12-7-2018

An Improved Method to Calculate Gas-Lift Valve Set Pressure and Valve Performance Curves

Khadhr A KH Altarabulsi
Louisiana State University and Agricultural and Mechanical College

AN IMPROVED METHOD TO CALCULATE GAS-LIFT VALVE SET PRESSURE AND VALVE PERFORMANCE CURVES

A Dissertation

Submitted to the Graduate Faculty of the
Louisiana State University and
Agricultural and Mechanical College
in partial fulfillment of the
requirements for the degree of
Doctor of Philosophy in Petroleum Engineering

in

The Department of Petroleum Engineering

by
Khadhr A KH Altarabulsi
B.S., Kuwait University – Kuwait, 2009
M.S., Kuwait University – Kuwait, 2014
May 2019

Acknowledgments

I would like to acknowledge my advisor, Dr. Paulo Waltrich for his kindness, continuous support, guidance, encouragement, and efforts during my journey to earn my Ph.D. Also, I would like to extend my gratitude to my committee members, Dr. Karsten Thompson, Dr. Dandina Rao, Dr. Ipsita Gupta, and Dr. Gerry Knapp. I appreciate your time, guidance and efforts for making this work successful.

I also would like to express my sincere appreciation to Dr. Renato Coutinho, Mr. Kenneth Decker, and Mr. Sergio Caicedo for their continuous help, support, superior guidance, and teaching.

I would like to acknowledge my parents, Ahmad Altarabulsi and Maryam Etani for their non-stop daily encouragement and prays. My sincere gratitude goes to my wife Anfal Al-Houli for being patient and supportive with me and our kids Ahmad and Fajer during this long journey.

I also would like to thank Mrs. Jeanette Wooden, Mr. Doug Hoy and Mr. Randy Hughes for their support and prompt help. Finally, I would like to thank my friends and colleagues: Dr. Mohammed Al-Dousari, Dr. Waleed Zaid, Dr. Abdullah Al-Ajmi, Dr. Redha Al-Hurr, Younes Al-Bulooshi, Dr. Waleed Al-Bazazz, Muzher Al-Musabeh, Hazem Fleifel, Ibrahem Al-Matri, Bruno Xavier, Ligia Tornisiello, Matheus Capovilla and Cooper Smidt for making my life more colorful and joyful during this journey in the USA.

Table of Contents

List of Symbols, Subscripts and Abbreviations

Symbol	Description
A	Area
$A_{1\text{-}11}$	Coefficient for Equation *2.11*
a	Coefficient for Equation *2.4*
b	Coefficient for Equation *2.4*
C_d	Discharge coefficient
c	Velocity of sound
C_v	Flow capacity of the valve
d	Diameter
F_k	Correction Factor for ratio of specific heats
g	Acceleration of gravity
K	bulk modulus of elasticity
k	Two sided Student coefficient
k	Ideal gas isentropic exponent
m	Mass
M_W	Molecular weight
n	Number of moles
n	Number of samples
n	Real isentropic exponent
P	Pressure
q	Volumetric flow rate
$\overline{q}$	Average measurements
R	Gas constant
T	Temperature
U	Expanded uncertainty
u_o	Experimental uncertainty
u_s	Device uncertainty
V	Volume
v	Specific volume
x	Pressure drop ratio
x_T	Terminal pressure drop ratio
Y	Expansion factor
Z	Compressibility factor
α	Linear thermal expansion coefficient
β	Isothermal secant bulk modulus
β	Volumetric thermal expansion coefficient
dp	Differential pressure increase
dv	Differential decrease in volume
ρ	Density
γ_g	Gas specific gravity

Subscripts	Description
1	Upstream
1	Initial conditions
2	Final conditions
10	Pressure of 10,000 psig, any temperature
Avg.	Average

BH	Static Bottomhole
c	Critical
d	Dome
g	Gas
i	Count number
m	Constant
max	Maximum
min	Minimum
o	Atmospheric pressure, any temperature
p	Port
Reff.	Reference
s	Standard state 77 °F
sc	Standard condition
T	Terminal
v	Valve depth
w	Water
wh	Wellhead conditions

Abbreviation	**Description**
API	American Petroleum Institute
AGA	American Gas Association
bbl	Barrel
DP	Standard Deviation
GLR	Gas-Liquid-Ratio
GLV	Gas-Lift Valve
IPO	Injection Pressure Operated
ISA	Instrumentation Society of America
LSU	Louisiana State University
OD	Outer Diameter
PPO	Production Pressure Operated
PVT	Pressure, Volume and Temperature
SCF	Standard Cubic Feet
VPC	Valve Performance Clearinghouse

Abstract

The main objective of this work is to improve the accuracy on calculations of design set pressure and performance curves (sizing equations) for Gas-Lift Valves (GLVs) at high pressure (real conditions). This improved calculation method is demonstrated to have an important effect on well unloading and production operations.

The analysis of the valve design set pressure includes an experimental evaluation of the effect of internal dome volume changes on the design set pressure due to the presence of silicone and thermal effects. The evaluation is carried out for different levels of GLV silicone fill, pressures and temperatures. Silicone fills covered 7.5, 10, 25, 50 and 75%. Initial pressure ranges are from 975 to 1,250 psig, and temperature range is from 60 to 175 °F. These experimental conditions cover the conventional operating range in the industry.

The analysis for the GLV flow equations includes a numerical study of the effect of using fluid properties at real conditions on the accuracy of gas-lift performance curves. A software is used to estimate the real fluid properties at high injection pressure for natural gas. These properties are used as a modification on the current model to account for the fluid properties at real conditions. The velocity of sound concept is used as a proof to validate the suggested modifications on the current model.

The results provide an enhanced model for improving the GLV design set pressure especially for refurbished GLV with large silicone fills. It also provided a successful well unloading design under all the investigated conditions, while utilizing other models lead to multi-point of injection problem. The new model overpredicts the design pressure by an average of 1.45% for all experimental points. The VPC model overpredicts the design pressure by an average of 2.71%, and the current practice (N_2) model underpredicts the pressure by -3.56%. Furthermore, the model

suggested for the GLV sizing equation provided a better improvement on estimating the flow through GLV especially in the critical region. Under the investigated conditions, the new improvement enhanced the flow rate estimate by 19%. This improvement may affect unloading operation of wells.

1. Introduction

There are many artificial lift methods utilized in the industry to aid in lifting the fluids from bottomhole to surface such as gas-lift, sucker rod pumps, Electrical Submersible Pumps (ESPs), Progressive Cavity Pumps (PCPs), plunger pumps, and jet pumps. Gas-lift (GL) is a commonly used artificial lift method, especially in offshore wells. Gas-lift method is common because it has many advantages such as reliability, covering a wide range of operating conditions, simple downhole assembly, need only limited space in the well, which is beneficial in offshore installations where the space is limited and costly (Bagci, 2017; Xu et al., 2013).

Gas-lift consist of injecting a certain amount of gas at the bottom of the production tubing through a GLV to increase the Gas-Liquid-Ratio (GLR) in the well, which in turn, reduces the fluid density, and consequently, lowers the hydrostatic pressure caused by the fluid column in the production tubing. However, one application precedes the intermittent/continuous gas injection: well unloading.

Well unloading is a procedure used to "kick-off" the wells after installation of completions or well shut downs. The well unloading operations aims to lower the hydrostatic pressure at bottomhole. This is often accomplished by utilizing a sequence of unloading GLVs along the production tubing that are capable to close at a certain set pressure, as shown in Figure 1.1. GLV set pressure is the desired opening/closing pressure of a valve needed at well conditions. The unloading process starts with injecting gas in the casing/annulus (P_{io}) towards the first GLV, when all the GLVs are open in the beginning at a certain set pressure. This would allow kill fluid to transfer from the casing to the tubing up to the surface as shown in following Figure 1.1 (a). When the gas starts flowing through the first GLV, it goes toward the tubing and mix with the liquid in the tubing.

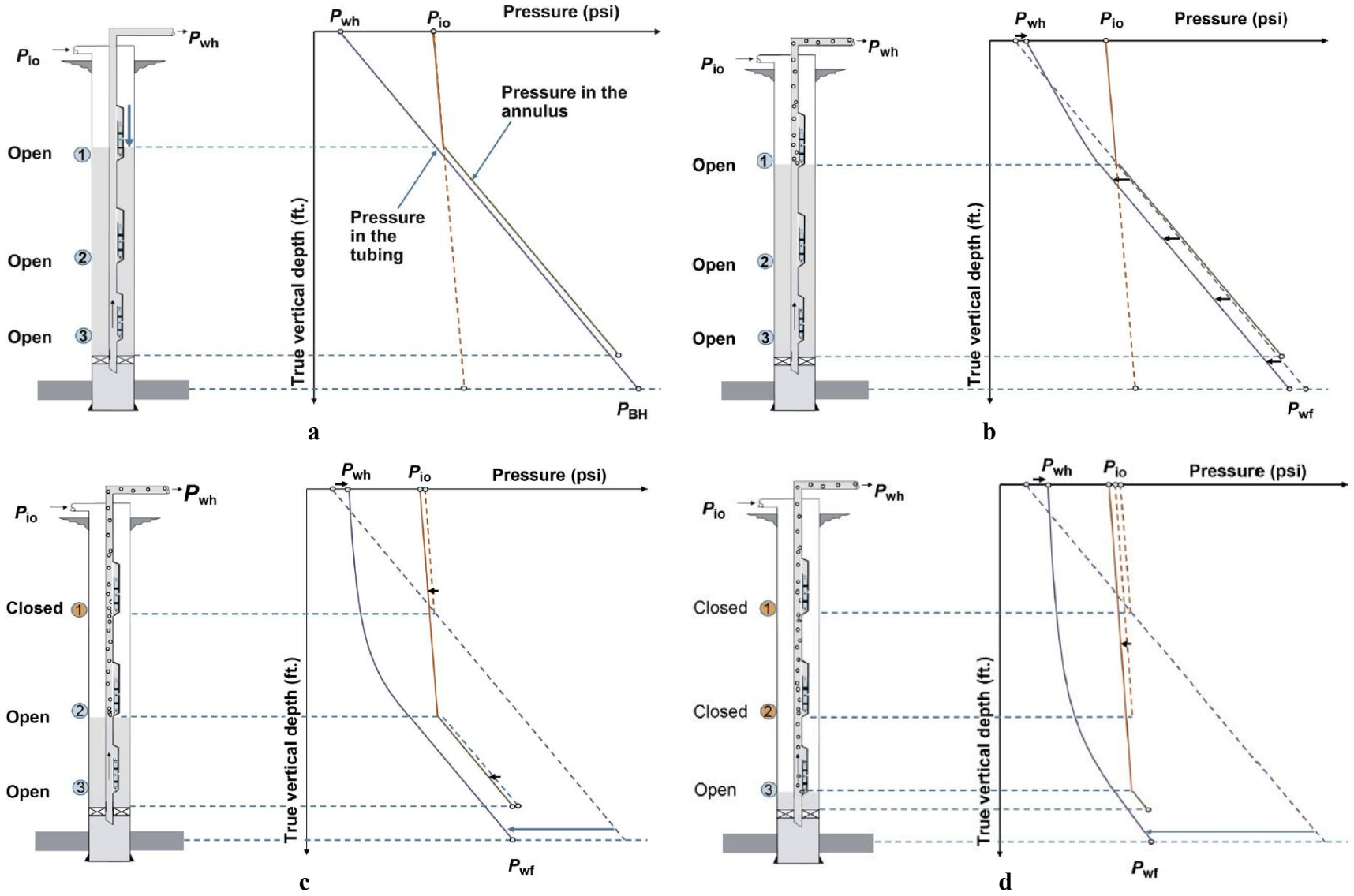

Figure 1.1. Typical unloading process using Gas-Lift valves [adapted from Hernandez (2016)].

As the gas mixes with the liquid in the tubing, the mixture density is reduced, which in turn, lowers the pressure along entire tubing as shown in Figure 1.1 (b). Gas keeps flowing through the first GLV but also keep pushing the liquid column in the casing. Once the gas reaches the second, the first GLV should close based on its design set pressure and gas keeps flowing through the second GLV as shown in Figure 1.1 (c). These process is repeated until the gas reaches the deepest valve where the first and second unloading valves closed as shown in Figure 1.1 (d) and the static bottomhole pressure (P_{BH}) is reduced to the target flowing bottomhole pressure (P_{wf}).

The valve at the deepest point is called the operating valve. Operating valve ensure injecting a certain amount of gas that is selected during the design stage to optimize the oil production rates. The valves above the operating valve are the "unloading" valves, which are designed primarily to unload the well.

1.1. Gas-Lift Valve Categories

Gas-lift valves are classified according to its application into two categories: unloading and production valves. Both categories as briefly described next.

1.1.1. *Unloading Valves*

Unloading valves mimic a variable orifice, and it is operated by pressure. An unloading valve has a set opening/closing pressure to allow the valve to open and close at a certain pressure and temperature. This mechanism is needed for successful well unloading as mentioned previously. The set opening/closing pressure for some valves has more sensitivity to the casing (injection) pressure and therefore, called Injection-Pressure-Operated valves (IPO). On the other hand, other types of valves are more sensitive to the tubing pressure and called Production-Pressure-Operated valves (PPO) (Hernandez, 2016; Takacs, 2005). IPO and PPO valves are also called calibrated/live valves (Hernandez, 2016). The opening and closing pressures are set at GLV workshops at a

temperature of 60 °F by injecting a certain amount of gas (usually nitrogen) inside its dome and bellows, as shown in Figure 1.2. Also, some IPO and PPO valves utilize a spring or both (spring and nitrogen) to control the set opening/closing pressure. The bellows are a metallic component that can expand and contract with pressure changes. The bellows are connected to the stem, which allows the stem to seal (close the valve) and unseal the seat (open the valve). Silicone is used as a vibration dampening fluid, which protect the bellows from sudden pressure changes (Takacs, 2005). A correction factor is used to determine the set opening/closing pressure at field conditions to account for the change in pressure on the nitrogen in the dome.

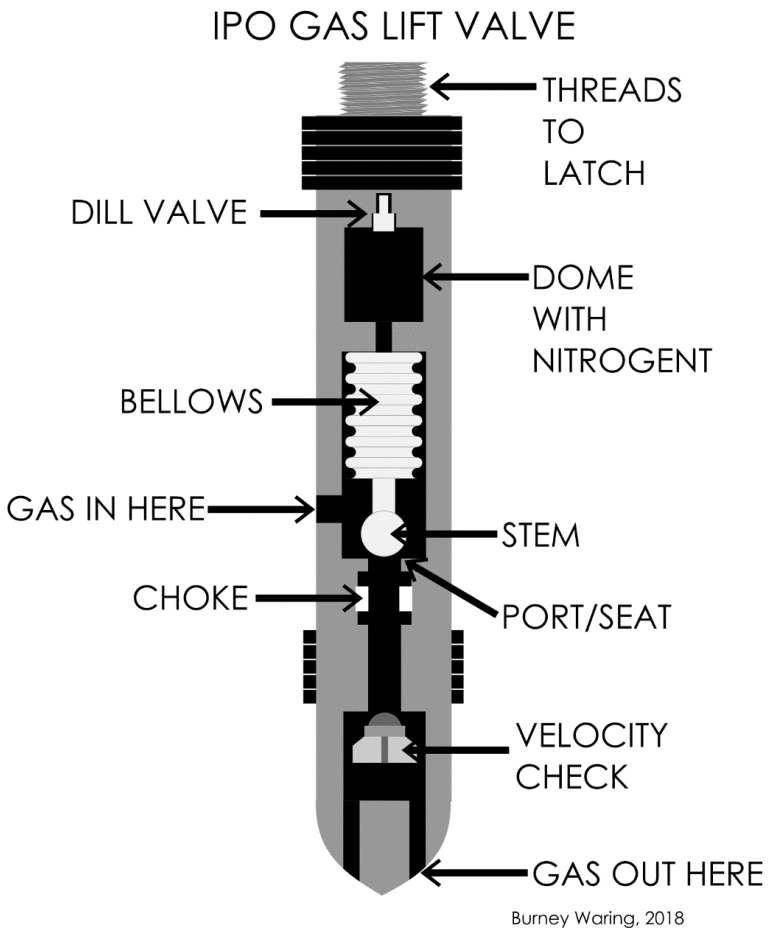

Figure 1.2. IPO gas-lift valve components [adopted from Warning (2018)].

The current correction factor described in the API (1999) and other references (Hernandez, 2016; Sutton, 2014; Takacs, 2005) does not include all the parameters affecting the set opening/closing pressure. These parameters are the silicone thermal expansion, silicone compression at high pressures and dome thermal expansion. More details about the factors that affect the set opening/closing pressure will be illustrated in the problem statement and the literature review. Inaccurate estimation of the set opening/closing pressure may fail unloading the well.Also, a certain volume of gas has to flow through the unloading valves during the well unloading process to, effectively, reduce the density in the tubing and successfully unload the well. The volume of gas flowing through a GLV depends on valve characteristics, injection and tubing pressures. Typically, the GLV performance curves are used during the valve selection process. These curves show the gas flow rate for a specific valve under different pressure conditions. Figure 1.3 shows a typical performance curve for an IPO valve as a function of injection/upstream and production/downstream pressures.

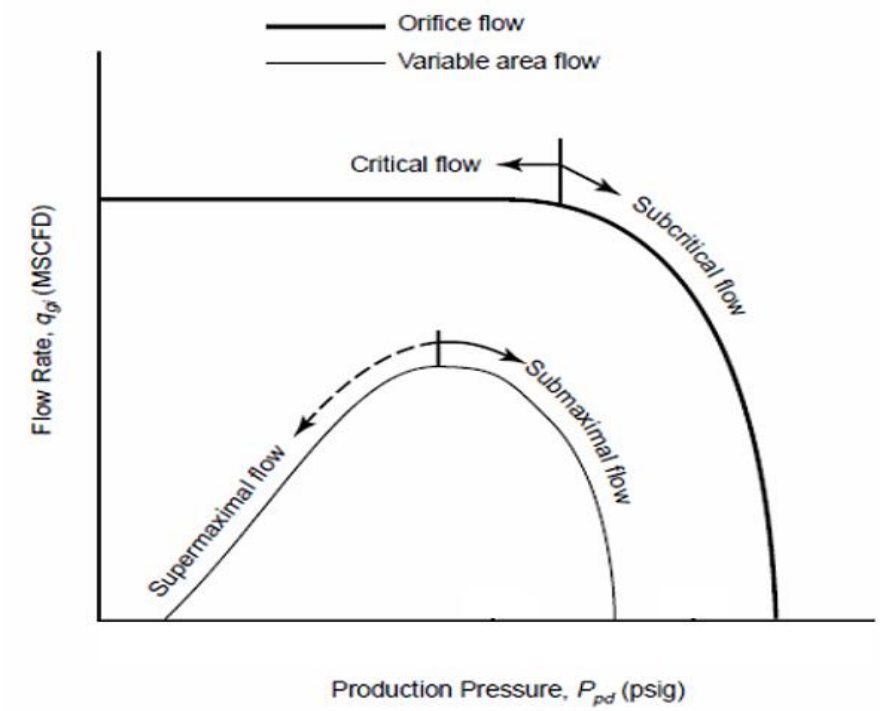

Figure 1.3. Typical gas-lift performance curves for an IPO GLV [adopted from API (2001)].

Two distinguished flow curves are observed in Figure 1.3. The upper curve is defined as an orifice flow. This type of flow occurs when the stem of the valve is fully open. The lower curve represents the throttling flow, where the stem of the valve is partially open, and the stem tip is only partially obstructing the gas flowing area. More details about the development of gas-lift valve performance curves are presented in section 2.2.3.

1.1.2. *Operating Valves*

Orifice GLVs are usually utilized as operating valves (Hernandez, 2016). However, IPO are also deployed as operating in some cases (Hernandez, 2016; Takacs, 2005). Orifice valves have a fixed-diameter orifice size to control the gas injection, as shown in Figure 1.4. The difference between orifice and IPO/PPO valves is that orifice valves are always open since there is no closing mechanism.

Figure 1.4. Typical orifice GLV [adapted from Hernandez (2016)].

When continuous gas-lifting is used, an optimized amount of gas should be injected. This concept is clearly illustrated in Figure 1.5. High gas rates lead to elevated mixture velocity, which

creates large frictional losses in the tubing and accelerational loss in the GLV, and consequently, large bottomhole pressures. High bottomhole flowing pressures reduce the liquid production rate (Beggs, 1991; Economides et al., 2012; Mukherjee et al., 1999). It can be seen from Figure 1.5 that, there is a small region (yellow-shaded area) to inject an optimized amount of gas where exceeding or decreasing this amount would lead to a serious reduction in the liquid production. The optimum amount is called the GLR limit.

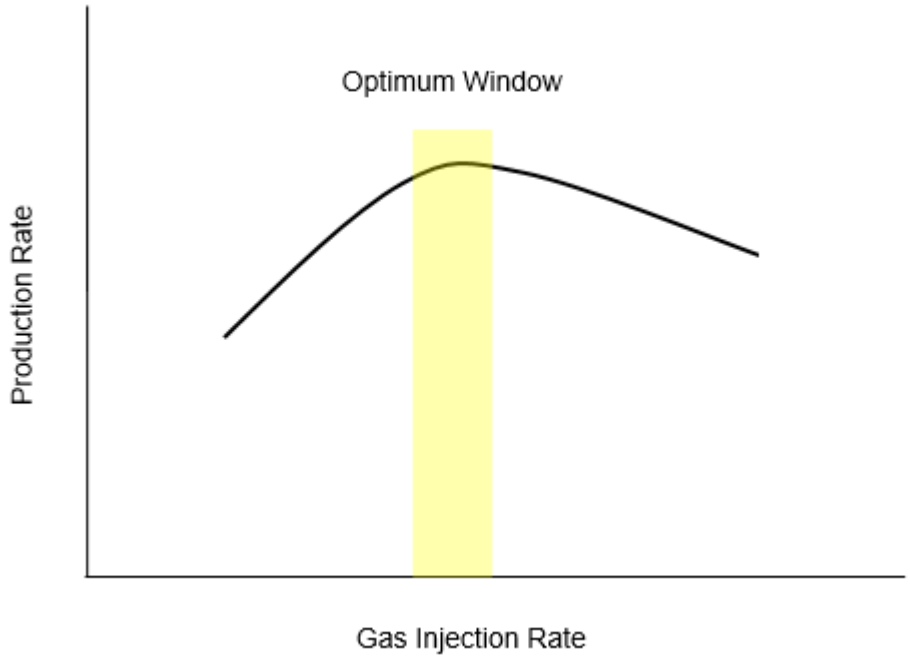

Figure 1.5. Gas injection rate vs. liquid production rate.

The GLV is a component in the gas-lift system which dictates the injected gas flow rate for gas-lift operations. The optimization of the gas injection is determined during the gas-lift design using both the Inflow Performance Relationship (IPR) and the Tubing Performance Relationship (TPR). After that, the GLV orifice size is selected based on its performance curves (similar to Figure 1.3). As mentioned earlier, these curves show the gas injection rate across that valve at a certain depth as a function of injection and production pressures. Since the pressure in the tubing

is not constant, it is important to use the performance curve to predict the performance of the GLVs at various tubing pressures. The gas flow rate through the valve controls the liquid production rate.

1.2. Gas-Lift Performance Curves

The gas-lift performance curves are generated in two ways: experimentally and theoretically. A typical orifice gas-lift performance curve is shown in Figure 1.3, and it illustrates the relationship between tubing/downstream pressure as a function of flowrate.

1.2.1. *Experimental Gas-Lift Performance Curves*

Generating the performance curves experimentally is very costly and time consuming. Also, the curves generated are limited to the test conditions (i.e., the range of pressures and temperatures deployed during the tests). These tests are generated using air, and a conversion factor is applied to convert it to the actual working fluid in the field (usually natural gas) (Takacs, 2005).

1.2.2. *Theoretical Gas-Lift Performance Curves*

Theoretical generation of the gas-lift performance curves has been used by the oil and gas industry for many years (Hernandez, 2016). More than ten theoretical methods were developed to generate these curves without performing costly experiments. These methods include mechanistic, statistical and unified models (Hernandez, 2016).

The Valve Performance Clearinghouse (VPC^{TM}) is a nonprofit consortium between the Louisiana State University (LSU) and the joint industry members. The objective of this consortium is to test and model GLVs. All the previously tested GLV data were incorporated in a software called the VPC^{TM} software. The VPC is a state-of-the-art software that allows the user to generate the GLV performance curves at field conditions using six theoretical methods. The best method (claimed by the developer Kenneth Decker) in this software is the VPC method, which provides

an accuracy of ±20% of the actual flow rate (Decker, 2014). This is because the VPC method requires GLV data that is obtained using actual dynamic flow tests under high pressure which, mimics the actual operating pressure conditions in the well. One other method is called the American Petroleum Institute (API) Simplified method (recommended by the API RP 19G2 (2010)) where it provides an accuracy of ±30% for port sizes less than or equal 3/16 inch. Both the VPC and the API Simplified methods utilize equation adopted from the Instrument Society of America standards (ISA, 1975). This equation has some assumptions for the fluid properties including ideal isentropic exponent in the gas expansion factor (Y), which is described in details in section 2.2.3. and 2.2.4. Other methods are also available such as the Thornhill-Craver equation (1946), Winkler-Eads (1993) correlation and Bertovic equation (1997). However, all the previous methods provide a lower accuracy than the VPC and API simplified methods (Decker, 2014). In addition, the latest edition of the API recommended practice for GLV performance testing (2010) recommended the use of the API simplified and if possible to use the dynamic flow tests to enhance the accuracy of the API simplified method. This step of including dynamic tests is implemented in the VPC method.

1.2.3. *Accuracy of the Set Pressure for GLVs*

To have a successful well unloading, the set opening/closing pressures for the GLVs have to be accurately determined. The opening/closing set pressures are determined on the workshops at 60 °F after that, a correction factor is imposed to this pressure to account for the temperature increase in the valve at setting depth. However, this factor does not account for volumetric changes of the silicone in the dome due to high pressures inside the dome and the volumetric thermal expansion of the silicone and dome itself. When the silicone expands, the dome volume occupied by gas reduces, which in turn, increase the dome pressure.

Furthermore, according to the VPC^{TM} (2014) software developer and ex-chairmen of the API group of the GLV performance testing (1993), Kenneth Decker, when the valve is re-furbished at workshops, technicians often add more silicone to the valve as a part of valve refurbishment with no specific reason (personal communication, April, 27, 2017). Silicone does not dissolve and does not leak, since the valve is sealed closed. This additional amount of silicone increases the silicone volume ratio with respect to the total dome volume. Adding more silicone increases the amount of the expanded silicone, which in turn, reduces the dome volume occupied by gas further, and hence, increasing the amount of the error in determining the correct opening/closing set pressures.

In addition, when liquid is subjected to a pressure change, its volume may change (reduce) due to its compressibility. The reduction of silicone volume increases the dome volume occupied by gas. Not accounting for this effect may also lead to error in the opening/closing set pressures design. Furthermore, when the bellows and dome are subjected to change in temperature, it expands and increases the volume of the dome and bellows. Therefore, ignoring the thermal expansion of the dome may affect the set pressure design. Experimental investigations have not been found in the literature to evaluate the impact of silicone and dome/bellows expansion due temperature increase, and silicone compression due to high pressures on set pressure of GLVs. The VPC method (2014) corrects for the thermal expansion of silicone but ignores the silicone compressibility and dome thermal expansion. In addition, the accuracy of nitrogen correlation used in the predicting the pressure is not known. Furthermore, the software is limited to the VPC members.

In some cases, IPO/PPO valves are utilized as operating valves for continuous gas-lift operations (Hernandez, 2016; Takacs, 2005). This is because IPO/PPO valves can maintain the gas injection rate by responding to tubing pressure changes, especially with wells that have

instability flowing problems. Therefore, in addition to its effect on well unloading operations, the accuracy on the design of set pressures may also affect the oil production rate of gas-lifted wells.

1.2.4. *Accuracy of GLV Sizing Equations under Real Conditions*

The key parameter in successfully designing gas-lift for oil wells (assuming accurate IPR curves) is the selection of an optimum gas injection rate. Deviation from the optimized rate of gas injection may dramatically decrease the liquid production rate (as shown in Figure 1.5). The orifice size of the GLV is selected based on the injection gas flow rate needed to reach the optimum liquid production rate. In addition to that, the amount of gas injection during the unloading process (using IPO/PPO valves) is important because the proper rate of gas has to be injected inside the tubing to reduce the density of fluid mixture and successfully unload the well.

Each GLV has its own performance curve, and there are different methods to generate such curves. As mentioned previously, one of these methods is generating the curves using theoretical equations. These equations are available in software such as the VPC^{TM} software (Decker, 2014). The second method is by testing the GLV experimentally under the needed field conditions. The pressure drop through the GLV is very sensitive to the gas flow rate injected, as shown earlier in the introduction (Figure 1.3).

This research focuses on two theoretical methods available in the VPC^{TM} software (Decker, 2014) specifically the VPC correlation (2014) and the API simplified correlation that represents the current recommended practice equation (2010). These methods are selected since it provides an accurate gas passage prediction in the GL valves (Decker et al., 2018) especially when compared to the commonly used (Hernandez, 2016; Takacs, 2005) Thornhill-Craver (1946) equation.

Many other equations are available such as Thornhill-Craver (1946), VPC limited (2014) and Winkler Eads (1993). These equations will be presented and discussed in section 2.2.1. The problem of applying the theoretical method comes from its accuracy, where it has been shown in the literature (AlTarabulsi et al., 2017; Hernandez, 2016) that the theoretical performance curves for such valves may not work appropriately for a wide range of fluid types, pressure, and temperature. One of the source of errors that may affect the accuracy of the theoretical performance curves comes from the assumptions used to develop these theoretical performance curves. The basis of the GLV performance curves utilizes the ideal gas concept in the form of an expansion factor, *Y,* to correct for gas expansion in the valve throat (API, 2010; Decker, 2014). However, the assumptions for the development of this expansion factor assumes ideal isentropic gas flow. These assumptions may deviate the theoretical model results from the actual behavior, especially when it is applied for high pressures and temperatures conditions (Buresh et al., 1964; Fagerlund, 1988; Riveland, 1992, 2012).

1.3. **Problem Statement**

This dissertation discusses two main problems:

a- The first problem deals with the accuracy of GLV design set opening/closing pressure and is discussed previously, in section 1.2.3.

b- The second problem deals with the accuracy of the GLV sizing equations under real conditions and is discussed previously, in section 1.2.4.

1.4. **Goals and Objectives**

The main goal of this dissertation is to propose an improved calculation method for the opening/closing set pressures and sizing equations for GLV performance curves. The following objectives are established to accomplish this goal.

1. Evaluate experimentally, the accuracy of the correction factor applied to the IPO/PPO valves represented by the negligence of the dome volume changes due to silicone thermal expansion, silicone compression, and dome thermal expansion.
2. Develop a model that accounts for the silicone thermal expansion, silicone compressibility and dome thermal expansion of the GLV set pressure and evaluate the developed model against models used currently in the industry.
3. Evaluate the effect of utilizing the non-ideal/real isentropic exponent in the gas expansion (Y) factor on the accuracy of the GLV sizing equations.
4. Validate the use of non-ideal/real isentropic exponent with the velocity of sound concept.
5. Evaluate the impact of utilizing the new models and improvements on the GLV design.

2. Literature Review

This chapter is divided into two parts. The first part provides a literature review related to the accuracy of GLV set pressure. The second part provides a literature review related to the accuracy of GLV sizing equations.

2.1. Accuracy on the Design of GLV Set Pressure

This section introduces the current practices in designing the set pressure for GLVs and the accuracy of the current nitrogen correlations used for this purpose. Also, it highlights the ignored effects that may affect the design set pressure for GLVs.

2.1.1. *Current Practice and the Use of Nitrogen Correlations*

During the period of 1950's and 1960's, many charts and tables similar to Figure 2.1 have been developed to account the temperature effect on the dome pressure using the test rack opening pressure (TRO) at 60 °F as a reference pressure. Kirkpatrick (1955), Winkler and Smith (1962) and Brown (1967) are some examples of commonly used charts and tables available at that time. These charts and tables were used due to the limited availability of computers at that time (Sutton, 2014). Winkler and Eads (1989) developed a method to perform the correction of the temperature effect using an equation rather than charts and tables for more accurate estimates. This empirical equation uses the dome pressure at workshop conditions (60 °F) and estimates the dome pressure at any temperature as follows:

$$P_d = P'_d + m(T_V - 60) \tag{2.1}$$

for $P'_d < 1{,}238\ psia$

$$m = -0.00226 + 0.001934P'_d + 3.054 \times 10^{-7}\ {P'_d}^2 \tag{2.2}$$

for $P'_d \geq 1{,}238\ psia$

$$m = -0.267 + 0.002298P'_d + 1.84 \times 10^{-7}\ {P'_d}^2 \qquad 2.3$$

where P_d is the dome pressure at setting depth, P'_d is the dome charge pressure at 60 °F, m is a constant that depends on the value of dome pressure at 60 °F, and T_v is the valve temperature at setting depth. The range of application for this equation is from 60 to 310 °F and from 200 to 3,000 psia (Winkler et al., 1989).

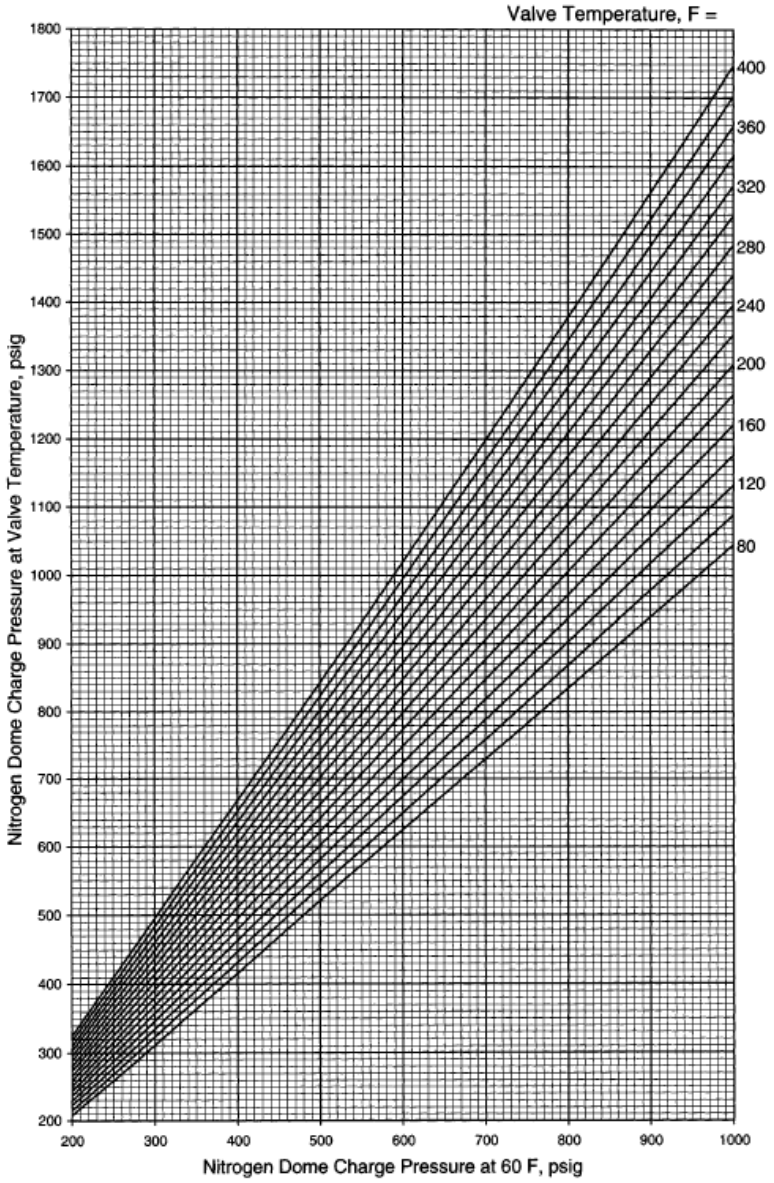

Figure 2.1. Correction factors for temperature effects on dome pressure filled with nitrogen [adapted from Takacks (2005)].

Another simple empirical equation was developed by Zimmerman (1982) that uses the dome pressure at workshop conditions (60 °F) and estimates the pressure at well as a function of temperature as follows:

$$P_d = bP'_d - a \tag{2.4}$$

$$a = 0.083(T_V - 60) \tag{2.5}$$

$$b = 1 + 0.002283(T_V - 60) \tag{2.6}$$

The recommended range of application of Equation *2.4* is limited to pressures up to 2,000 psig and temperatures up to 220 °F. The accuracy of this equation was not evaluated.

Another approach to compensate the temperature effects on the set pressure is by using real gas law and conservation of mass assuming a constant volume. An expression relating the set pressure change between the workshop conditions (60 °F) and downhole conditions is as follows (Takacs, 2005):

$$P_1 = \frac{P_2 Z_1 T_1}{Z_2 T_2} \tag{2.7}$$

where P_1 is the dome pressure charged at workshop conditions (P_1 and $T_1 = 60$ °F), Z_1 is the nitrogen compressibility factor at workshop conditions, T_2 is the temperature at the valve setting depth, and Z_2 is the nitrogen compressibility factor at valve setting depth and design pressure (at P_2 and T_2). Equation *2.7* needs iteration since P_1 is a function of Z_1.

Since Equation *2.7* depends on the compressibility factor evaluated at workshop and valve depth conditions, many equations were developed to estimate the compressibility factor for nitrogen. Takacs (2005) developed a nitrogen compressibility factor equation by curve fitting the experimental data from Sage and Lacey (1950), and claimed that the accuracy is better than ±0.1% at pressures less than 2,500 psia (Sutton, 2014; Takacs, 2005). The data range used for this curve

fitting is from 0 to 3,000 psia and from 60 to 400 °F. The following equation is the nitrogen compressibility factor developed by Takacs (2005) :

$$Z = 1 + b\,P + c\,P^2 \tag{2.8}$$

$$b = (1.207 \times 10^{-7} T_{°F}^{3} - 1.302 \times 10^{-4} T_{°F}^{2} + 5.122 \times 10^{-2} T_{°F}^{-2} - 4.781)10^{-5} \tag{2.9}$$

$$c = (-2.461 \times 10^{-8} T_{°F}^{3} + 2.640 \times 10^{-5} T_{°F}^{2} - 1.058 \times 10^{-2} T_{°F}^{-2} + 1.880)10^{-8} \tag{2.10}$$

where *Z* is the nitrogen compressibility factor, *P* is the pressure in psia, *T* is the temperature in °F. More recently, a new expression (Equation *2.11*) was developed by Sutton (2014) to estimate the compressibility factor of nitrogen for a wider range of pressure and temperature conditions. The range of applicability of Equation *2.11* is from 100 to 15,000 psia and from 60 to 400 °F. The minimum error is - 0.31% and the maximum error is 0.19% for the entire range.

$$Z = 1 + \left(A_1 + \frac{A_2}{T_r} + \frac{A_3}{T_r^3} + \frac{A_4}{T_r^4} + \frac{A_5}{T_r^5}\right)\rho_r + \left(A_6 + \frac{A_7}{T_r} + \frac{A_8}{T_r^2}\right)\rho_r^2 - A_9\left(\frac{A_7}{T_r} + \frac{A_8}{T_r^2}\right)\rho_r^5 + A_{10}(1 + A_{11}\rho_r^2)\left(\frac{\rho_r^2}{T_r^3}\right) exp(-A_{11}\rho_r^2) \tag{2.11}$$

$$\rho_r = \frac{Z_c P_r}{Z T_r} \tag{2.12}$$

$$A_1 = 0.414453,\ \ A_2 = -0.885611, A_3 = -1.372537, A_4 = -1.307205$$

$$A_5 = 2.943774, A_6 = 0.244662, A_7 = -0.253387, A_8 = 0.281159$$

$$A_9 = 0.313724, A_{10} = 0.307269, A_{11} = 0.135200, Z_c = 0.2916$$

where *Z* is the nitrogen compressibility factor, A_1-A_{11} are coefficients, ρ_r is the reduced density for nitrogen, T_r is the reduced temperature for nitrogen, P_r is the reduced pressure for nitrogen. Equation *2.11* uses a modified version of the equation of state introduced by Dranckuk and Abou-Kassem (DAK) (1975).

Equation *2.11* (Sutton-modified DAK) is selected in this study since it covers a wider range of application, compared to other correlations. Sutton (2014) presented a study comparing the accuracy for both correlations. The outcomes of this study showed that the error in pressure using Tacaks equation increases slightly starting from 1,500 to 3,000 psig where the maximum error is around -12 psig (-0.4%). On the other hand, when using Sutton modified DAK using the same pressure range would result in a lower error where the maximum error is around -1.5 psig (-0.05%).

2.1.2. ***Design Set Pressure for IPO GLV***

The current recommended practice (API, 1999) calibrates the nitrogen-charged IPO valve set pressure based on its opening pressure. The equation used to estimate the opening pressure at well conditions is as follows (Takacs, 2005):

$$P_{vo} = \frac{P_d}{1-R} - P_t \times PPEF \tag{2.13}$$

$$PPEF = \frac{R}{1-R} \tag{2.14}$$

$$R = \frac{A_p}{A_b} \tag{2.15}$$

where P_{vo} is the valve opening pressure at well conditions, P_t is the tubing/production pressure, *PPEF* is the production pressure effect factor, A_p is the area of the port, A_b is the area of the bellows and R is a geometrical constant. The right-hand side of Equation *2.13* is called the Production Pressure Effect (PPE). This term represents the contribution of the pressure coming from the production/tubing toward the valves' opening pressure. As shown in Equation *2.13*, larger port sizes would provide larger contribution coming from tubing/production (Takacs, 2005). The following Table 2.1 shows 1 in OD IPO GLV (Camco BK-1) with the PPEF for each port size for the same valve (Takacs, 2005). It can be seen that the PPEF increases significantly, as a function

of valve's port size. Figure 2.2 shows the location of the port and bellow area in a typical nitrogen-chraged GLV.

Table 2.1. Camco BK-1 IPO GLV port sizes with the production pressure effect.

Port Size (*in*)	Production Pressure Effect (PPEF)
1/8	0.073
3/16	0.135
1/4	0.230
5/16	0.456
3/8	0.712

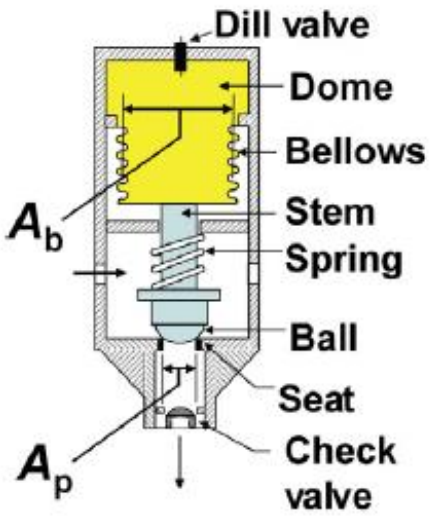

Figure 2.2. Illustration of the port and bellow area in a nitrogen-charged IPO GLV [adapted from Hernandez (2016)].

2.1.3. *Ignored Effects on the Design of GLV Set Pressure*

The corrections presented in section 2.1.1 account only for the temperature effect on the nitrogen in the dome. However, there are three other important factors that may affect the set pressure for a GLV:

1. Thermal expansion of silicone;
2. Thermal expansion of dome (metal);

3. Compressibility of silicone.

These factors will be discussed separately in the following sections.

2.1.3.1. *Thermal Expansion of Silicone*

Nitrogen charged valves are filled with a viscous fluid called silicone. When the temperature increases, the silicone fluid expands decreasing the volume of the dome occupied by the nitrogen, which in turn, increases the dome pressure. Silicone has a coefficient of thermal expansion five times that of water (Corning, 2017; OpenStaxCollege, 2012). The larger the amount of silicone fluid inside the dome, the larger the volume of expanded silicone, and therefore, the higher the effect on changing the GLV set pressure. Figure 2.3 shows the volumetric silicone expansion as a function of temperature.

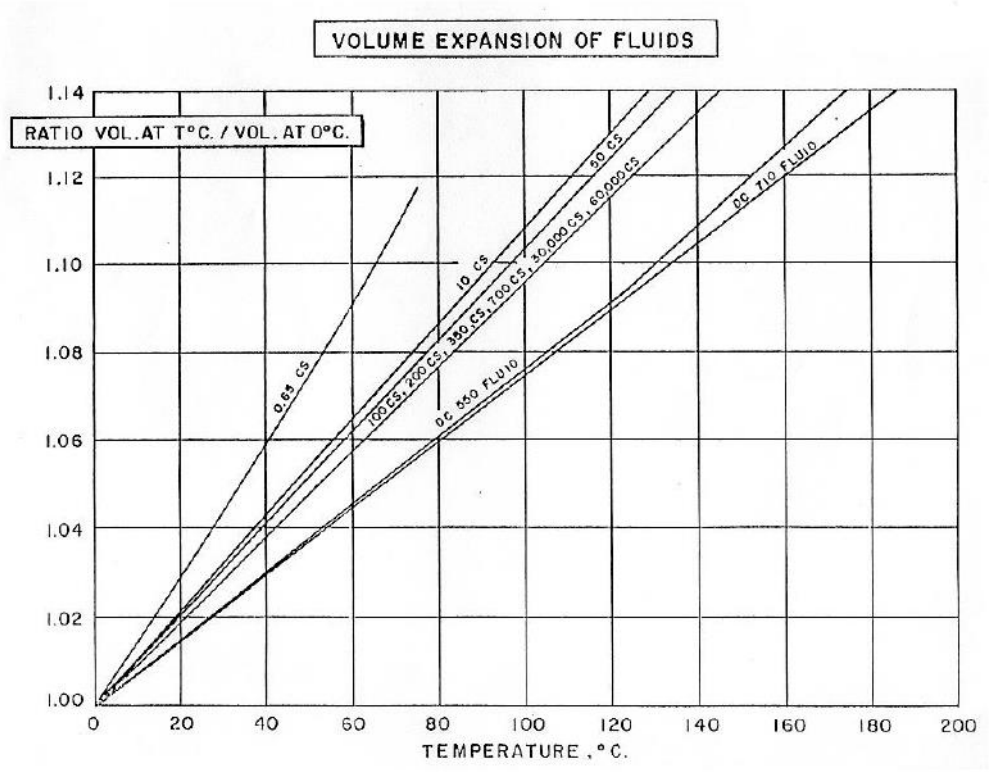

Figure 2.3. Typical silicone volumetric expansion at elevated temperatures [adapted from Corning (2017)].

Typically, DOW Corning (DC) 500 serious silicone is used to fill the dome in GLVs. Based on Figure 2.3, if the temperature increases from 60 °F to 212 °F, the volumetric expansion of the silicone will increase by 6.67%. This rise may affect the GLV set pressure, especially when the valve is utilized at high pressure and temperature applications.

Consider a theoretical example for a 1 in IPO valve that has a dome volume of 2.7 in^3 and a silicone volume of 0.7 in^3. If the valve is set to open at 2,000 psig, when the silicone thermal expansion of 6.67% is considered, the new opening pressure considering the thermal expansion is 2,047 psig. The unloading operation may fail especially if there is no extra pressure available to exceed the 47 psi caused by silicone expansion.

This effect may extend to other unloading valves, particularly when each valve is filled with a different amount of silicone fluid. Therefore, each valve will have a different amount of expanded fluid and thus, different opening pressures, which may negatively affect the unloading operation may cause multi-point of injection during unloading and production operations.

Also, this issue is not detectable in the workshop since the valves are tested at a single temperature of 60 °F. Therefore, the effect of different silicone filling will be undetectable since the silicone has not expanded significantly.

The problem of utilizing different amount of silicone fluid may occur when using refurbished valves. During the refurbishing process, technicians often add silicone fluid to the valve dome. The only calculation method which includes the effect of silicone expansion is the one included in the VPC™ software (Decker, 2014).

The VPC method includes a silicone thermal expansion factor. However, according to a personal communication with the software developer (Decker, (personal communication, April,

27, 2017) the effect of the thermal expansion on the dome pressure has not been verified with actual test data.

Also, it does not include the effect of silicone compressibility and dome thermal expansion. Furthermore, the nitrogen correlation and its accuracy is not specified in the VPC software method and the software is limited to the VPC members.

The practice of having multi-point of injection is not recommended in the continuous gas-lift design since it significantly, affects the efficiency of the process during the unloading and production stages.

Starting with the unloading stage, when the gas is injected through two valves simultaneously, the total amount of gas injected from the surface (compressor) is split to flow in two valves.

When this happens, the gas lift system (compressor) may not be able to provide adequate amount and gas pressure to overcome the production/tubing pressure at lower valves. Therefore, the gas will not be transferred to the lower valves, which in turn, may fail the unloading operation (Hernandez, 2016; Takacs, 2005). On the other hand, when multiple point of injection occurs during the production stage, it reduces the liquid production from the well. Sometimes, in order to increase the production to its desired (design) rate, a significant amount of gas may be needed.

The following example in Figure 2.4 compares the effect of single point and multi-point of injection for a gas-lifted well (Takacs, 2005).

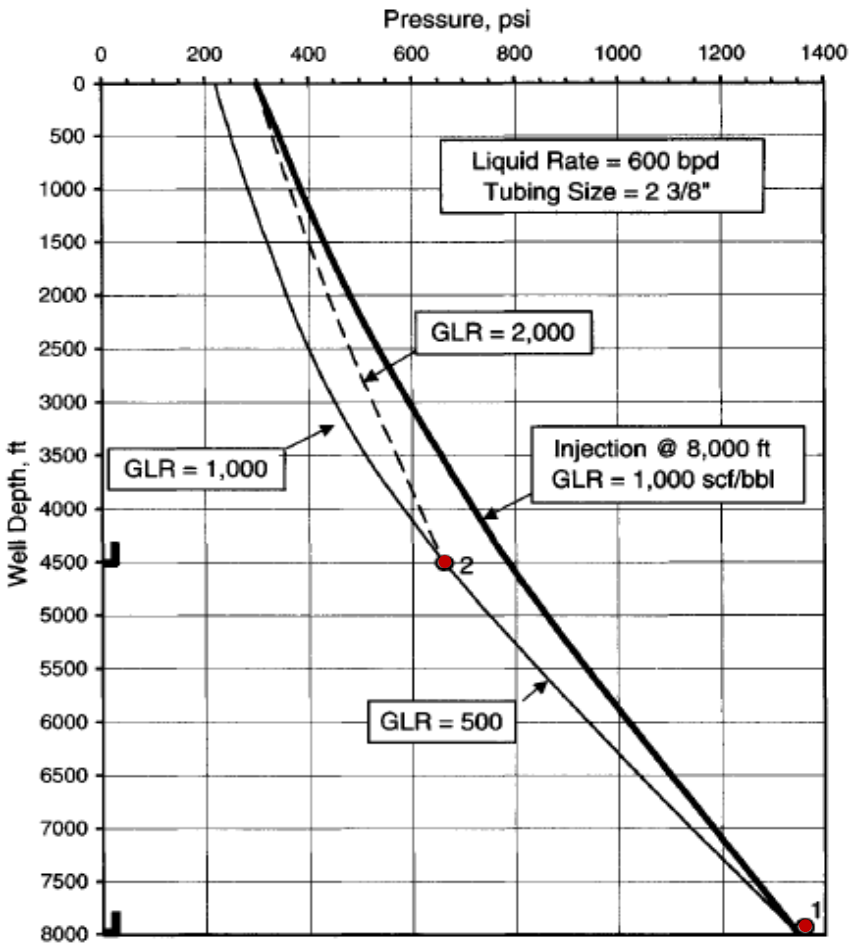

Figure 2.4. single point and multipoint gas injection in a continuous GL well [adopted from Takacs (2005)].

As can be seen in Figure 2.4, when injecting through a single point at a depth of 8,000 ft (point 1), a total GLR of 1,000 SCF/bbl is needed to allow a production rate of 600 bbl/d with wellhead pressure of 300 psig as shown in Figure 2.4. On the other hand, if two valves are open (multi-point of injection problem) and the gas injection is divided evenly (500 SCF/bbl) through these valves in points 1 and 2 simultaneously, it results in a lower wellhead pressure of 225 psig. Therefore, the well is not capable to flow against the required wellhead pressure of 300 psig. In order to restore the production with the same required wellhead pressure, a total of 2,000 GLR is needed at point 2 (shown in the dashed line, Figure 2.4). This additional amount of gas requires more compression and compression cost is the largest operating cost in the gas-lift (Takacs, 2005).

In addition, this additional amount of gas may not be available at the system, which may cease the unloading/production operations. The detection of multi-point of injection requires the use of formation evaluation techniques. These techniques play a major role in both designing and troubleshooting wells operated by GL. Two common techniques are highlighted in this discussion. These are the pressure survey log and the temperature survey log. Typically, the pressure and temperature surveys are performed together and performed under two well conditions, static and dynamic (flowing well).

Static and dynamic pressure and temperature logs can be performed in discrete stops and continuous manner depending on the tools available and budget. Static pressure survey is used to measure the static bottomhole pressure, static fluid level and static gradient of well fluids (API, 1994). On the other hand, static temperature survey measures the geothermal well gradient and static reservoir temperature. These parameters are key inputs in the GL design for a well especially when nitrogen charged IPO valves are used.

Dynamic pressure and temperature surveys can be used (along with other parameters) to analyze and select a proper multi-phase flow correlation/model for the well and other wells operating in the same field. Also, to update and estimate the current productivity index and formation damage of the well by varying the gas injection rate and measuring the production change. Also, it can locate the operating valve (point of injection). Furthermore, it can be used to diagnose multi-point of injection problems as will be shown in the following example [adopted from Hernandez (2016)].

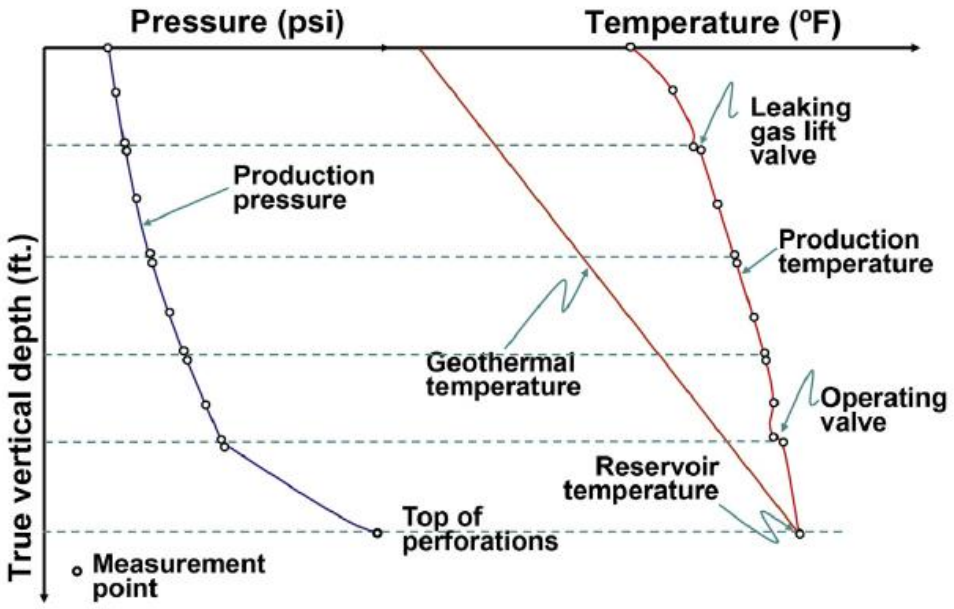

Figure 2.5. Pressure and temperature survey logs for a well having a multi-point of injection [adopted from Hernandez (2016)].

Figure 2.5 shows dynamic pressure and temperature surveys as a function of depth performed in discrete-stops for a well having multi-point of injection problem. As can be seen from the same Figure 2.5 that the first valve is leaking. This is because its temperature survey log responses show cooler than normal temperature gradient (due to gas expansion) compared to the general well trend. Also, following the same technique is used to locate the operating valve. As can be seen from the same Figure 2.5 that the operating valve can be located by observing the change in pressure and temperature gradients. Recently, new sensors are developed capable of performing the pressure and temperature surveys in continuously fashion rather than discrete stops (Hernandez, 2016). These sensors can detect temperature changes as small as 0.001 °F (Hernandez, 2016). Utilizing this technique increases the accuracy of the measurements and, therefore, the precision in the identification of leaks and other problems up to one foot. Such accuracy is not achievable when the conventional discrete method is utilized. The following Figure 2.6 shows the results of continuous pressure and temperature survey logs survey in a well (Hernandez, 2016).

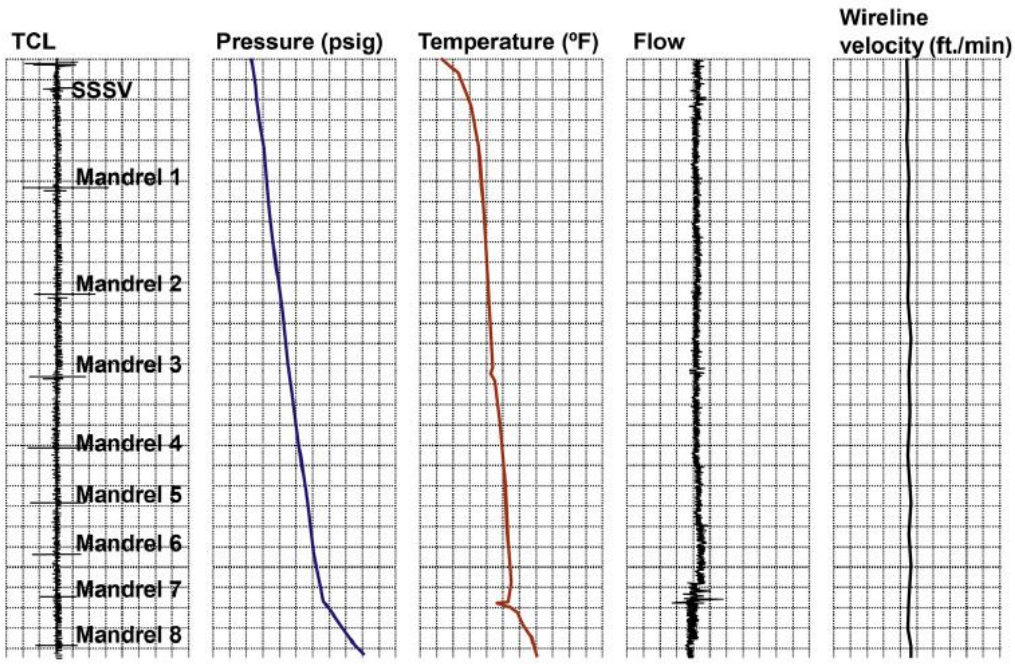

Figure 2.6. Continuous flowing pressure and temperature survey [adopted from Hernandez (2016)].

It can be seen from Figure 2.6 that there is a very small leak in mandrill # 3 and the operating valve is located in mandrill # 8. Sometimes tubing leaks take place near mandrills due to corrosive fluids such as CO_2 (Hernandez, 2016). If the conventional discrete method is used, the results may lead to the wrong conclusion of faulty GLV (instead of whole near the GLV mandrill) and may lead to unnecessary valve replacement instead of completion pullout, which takes time and money.

2.1.3.2. *Thermal Expansion of Dome*

Volumetric thermal expansion coefficient is smaller in solids than in liquids. However, the thermal expansion of the liquid silicone and metal dome should be considered. Table 2.2 compares the volumetric thermal expansion for water, silicone and stainless steel 316 (Metals, 2001; OpenStaxCollege, 2012).

Table 2.2. Thermal expansion coefficients at 68 °F.

Subject	Volumetric Thermal Expansion Coefficient $\left(\frac{in^3}{in^3}°F\right)$
Stainless steel 316	0.0000275
Water	0.0001167
Silicone	0.000533

The volumetric thermal expansion for a solid after being subjected to temperature change can be estimated by the following expression (Ho et al., 1998):

$$V_f = V_o(1 + \beta \Delta T) \tag{2.16}$$

where V_f is the final solid volume after being subjected to temperature increase, V_o is the initial volume, ΔT is the temperature difference between initial and final conditions and β is the volumetric thermal expansion coefficient.

2.1.3.3. *Compressibility of Silicone*

The compressibility of a fluid is the measure of the volume reduction of a fluid when it is subjected to a certain pressure change (Munson et al., 2010; Tichy et al., 1968). The compressibility of the fluids is expressed by the bulk modulus of elasticity, and it is expressed as follows (Munson et al., 2010; Streeter, 1969):

$$K = -\frac{\Delta P}{\Delta V / V} \tag{2.17}$$

where K is the bulk modulus of elasticity, ΔP is the pressure increase, ΔV is the decrease in volume due to pressure increase, and V is the original volume.

Fluids are usually considered incompressible especially at low-pressure applications. On the other hand, the effect of compressibility increases significantly at high pressures (Streeter, 1969).

Moreover, silicone fluids are considered very compressible fluids compared to other fluids (e.g. Water) (Corning, 1966).

A correlation was developed from experimental data to account for the silicone compressibility depending on pressure, temperature and density (Tichy et al., 1968). The claimed average error from experimental data is ±1.18%, and it covers the range from 32 to 400 °F and pressures up to 500,000 psig.

This correlation is used by DOW Corning (2017) to generate the data for Figure 2.7, which shows the silicone compressibility for a typical silicone fluid as a function of pressure and temperature (Corning, 2017). Tichy & Winer (1968) method is used in this study to estimate the silicone compressibility for the silicone fluid used in the experiment (DC 510 CS 500).

It can be seen from Figure 2.7 that the compressibility of the silicone increases as the pressure and temperature increase.

The compressibility of the silicone affects the dome pressure estimation, as it changes the nitrogen volume in the GLV dome. Therefore, it is essential to investigate and account for the effect of silicone compressibility on dome pressure calculations.

2.2. **Accuracy of GLV Sizing Equations for High-Pressure and High-Temperature**

This section introduces the current industrial practice in generating the GLV performance curves using experimental and theoretical methods. In addition, it shows the GLV orifice components and the velocity of the sound concept since these concepts will be used in analyzing the results. Also, the development of the GLV sizing equation utilized in the industry with its limitations.

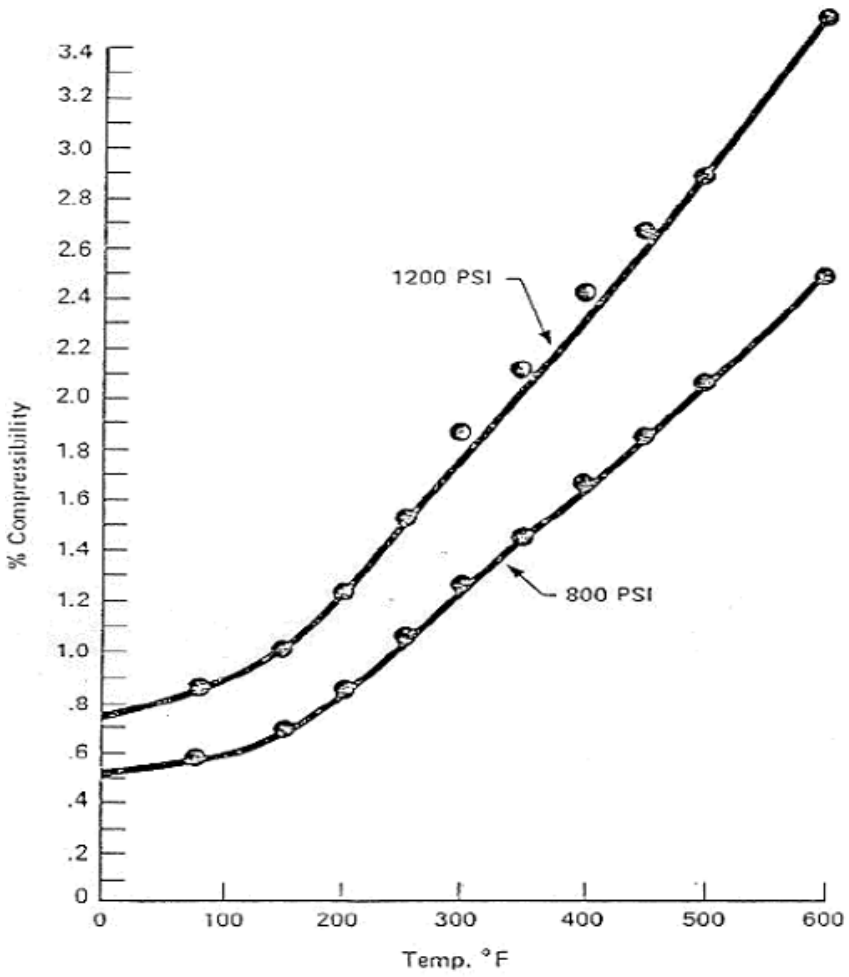

Figure 2.7. Typical silicone compressibility at elevated pressures and temperatures [adapted from Corning (2017)].

2.2.1. *Gas-Lift Valve Performance Curves*

The GLV performance curves are used to select the orifice/port size for GLV under certain pressure and temperature. Since these curves show the injection capacity of a valve as a function of injection pressure, tubing pressure and temperature. The amount of gas injected through a GLV is important for unloading and normal well operations. During the unloading operation, multiple unlading valves are utilized to allow a stepwise operation of fluid displacement from casing and tubing. An adequate amount of gas is necessary to pass through the upper valve to reduce fluid gradient in the tubing. When the tubing gradient is reduced properly, an injection will occur in the consecutively lower valve because of differential pressure between the casing and tubing. If the

amount of gas is not sufficient to achieve design tubing gradient, gas will not pass through the lower valve and the unloading operation may fail (Takacs, 2005). The amount of gas passage is also important for operating valves. As shown previously in Figure 1.5, a small change in the amount of gas injected would induce large changes in the production rate. To generate these GLV performance curves, two methods are available:

1. Experimental dynamic flow test under field pressure and temperature conditions.
2. Theoretical correlations.

Among theoretical correlations, there are five common methods available in the literature to generate the performance curves for the GLVs:

i) VPC correlation (2014)
ii) API Simplified correlation (2010)
iii) Thornhill-Craver equation (1946)
iv) VPC limited correlation (2014)
v) Bertovic equation (1997)

The first three methods will be briefly discussed next.

2.2.1.1. *VPC correlation (2014)*

The VPC correlation utilizes a mechanistic model that utilizes a force balance equation to predict the flow under dynamic conditions within ±20% (Decker, 2014). This correlation can be applied to both orifice and calibrated/live valves. In this correlation, the pressure acting on the stem of the valve is calculated using ISA-575.02 Standard control valve sizing equations to predict the gas flow through the GLV (ANSI/ISA, 1977). This model requires some experimental data for each GLV, such as dynamic flow tests, valve opening pressure at 60 °F (TRO), load rate (A_{bl}), maximum effective stem travel (max. effective d_x), flow coefficient (C_v) and critical pressure ratio (x_T) as a function of stem travel (d_x).

As mentioned previously, the dynamic flow tests are the tests used to generate GL performance curves similar to Figure 1.3. Load rate is a measure of the stiffness of the bellows under a certain pressure which affects the stem movement. Maximum effective stem travel is the maximum travel of a stem before bellow stacking. Flow coefficient is a measure of the flow capacity of a valve. An orifice GLV has a fixed flow capacity for each port size. On the other hand, a calibrated valve has a variable flow coefficient per port size and is estimated as a function of stem travel. Critical pressure ratio (x_T) is the pressure drop required to attain critical (choked) flow. An orifice GLV has a fixed critical flow per port size. Conversely, a calibrated valve has a variable critical pressure ratio per port size and is estimated as a function of stem travel. More about the critical flow is discussed in section 2.2.2. The development of the equation and its limitations will be discussed in detail in section 2.2.3 and 2.2.4.

2.2.1.2. *API Simplified Correlation (2010)*

This method is the latest API recommended practice stated in the API 19G2 RP (2010). It has an accuracy of ±30% for GLVs with port sizes less than or equal 3/16 in, and it presents an overprediction around 50% for ports larger than 3/16 in (Decker, 2014). This correlation requires many data, such as flow coefficient, critical pressure ratio, and load rate. However, the equation used to estimate the flow rate is similar to the equation used in the VPC correlation, and it shares the same assumptions of an ideal gas with isentropic exponent utilized in the expansion factor. The difference between the VPC correlation and API Simplified comes in the procedure of calculating the stem position of the valve using static force equation (Decker, 2014). The VPC uses the dynamic flow tests under high pressure (generating GLV performance curves experimentally) to calculate the stem position under dynamic conditions. On the other hand, The API simplified does not require dynamic flow tests (generating GLV performance curves experimentally) since it uses

the static force equation to calculate the stem position. Therefore, the VPC requires more expensive experimental tests than the API Simplified method but generate more precise flow rate estimates.

2.2.1.3. *Thornhill-Craver Empirical Equation (1946)*

The Thornhill-Craver empirical equation (Equation *2.18*) was originally developed for 6 in long cylindrical shaped surface chokes, with beans opening range between 1/8 and 3/4 in, and it assumes a fully open port, which is not always the case in live/calibrated GLVs. It has been used for decades to estimate the flow rate through GLVs. Moreover, GLV has a different geometry (entrance and exits ports, openings, internal passageway paths and reverse flow check valve as shown in the following Figure 2.8), for this reason, Thornhill-Craver (1946) has a poor accuracy in predicting the performance of IPO/PPO GLVs, where it overpredicts the gas flow rate by 200% in most cases (Decker, 2014).

Figure 2.8. Orifice GLV geometry [adapted from Coutinho (2018)].

The Thornhill-Craver (1946) predicts the flow using the following equation:

$$q_g = 155.5\, C_d A_p P_1 \frac{\sqrt{2g\left(\frac{k'}{k'-1}\right)\left(r^{\frac{2}{k'}} - r^{k'+\frac{1}{k'}}\right)}}{\sqrt{T\gamma_g}} \qquad 2.18$$

where q_g is the gas flow rate, C_d is the valve discharge coefficient, A_p is the seat flowing area (orifice size), P_1 is the upstream pressure, g is the acceleration of gravity, k' is the specific heat ratio of the injected gas, r is the downstream to upstream pressure ratio, γ_g is the gas specific gravity, and T is the upstream-injected gas temperature.

2.2.2. ***Fluid Flow in GLV Orifice and the Velocity of Sound Concept***

In order to illustrate the development of GLV sizing equation effectively, it is needed to illustrate some theoretical concepts related to fluid flow in GLV orifice and velocity of sound.

2.2.2.1. *Fluid Flow in GLV Orifice*

This section will illustrate important concepts related to the fluid flow in GLV orifice. A GLV orifice flow model is used to characterize the flow through GLVs since the flow through the GLV is controlled by an orifice shaped restriction (valve port). As mentioned earlier, a GLV has additional restrictions when compared to an orifice, such as entrance and exit ports, internal passageway paths and reverse check valve. However, the following discussion focuses only on the main flow control component in a GLV, which is the orifice.

Figure 2.9 shows a schematic of a typical GLV orifice (squared-edge orifice) along with the pressure distribution on each location.

As illustrated in Figure 2.9, the flow stream in the orifice is divided into four locations. Location 1 represents the flow at upstream conditions where the injection pressure is measured before entering the orifice (restriction). Location 2 represents the flow at orifice entrance where the diameter (area) is reduced. Location 3 represents the orifice throat or the *vena contracta*, which

is the smallest area in the flow stream. *Vena contracta* typically has a smaller diameter than the orifice diameter, therefore, when the flow stream reaches *vena contracta*, the flow velocity increases to its maximum value (due to the conservation of mass) and the pressure drop reaches its maximum value (due to the conservation of energy). Location 4 represents the flow at downstream conditions (tubing/production pressure in gas-lifted wells).

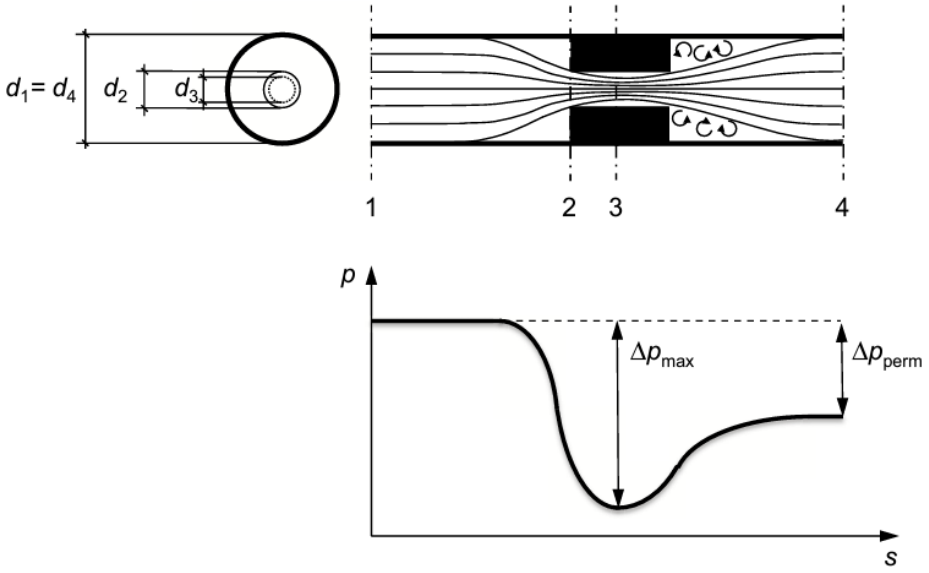

Figure 2.9. Schematic of an orifice with pressure distribution in each section [adapted from Jansen (2017)].

In Location 4, the flow velocity and the pressure drop are decelerated due to area increase (conservation of mass and energy). It is important to mention that the velocity and pressure values are not restored to its original values due to energy losses occurred during the flow through a choke (Driskell, 1983; Jansen, 2017).

The flow in an orifice is divided into two regions, critical and subcritical as shown in Figure 1.3. Subcritical flow region is recognized by an increase in the flow rate as the downstream pressure decreases at a constant injection pressure. This region is shown on the right side of Figure 1.3. Critical flow occurs when the velocity of the flowing fluid reaches the local velocity of sound in the medium and any further reduction in the pressure downstream to the orifice will not increase

the flowrate at a constant injection pressure (Location 1). This region is shown on the left side of Figure 1.3. As mentioned above, the *vena contracta* is the smallest area available for streamflow. Therefore, the critical (choked) flow occurs in the Location 3. To have a better understanding of the critical flow conditions, the following section (2.2.2.2) discusses the factors that affect the velocity of sound in a medium for ideal and real gases.

2.2.2.2. *The Velocity of Sound for Ideal and Real Gases*

Understanding the velocity of sound phenomenon is essential to characterize flow through restrictions because it directly impacts the pressure drop and flow rate at which the critical flow occurs. This section will discuss the effect of different fluid properties in the velocity of sound for real gases.

Pressure disturbances occurring at any point is propagated with a certain velocity. The velocity at which the pressure disturbances propagate is called velocity of sound (c) (Munson et al., 2010). The equation that relates the sound wave propagation in a perfect gas is derived from conservation of mass and momentum equations under the assumption of isentropic process. The final expression is as follows (Munson et al., 2010; Rayleigh et al., 1945):

$$c = \sqrt{k\,R\,T} \tag{2.19}$$

where k is the ideal isentropic exponent, R is the gas constant and T is the temperature.

The isentropic exponent is reduced to the ratio of specific heats under the assumption of an ideal gas. Also, for ideal gases, it is assumed to be a constant value since it depends only on the gas composition (Munson et al., 2010; Streeter, 1969; Wylie et al., 1978). Therefore, the velocity of sound for a perfect gas is a function of absolute temperature only as shown in Equation *2.19*. In real gases, the velocity of sound under the assumption of isentropic process is expressed as follows (Johnson, 1972; Kouremenos et al., 1987; Kouremenos, 1986; Nederstigt, 2017):

$$c = \sqrt{n\,Z\,R\,T} \tag{2.20}$$

where n is the real gas isentropic exponent and Z is the compressibility factor. The variation in the real isentropic exponent (n) at high pressure and temperature would result in significant changes in the velocity of sound estimates (Streeter, 1969). Further discussion about how the real isentropic exponent (n) changes as a function of pressure and temperature is discussed in section 2.2.4.

A study conducted on natural gas to estimate the velocity of sound assuming real gas properties showed that temperature change is more significant than the pressure change, especially at high pressure (Smith et al., 2010).

For example, when using natural gas as a working fluid, a change of 1 °F at 1,000 psi would change the velocity of sound by 2.1 ft/s. On the other hand, a 10 psi change in pressure would cause only 0.1 ft/s changes in the velocity of sound (Smith et al., 2010).

The American Gas Association (AGA) developed a method called the AGA report 10 (2003) to estimate the velocity of sound in natural gas with high accuracy as shown in Figure 2.10 (AGA, 2003). The equations used to estimate the speed of sound and other gas properties such as the real isentropic exponent are very complex and it is best solved by using a computer software (Smith et al., 2010). This is because these equations requires the computation of several partial derivatives as a part of its procedure (Smith et al., 2010). Therefore, the FLOWSOLVE (2017) software will be used to estimate the velocity of sound and the isentropic exponent.

This method accounts for the real gas effects discussed earlier. It can be seen from Figure 2.10 that the estimation of the velocity of sound presents high accuracy (Max. 1% difference). The accuracy of the velocity of sound estimates will be used later during the discussion of how the critical pressure drop and the critical flow would change with fluids exhibiting real gases in the analysis section. Also, it will be used to validate the new suggestions made on GLV sizing equations to account for real gas behavior.

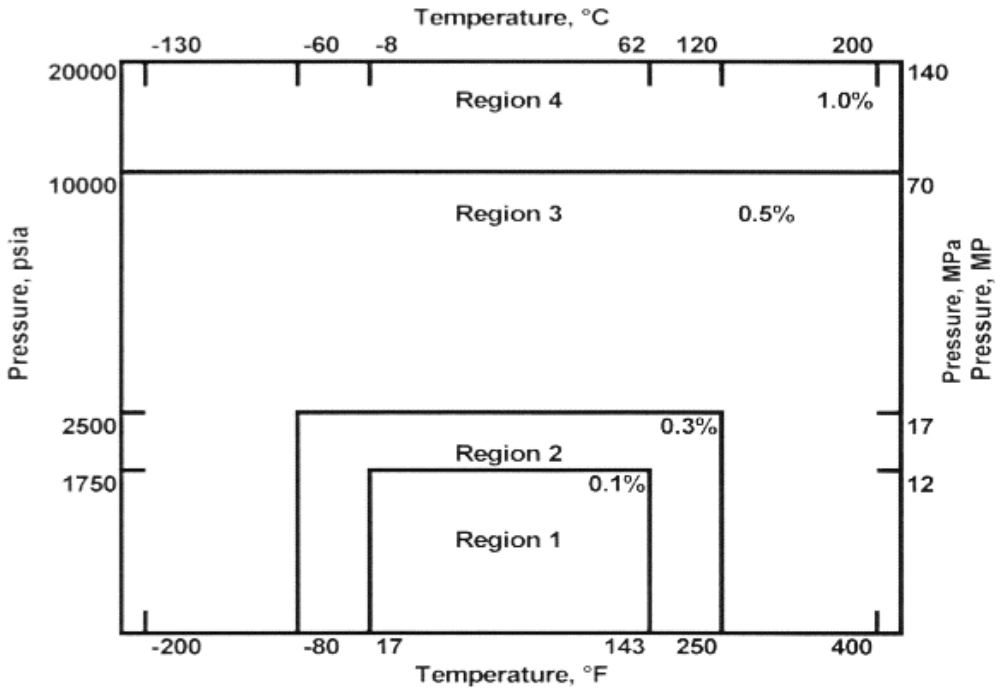

Figure 2.10. Uncertainty of velocity of sound estimation as per AGA report 10 method [adapted from Nasrifar et al (2006)].

2.2.3. ***Development of GLV Sizing Equation***

Since this research focuses on the ISA (1975) equation used in the VPC and API Simplified flow models, it is necessary to illustrate the development of this equation and its assumptions.

Some of the following explanation of the development of valve sizing equation is adopted from Riveland (2012). The ISA equation (used in the VPC and API Simplified) used to estimate the flow through a GLV originates from the equation of flow for incompressible fluids (Equation *2.21*). This equation relates the flow rate (q) with the pressure drop across the restriction (ΔP), specific gravity (γ) and the flow capacity of the valve (C_v) (empirical coefficient determined experimentally) (Driskell, 1983; Riveland, 2012).

$$q = C_v \sqrt{\frac{\Delta P}{\gamma}} \qquad 2.21$$

The basic derivation of Equation *2.21* comes from combining the conservation of mass and conservation of energy equations assuming incompressible isentropic flow. The flow capacity of the valve (C_v) is added to account for many factors including irreversible losses such as (discharge coefficient, C_d), velocity of approach and contraction coefficient (Driskell, 1983).

Two modifications are required to adjust the Equation *2.21* for compressible fluids. The first adjustment is to account for density changes with pressure and temperature. This is done by adding the compressibility factor (Z). The second adjustment is to correct for the gas expansion in the valve throat. When the gas is accelerated through the valve throat (between Locations 2 and 3, Figure 2.9) due to area reduction, its pressure is decreased (conservation of energy). When gas pressure decreases between the inlet (Location 2, Figure 2.9) and throat (Location 3, Figure 2.9), its volume increases and density decreases between these locations, which in turn, decrease the gas flow rate since gas expansion adds resistance to the flow through a restriction (Sines, 2015). To account for this reduction in the flow due to gas expansion, a correction factor has to be introduced. This factor was introduced by Driskell (1969) and is called the expansion factor (Y). The expansion factor for liquids is equal to *one* since the liquids are assumed incompressible, therefore; there is no reduction in the flow due to expansion.

Expansion factor used for ISA (1975) equation was developed based on experimental observation. This observation states that expansion factor attains a linear relationship with the pressure drop ratio across the valve for most valve types within an acceptable tolerance of ±2% (Driskell, 1969). Also, it was proven by differential calculus that the maximum flow for any valve is reached when expansion factor reaches 2/3 (Driskell, 1969). In addition, for each valve, there is an empirical effective maximum pressure drop called the terminal pressure drop ratio (x_T).

Terminal pressure drop ratio is pressure drop ratio (P_2/P_1) at which the critical flow occurs. This pressure ratio has to be determined experimentally since it depends on the valve geometry (Driskell, 1969, 1983; Riveland, 2012). When this limiting pressure is attained, any further reduction in the pressure downstream will not induce an increase in the flow. This phenomenon is known as the critical/choked flow, as discussed earlier.

The linear expression for expansion factor with the pressure drop ratio is derived based on the following conditions (Driskell, 1983):

1- Expansion factor (Y) equals to *one* (incompressible fluid) when the pressure drop ratio (x) equals to *zero*.

2- Expansion factor equals 2/3 when the pressure drop ratio (x) is equal to the terminal pressure drop ratio (x_T).

From the above conditions and using the equation of a straight line, the final expression of the expansion factor is:

$$Y = 1 - \frac{x}{3\,x_T} \qquad 2.22$$

The maximum pressure drop ratio allowed in this equation is limited to the terminal pressure drop ratio (x_T). When the pressure drop ratio (x) is equal to the terminal pressure drop ratio (x_T), Equation *2.22* reduces to $Y = 2/3$, which results in the maximum flow rate across the valve. Equation *2.22* is applicable only for the working fluid used to determine x_T (commonly air). When other fluid is used, a correction factor has to be added to account for the change in fluid properties that affects the terminal pressure drop.

The expansion of gas inside the valve throat is assumed to be isentropic, and therefore, the thermodynamic process from the valve inlet to the throat can be expressed thermodynamically by Equation *2.23*. From Equation *2.23*, it is clear that the isentropic expansion of ideal gas depends

on the ideal isentropic exponent (k). Higher isentropic expansion leads to a greater gas density when the pressure is reduced. Greater gas density means lower expansion, which yields higher flow.

$$Pv^k = constant \tag{2.23}$$

where v is the specific volume and k is the ideal gas isentropic exponent.

Based on experimental work done on nozzles and orifice plates using air and steam with ideal gas isentropic exponents range 1.08 and 1.65 (ASME, 1959; Cunningham, 1951), it was concluded that the following correction factor is applicable with an accuracy of 5% (Driskell, 1969, 1970, 1983):

$$F_k = \frac{k_{gas}}{k_{air}} \tag{2.24}$$

where k_{gas} the ideal gas isentropic exponent of the fluid intended to be used in the GLV (usually natural gas with $k = 1.3$), k_{air} is the ideal gas isentropic exponent for air which is equal to 1.4 under ideal conditions. The final expression of the expansion factor is as follows:

$$Y = 1 - \frac{x}{3\, F_k\, x_T} \tag{2.25}$$

It can be concluded from Equation *2.25* that as the pressure drop ratio (x) increases, the expansion factor decreases. When the expansion factor (Y) decreases, it means that the gas inside the throat expands more, occupying more volume in the throat and reducing its density. Thus, reducing the flow.

Compiling Equation *2.21* with *2.25* and adding the compressibility factor correction, yield the final equation for sizing valves for gas:

$$q_g = 32.64\, C_v\, Y\, P_1 \sqrt{\frac{x}{T\, Z\, \gamma_g}} \qquad 2.26$$

where P_1 is the pressure upstream to the valve (Location 1, Figure 2.9), T is the temperature upstream the valve (Location 1, Figure 2.9), Z is the compressibility factor upstream the valve (Location 1, Figure 2.9) and γ is the gas specific gravity.

Equation *2.26* is used by the ISA and adopted by the VPC and API Simplified in GLV sizing applications (Decker, 2014; ISA, 1975).

2.2.4. *Assumptions and Limitations of GLV Sizing Equations*

The standard practice in using the ISA equation (used in the VPC and API Simplified correlations) is to assume a constant ideal gas isentropic exponent (k) for any condition (pressure and temperature) in which the correlation will be applied.

This assumption is valid under the ideal gas flow, where the pressure does not induce large changes in the gas properties. On the other hand, when the gas is submitted to high pressures and temperatures, the ideal gas assumption is no longer valid, and constant ideal gas isentropic exponent should not be used (Fagerlund, 1988; Riveland, 1992, 2012).

Figure 2.11 shows how the isentropic exponent for natural gas varies with pressure and temperature. Data obtained using the FLOWSOLV software utilizing the AGA report 10 method (AGA, 2003; SOLV, 2017).

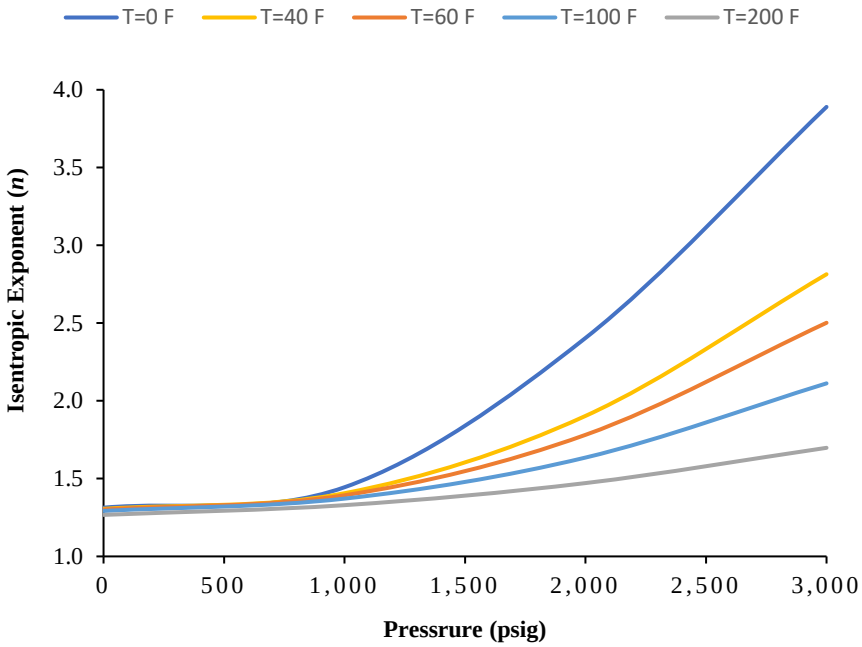

Figure 2.11. Real isentropic exponent (n) for natural gas at elevated pressure and temperature.

Figure 2.11 shows that the real isentropic exponent (n) for natural gas is almost constant (around 1.35) with all temperature ranges from atmospheric pressure until around 800 psig. For pressures above 800 psig, the isentropic exponent increases with the pressure increase. It is also observed that for pressures higher than 800 psig, the lower the temperature, the higher the isentropic exponent. As mentioned above in Equation *2.26*, higher isentropic expansion leads to higher expansion factor (less resistance to flow), and, consequently, increases the flow rate prediction.

Many methods have been developed to account for real isentropic exponents in the valve industry (Buresh et al., 1964; Fagerlund, 1988; Riveland, 1992, 2012).

Fagerlund (1988) suggested using the real isentropic exponent at upstream conditions (Location 1, Figure 2.9) instead of using the ideal isentropic exponent (k). Therefore, the ideal gas isentropic exponent correction factor $F_k = k/1.4$ becomes $F_n = n/1.4$. A similar approach is used in the latest API (2014) recommended practice for sizing pressure reliving valves. This suggestion is

not applied on sizing GLVs. The effect of using the real isentropic exponent for GLVs is shown in section 4.2.1. In addition, the validity of this suggestion is evaluated using the velocity of sound concept in section 4.2.2.

3. Methodology

This chapter is divided into two sections since this research has two main topics. The first section shows the methodology for the accuracy of GLV design set pressure. The second section shows the methodology for the accuracy of GLV sizing equations.

3.1. Methodology for the Accuracy of GLV Design Set Pressure

This section is divided into three parts. The first part shows the experimental setup and procedure used in this research. The second part discusses the three models (N_2, VPC, and the model developed in this study) evaluated in this research for predicting theoretically, the dome/chamber pressure at different conditions. Finally, the third part shows error propagation to the GLV unloading design.

3.1.1. *Experimental Setup and Procedure*

The purpose of this experiment is to investigate the effect of some ignored factors in the current practices that may affect the accuracy of GLV set pressure. These factors are the silicone thermal expansion, silicone compressibility, and dome thermal expansion. In addition, to use the experimental results to evaluate the current and the newly developed model in this research that accounts for these ignored factors.

This section is divided into two parts. The first part shows the experimental setup and the second part shows the experimental procedure used to evaluate the impact of the silicone expansion and silicone/gas volume ratio in the dome pressure.

3.1.1.1. *Experimental Setup*

3.1.1.1.1. Instrumented Chamber

The left-hand side of Figure 3.1 shows typical nitrogen charged IPO valve showing the dome and the bellow locations. In this experiment, GLV dome will be represented with a cylindrical chamber shown on the same figure to the right.

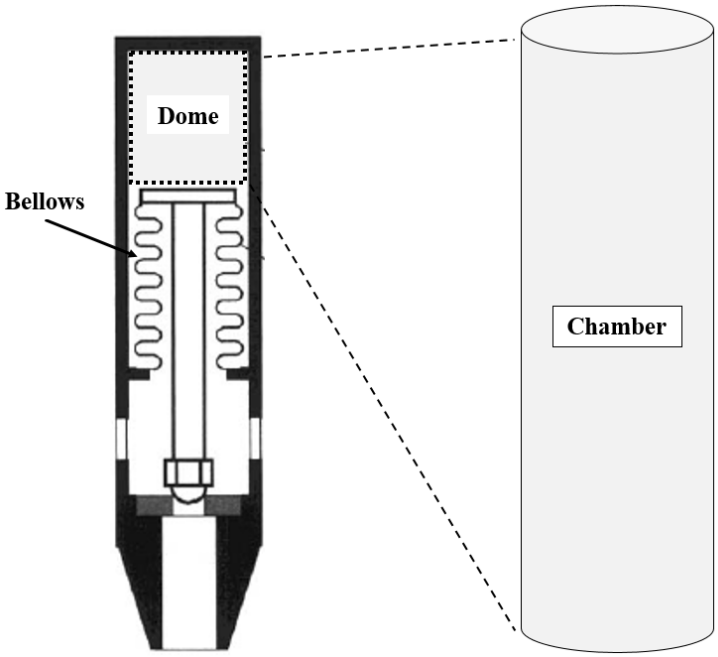

Figure 3.1. Typical IPO valve (left) and IPO valve representation by a chamber (right)[adapted from Takacs (2005)].

Figure 3.2 Shows the physical chamber used in the experiment to represent the GLV dome. It has a volume of 18.3 in^3 and made of stainless steel 316 material. The cylinder has a maximum operating pressure of 1,800 psig at 60 °F and 2,120 psig at 200 °F. The cylinder is connected to pressure, and temperature transducers and the bottom end is connected to a needle valve to allow for charging and sealing the chamber.

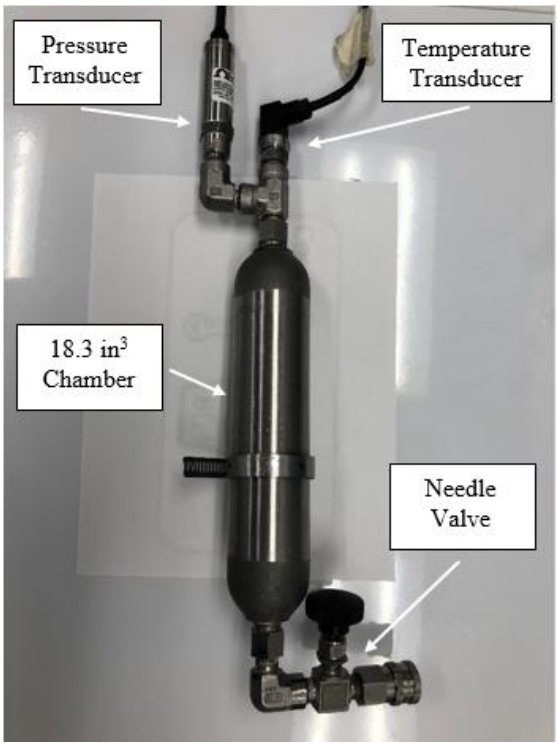

Figure 3.2. The instrumented chamber.

The pressure transducer has a range of 0 to 2,500 psig with NIST calibration and accuracy of 0.05% of full range. The temperature transducer is a class A RTD with an accuracy of 0.56 °F (for the temperature range used in this experiment). The pressure and temperature transducers are connected to a National Instruments® data acquisition system. This system is used to record the experimental data.

3.1.1.1.2. Charging Manifold System

The Charging manifold system is used to charge and discharge the nitrogen safely from the test cylinder. The system is composed of a high pressure nitrogen bottle and a manifold. The nitrogen bottle has a pressure of 2,200 psig filled with 99.99% ultra-purity nitrogen and connected to a pressure regulator and a charging manifold. The charging manifold has four outlets. Two outlets are used for pressure measurement in the system via a master pressure gauge (grade 3A 0.25% accuracy) and a pressure transducer with an accuracy of 0.1% of full scale (0 to 7,500 psig).

One outlet is used for venting/exhausting the gas and equipped with a muffler to mute the gas sound during ventilation for safety. The fourth outlet is used to charge the chamber with nitrogen. Each outlet is equipped with a ball valve for proper system isolation. The following Figure 3.3 shows the charging manifold system.

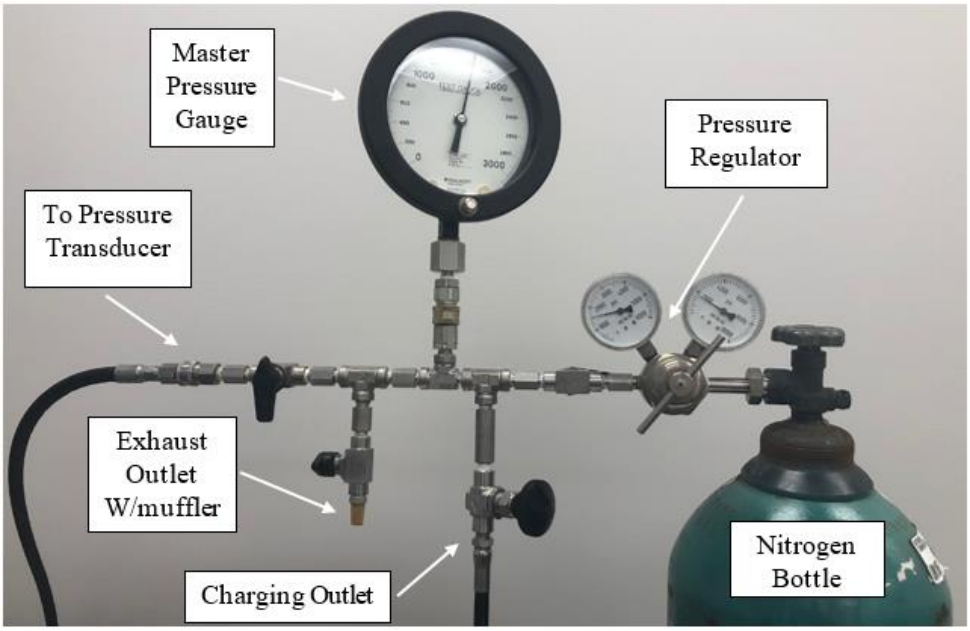

Figure 3.3. The charging manifold system.

3.1.1.1.3. Temperature Controlled Hot Water Bath

The temperature controlled hot water bath is composed by an insulated 2 ft^3 water tank and three 1,500W coil heater. The coil heater is connected to a temperature controller. A water pump is used to circulate the hot water at a flow rate of 0.28 ft^3/min, it is needed to guarantee an even temperature distribution in the hot water bath. The instrumented chamber is held in a stand and submerged in a temperature controlled hot water bath. Figure 3.4 shows a schematic of the main experimental setup.

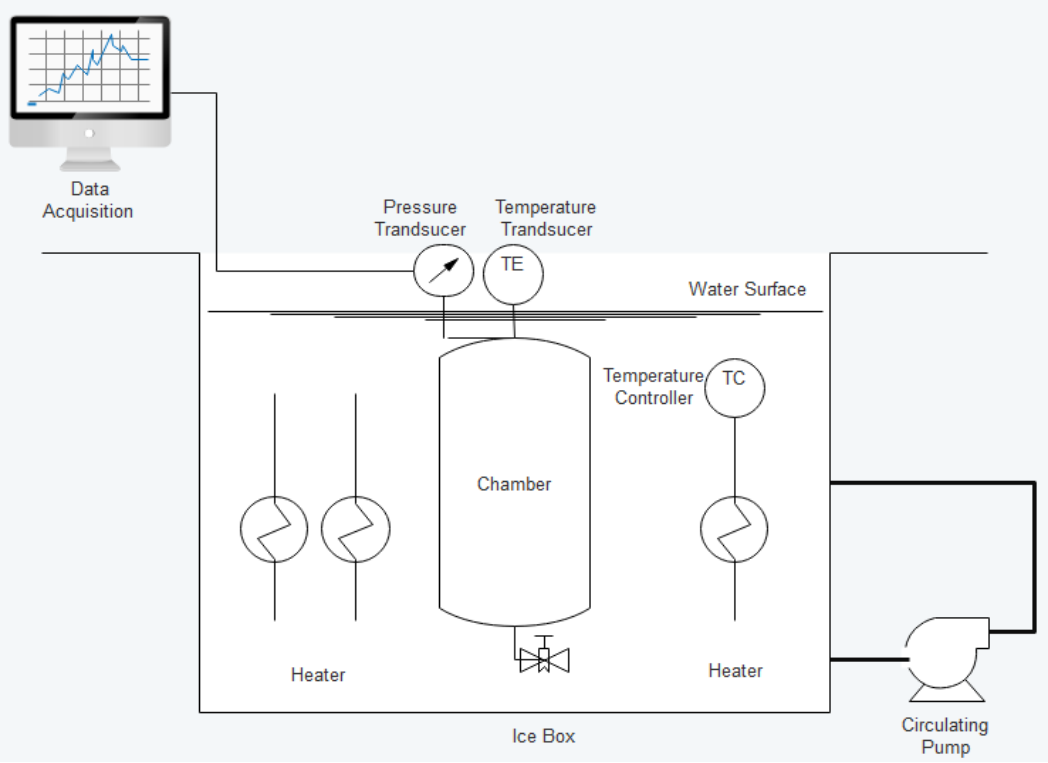

Figure 3.4. Schematic of the complete setup for heating the chamber.

3.1.1.1.4. Measurements Uncertainties

The measurement uncertainty is estimated using the recommended procedures described in the ISO (1998) document (Waltrich, 2012). These procedures are based on the average parameter ($\overline{q}$) and standard deviation (*DP*) calculations as follows:

$$\overline{q} = \frac{1}{n}\sum_{i=1}^{n} q_i \qquad 3.1$$

$$\mathrm{DP} = \sqrt{\frac{\sum(\mathrm{q_i} - \overline{\mathrm{q}})^2}{\mathrm{n} - 1}} \qquad 3.2$$

$$U = k\sqrt{u_o^2 + u_s^2} \qquad 3.3$$

where $\overline{q}$ is the average reading for the parameter needed to be measured (pressure and temperature in this experiment), *n* is the number of measurements taken in the experiment, *k* is the two-sided, Student coefficient for 95% probability and equals to 2, *U* is the expanded uncertainty, u_s is the

uncertainty from measuring device provided by the manufacturer, u_o is the standard uncertainty from experimental measurements.

In this experiment, the standard uncertainty is considered as a time-independent, direct measurement variable and obtained as follows:

$$u_o = \frac{DP}{\sqrt{n}} \qquad 3.4$$

Using the above procedures results in pressure and temperature measurement uncertainties of 2.9 psig and 1.1 °F respectively.

3.1.1.2. *Procedures*

1- Silicone fluid (DC510 500 CS) is used to fill the volume of the chamber to a desired ratio of the total volume. The silicone volume is measured by weighting the silicone container before and after purring the silicone into the chamber. The silicone fluid used in the experiment has a density of 62.4 lb/ft^3.

2- The chamber is charged to the desired pressure at room temperature (typically 70 °F) using the charging manifold system (Figure 3.3).

3- The chamber is submerged in the temperature controlled chilled water bath until it reaches 60 °F.

4- The pressure reading inside the chamber is recorded when the temperature is stabilized at 60 °F using the data acquisition system.

5- The chamber is moved from the chilled water bath and submerged in the temperature controlled hot water bath.

6- The chamber is heated by turning on the coiled heaters to reach the desired temperature, i.e., 100 °F.

7- The pressure reading inside the chamber is recorded when the temperature is stabilized at 100 °F using the data acquisition system.

8- Steps 6 and 7 are repeated, and temperature is measured in steps until a final temperature of 175 °F is achieved.

Experimental pressure results are compared with the pressure results estimated using three different theoretical models (N_2, VPC, and the model developed in this study) that will be discussed in the following section 3.1.2. Also, the experimental results obtained from step 8 are fitted by linear regression. The equations resulted from previous experimental data (fitted by linear regression) gives the final dome pressure (P_2) as a function of initial pressure (P_1) at 60 °F, final temperature (T_2) and silicone fill ratio. These equations are used for the evaluation of error propagation presented in section 3.1.3. Table 3.1 presents the test matrix for the experiments. The total number of experimental points is 78.

Table 3.1. Test matrix.

Initial Pressure @60 °F (*psig*)	Silicone fill (%)	Temperature Steps (°F)
975	0; 7.5; 10; 15; 25; 50 and 75	60; 100; 130; 150 and 175
1,250	0; 25; 50 and 75	60; 100; 130; 150 and 175
1,500	0; 25; 50 and 75	60; 100; 130; 150 and 175

3.1.2. *Development of Models to Estimate GLV Dome Pressure*

A GLV dome is typically charged with a certain pressure (P_1) and temperature (T_1) at the workshop. When the GLV is installed in a well, its pressure and temperature changes (mostly increases). This effect is represented in this experiment by charging the chamber initially with a certain pressure (P_1) and temperature (T_1) and measured chamber volume occupied by nitrogen (V_1) to represent charging the valve at workshop conditions (60 °F). After that, the chamber is heated in a hot water bath, and its the final pressure, temperature, and chamber volume occupied by nitrogen will be presented by (P_2), (T_2) and (V_2).

Since the mass of nitrogen in the chamber/dome is preserved. Therefore, the mass at initial conditions (P_1, T_1, and V_1) equals the mass at finial conditions (P_2, T_2, and V_2).

$$m_1 = m_2 \tag{3.5}$$

Using the real gas law

$$PV = Z\frac{m}{M_W}RT \tag{3.6}$$

Rearranging

$$m = \frac{PVM_W}{ZRT} \tag{3.7}$$

Substituting in Equation *3.5* and rearranging for the pressure at finial conditions results:

$$P_2 = \frac{P_1V_1Z_2T_2}{V_2Z_1T_1} \tag{3.8}$$

Three models are evaluated in this experiment. These models are the nitrogen model (N_2), which represents the current practice, the VPC model and the model developed in this study.

All the models utilize Equation *3.8* in the prediction of final pressure. The only change between these models is in the way of estimating the volume occupied by the nitrogen at final conditions (V_2). The difference between the VPC and the model developed in this study is that this study model includes the silicone compressibility and dome thermal expansion in estimating (V_2).

Figure 3.5 summarizes the process to define the volume (V_2) at final conditions in each model by showing the physical effects included in each model:

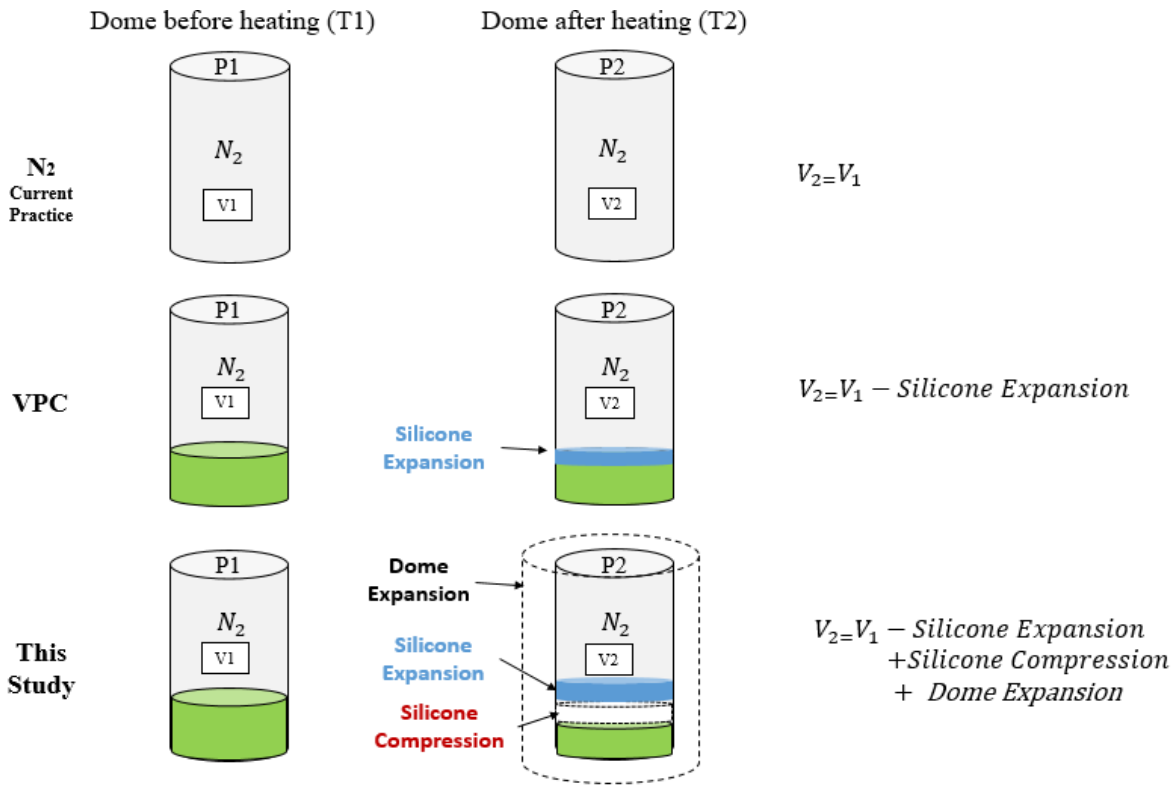

Figure 3.5. Summary of the physical effects included in the models.

The previous Equation *3.8* requires the use of an accurate nitrogen correction. Therefore, Sutton modified DAK (2014) correlation is used for all the models. It is assumed that the current practice and the VPC utilizes the same correlation (Sutton modified DAK) since the VPC manual does not contain this information. Therefore, the results shown in this study may present a better estimate than the actual for the current practice and the VPC models.

Also, Equation *3.8* requires iteration since the compressibility factor at finial condition (Z_2) is a function of final pressure (P_2) needs to be estimated. A VBA code using Sutton modified DAK has been written to perform the iteration and estimate the final pressure (P_2).

3.1.2.1. *Volume Calculations*

This section shows the methods used to estimate the silicone volumetric expansion, chamber volumetric thermal expansion, and silicone volumetric compression.

3.1.2.1.1. Silicone Volumetric Expansion

Silicone volumetric expansion is estimated using the following equation:

$$V_{Silicone\ Expansion} = V_{silicone}\,\beta(T_2 - T_1) \tag{3.9}$$

where $V_{Silicone\ Expansion}$ is the amount of silicone expanded, β is the volumetric thermal expansion coefficient for silicone and equals to 0.000533 $\frac{in^3}{in^3}°F$ (Corning, 2017), $V_{Silicone}$ is the initial amount of silicone in the chamber, T_2 is the temperature at final conditions, T_1 is the temperature at initial conditions and equals to 60 °F.

3.1.2.1.2. Chamber Volumetric Expansion

Chamber volumetric expansion is estimated using the following equation:

$$V_{Chamber\ Expansion} = V_{Chamber}\,\beta(T_2 - T_1) \tag{3.10}$$

where $V_{Chamber\ Expansion}$ is the volume of chamber expanded, β is the volumetric thermal expansion coefficient for the chamber material which is stainless steel 316 and equals to 0.0000267 $\frac{in^3}{in^3}°F$ (Metals, 2001), $V_{Chamber}$ is the initial internal chamber volume, T_2 is the temperature at final conditions, T_1 is the temperature at initial conditions and equals to 60 °F.

3.1.2.1.3. Silicone Volumetric Compression

The silicone volumetric compression is estimated using the following equation:

$$V_{Silicone\ Compession} = \frac{(P_2 - P_1) \times V_{Silicone}}{K} \tag{3.11}$$

where $V_{Silicone\ Compression}$ is the amount of silicone compressed, P_2 is the chamber pressure at final conditions, P_1 is the chamber pressure at initial conditions, $V_{Silicone}$ is the initial silicone volume inside the chamber and K is the bulk modulus of silicone (reciprocal of compressibility).

3.1.2.1.4. Estimation of Silicone Compressibility using Tichy's (1968) Method

As mentioned in the literature review, Tichy (1968) developed a procedure that estimates the compressibility of silicone as a function of its standard state density, pressure and temperature. The standard state density is the density of silicone fluid at 77 °F. The procedure requires the use of multiple figures presented in the paper. Therefore, in order get an accurate estimate using these figures, a digitizer software (Rohatgi, 2010) was used to digitize all the figures in that paper. After that, all the plots are fitted using polynomial equations. These polynomial equations are used to predict any value needed for the experiment. The following steps show how to obtain silicone compressibility using Tichy's method using and polynomial equations obtained from digitized figures presented in that paper (Tichy et al., 1968):

1- Equation *3.12* (obtained from fitting a linear regression curve) shown below is used to obtain the reference density at a needed temperature (*T*).

$$Reference\ Density = -0.0005\,T + 1.0355 \qquad 3.12$$

2- Both reference density obtained from step 1 and temperature selected is used to obtain the isothermal bulk modulus β_{10} from the following equations that can be used to obtain β_{10}. These equations are developed by fitting polynomial regression presented in Tichy's paper (1968). Linear interpolation is used to estimate any unavailable reference density data.

For reference density of 68.67 (lb/ft^3):

$$\beta_{10} = 0.0015T^2 - 0.6951T + 351.45 \qquad 3.13$$

For reference density of 65.55 (lb/ft^3):

$$\beta_{10} = 0.0007T^2 - 0.2898T + 270.56 \qquad 3.14$$

For reference density of 62.43 (lb/ft^3):

$$\beta_{10} = -5 \times 10^{-7}T^3 + 0.0005T^2 - 0.1925T + 215.78 \quad (3.15)$$

For reference density of 59.31 (lb/ft^3):

$$\beta_{10} = -3 \times 10^{-7}T^3 + 0.0005T^2 - 0.2563T + 190.27 \quad (3.16)$$

For reference density of 56.19 (lb/ft^3):

$$\beta_{10} = 0.0005T^2 - 0.3674T + 184.33 \quad (3.17)$$

For reference density of 53.06 (lb/ft^3):

$$\beta_{10} = 0.0005T^2 - 0.405T + 175.19 \quad (3.18)$$

For reference density of 49.94 (lb/ft^3):

$$\beta_{10} = 0.0004T^2 - 0.3647T + 161.08 \quad (3.19)$$

For reference density of 46.82(lb/ft^3):

$$\beta_{10} = 0.0005T^2 - 0.405T + 175.19 \quad (3.20)$$

For reference density of 43.70 (lb/ft^3):

$$\beta_{10} = 0.0005T^2 - 0.4346T + 150.68 \quad (3.21)$$

3- Using β_{10} obtained from step 2 and pressure selected, estimate the isothermal secant bulk modulus β from the following formula:

$$\beta = m(P) \times \beta_{10} + c(P) \quad (3.22)$$

where *m* and *c* are the slope and intercept as per Table 3.2 and *P* is the pressure needed. Linear interpolation is used to estimate the slope and intercept for any pressure not presented in Table 3.2.

Table 3.2. Slopes and intercepts for Equation under different pressures [adopted from Tichy (1968)].

Pressure (*psig*)	m(P), Slope	c(P), Intercept
0	0.8856	-26.63
5,000	0.9394	-13.34

3.1.3. *Error Propagation from N_2, this Study and VPC on Typical IPO GLV Unloading Design*

1- Perform IPO GLV design calculations following the recommended design procedures and well data presented in example # 1 in the API 11V6 recommended practice (1999). The maximum injection pressure used is 1,200 psig, and the injection pressure drop between the valves is 10 psi to ensure closing upper valves. The following Figure 3.6 shows the pressure and temperature survey logs that can be used to represent the tubing flowing pressure and flowing tempertature data for the well used. The following Table 3.3 summarizes the results from this step (1).

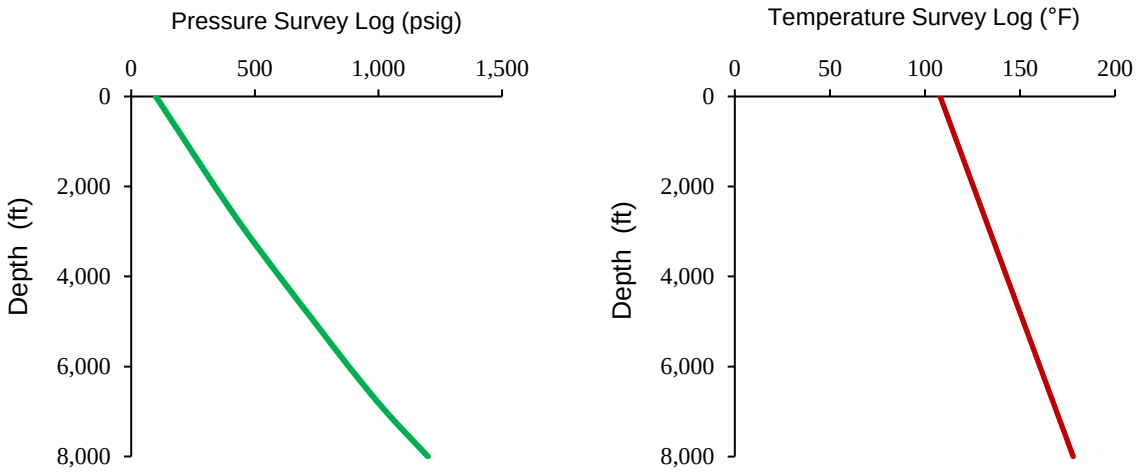

Figure 3.6. Pressure and temperature survey logs for the well used in the design.

Table 3.3. Summary of unloading valve design calculations.

Valve #	Depth (*ft*)	Temperature (°*F*)	Dome Pressure ($P_{2\ design}$) at Depth (psig)	Surface Opening/Injection Pressure (psig)
1	2,483	130	1,192	1,200
2	4,433	147	1,260	1,190
3	5,901	159	1,311	1,180
4	6,967	169	1,346	1,170
5	7,716	175	1,368	1,160

2- Using design dome pressure needed at depth ($P_{2\ design}$) shown in column 4, Table 3.3, estimate the dome pressure at needed at workshop conditions (P_1) and 60 °F using the

current practice, the model developed in this study and the VPC models. The equations used for each model are shown previously in section 3.1.2.

3- Using (P_1) obtained in the previous step (2) and valve temperature at depth shown in column 3, Table 3.3, estimate the experimental dome pressure at depth ($P_{2\ experiment}$) using equations obtained experimentally in section 3.1.1.2.

4- Calculate the valve opening pressure based on the design opening/injection pressure shown in column 5, Table 3.3 using ($P_{2\ experiment}$) and Equation *2.13* for each model and compare.

3.2. Methodology for the Accuracy of GLV Sizing Equations

To evaluate the impact of utilizing the real isentropic exponent instead of the ideal isentropic exponent on GLV sizing equations, the following theoretical methodology is performed.

1 - Generate the GLV performance curves for 24/64 in orifice GLV with a valve flow capacity (Cv) of 3.5 and the terminal pressure drop ratio (x_T) of 0.54. This valve is used as an operating valve and has a large flow rate capacity. Large flow rate capacity valves are used in wells with high production rates. Therefore, the error of gas flow rate estimate and its effect on the production rate that may result due to using ideal isentropic exponent is expected to be large representing worse scenario. The first case assumes an ideal isentropic exponent of (k=1.3) using the GLV sizing Equations *2.25* and *2.26*. This step represents generating the performance curves theoretically using the current recommended practice.

2 - Generate the GLV performance curves assuming real gas isentropic exponent factor using isentropic exponent for natural gas evaluated at upstream conditions (n) represented by location 1 in Figure 2.9 using the Equations *2.25* and *2.26*;

3 - The real natural gas isentropic exponent is estimated using the FLOWSOLV software utilizing the AGA report 10 method (AGA, 2003; SOLV, 2017).

4 - Evaluate the difference in the resultant performance curves generated from the assumption of ideal gas and real gas isentropic expansion factors (step 1 and step 2);

5 - Validate the difference in the performance curves from step 4 results with the velocity of sound concept;

6 - The velocity of sound is estimated at pressure and temperature using FLOWSOLV software utilizing the AGA report 10 method (AGA, 2003; SOLV, 2017).

7 - Repeat steps 1 to 6 using an IPO GLV with 3/16 in port size since this valve is commonly used in the industry to design the unloading operation (API, 1999). This methodology can be applied to any orifice and IPO valves;

4. Results and Discussion

This chapter is divided into two sections since this research has two different main topics. Each section discusses the results for a specific topic. The first topic is the accuracy of GLV design set pressure and the second topic is the accuracy of GLV sizing equations.

4.1. Accuracy of GLV Design Set Pressure

The following subsections show the results related to aspects that may affect the accuracy of GLV set pressure. Section 4.1.1 shows theoretical and experimental results related to the effect of thermal expansion of a GLV dome on its set pressure since this effect is ignored in the current recommended practice. Section 4.1.2 shows a correlation developed using Tichy's (1968) empirical method to account for silicone compressibility for the silicone DC 510 CS 500 used in the experiment. Section 4.1.3 shows experimental results illustrate how the silicone volume ratio in the GLV dome influence the set pressure. Section 4.1.4 shows experimental results to evaluate the accuracy of a GLV set pressure based on the consideration of different volumetric effects mentioned earlier (silicone thermal expansion, silicone compression, and dome thermal expansion) as a function of initial dome charge pressure (P_1). Section 4.1.5 evaluates experimental pressure results ($P_{2\ experiment}$) against different models developed to estimate the GLV set pressure ($P_{2\ model}$). Finally, section 4.1.6 shows the effect of error propagation of different models on typical IPO GLV unloading design following the latest API (1999) recommended practice.

4.1.1. *Effect of Dome Thermal Expansion*

The objective of this analysis is to evaluate the effect of the volumetric increase of GLV dome volume due to thermal expansion. The dome volumetric thermal expansion is ignored by the current recommended practice in designing GLV set pressure. Including this effect may enhance

the accuracy of the GLV set pressure. Figure 4.1 illustrates the effect of volumetric expansion of the chamber (or GLV dome) on the final chamber pressure (P_2). As shown in Figure 4.1, when the chamber is subjected to heat, its volume increases due to the increase of the kinetic energy of its molecules, which in turn, increase the vibration and thus, the space between the molecules, therefore, increasing the total volume.

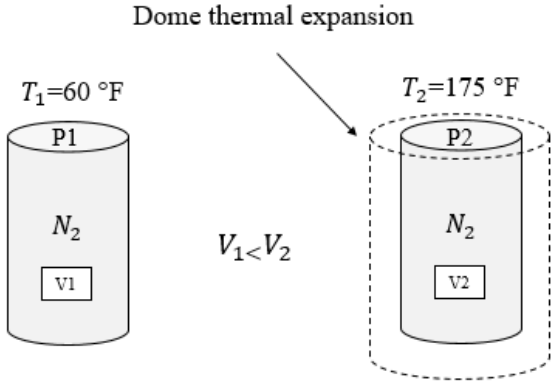

Figure 4.1. Effect of volumetric thermal expansion on the final chamber pressure (P_2).

This work compares final system pressure (P_2) assuming no thermal expansion (constant volume, case 1) and assuming volume change due to thermal expansion (case 2). The thermal expansion due to temperature increase would result in higher chamber volume and, consequently, lower system final pressure (P_2) as per Equation *3.8*:

$$P_2 = \frac{P_1 V_1 Z_2 T_2}{V_2 Z_1 T_1} \qquad 3.8$$

The chamber used in this experiment is made of a stainless steel 316 with volumetric thermal heat expansion coefficient of 0.0000275 $\frac{in^3}{in^3}$°F (Metals, 2001)**.** Figure 4.2 shows the theoretical percentage volumetric thermal expansion with respect to the volume of the chamber at 60 °F versus the temperature developed using Equation *3.8*. The temperature range in Figure 4.2 is from 60 °F to 200 °F since the maximum temperature performed in the experiments is 175 °F.

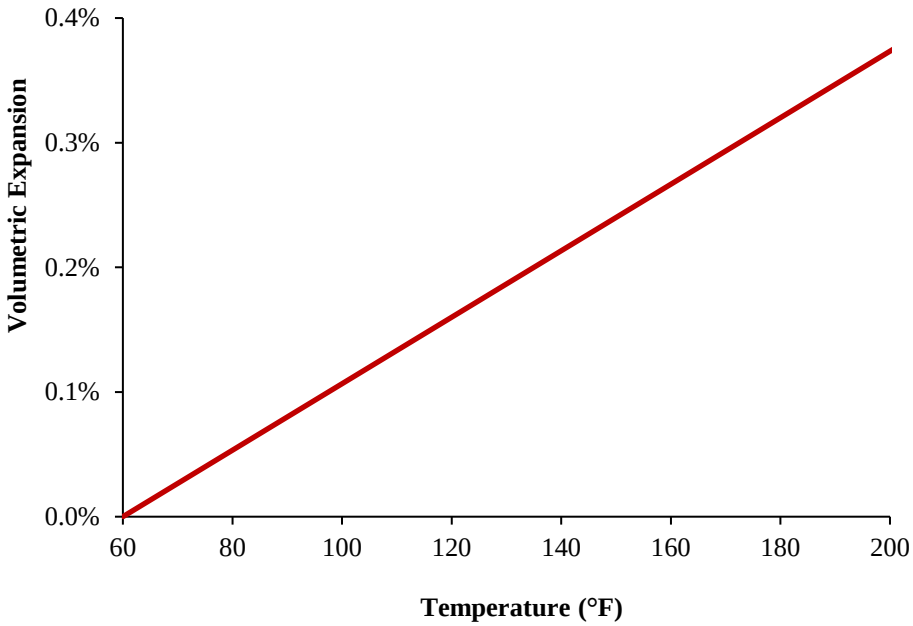

Figure 4.2. Theoretical volumetric thermal expansion for stainless steel 316.

It is seen from Figure 4.2 that the volumetric expansion is a linear function of temperature (until 212 °F). The maximum theoretical volumetric thermal expansion of the chamber during the experiments is 0.31% at 175 °F.

Figure 4.3 present results for the effect of including the volumetric thermal expansion on the final system pressure (P_2) for an initial chamber pressure (P_1) of 1,495 psig, and the maximum temperature (T_2) of 175°F. These pressure and temperature conditions are similar to the range of experimental condition of the upcoming experiments, which includes silicone.

Figure 4.3 compares the experimental pressure results with theoretical pressure results (estimated by Equation *3.8*) neglecting chamber volumetric expansion due to thermal effects ($V_1 = V_2$) and including chamber volumetric changes due to thermal expansion ($V_1 < V_2$).

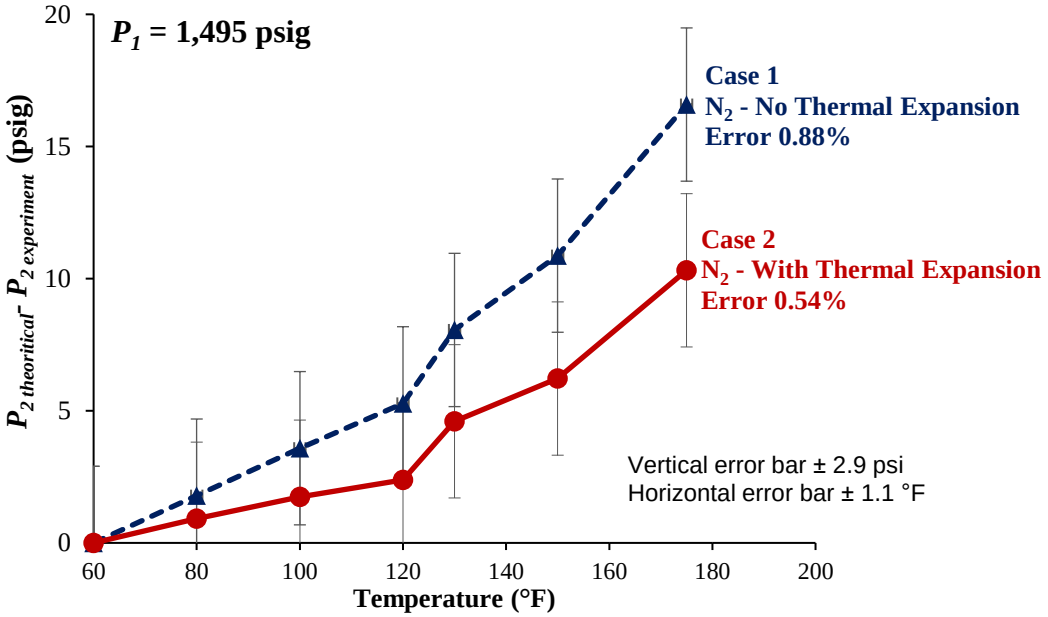

Figure 4.3. Effect of volumetric expansion in reducing the errors at P_1=1,495 psig.

The dashed line in Figure 4.3 represents the difference between the experimental and the theoretical results for the case neglecting volumetric thermal effects (case 1 discussed previously), and the solid line represents the difference between the experimental and the theoretical results including the volumetric thermal expansion effects (case 2 discussed previously). The maximum errors with respect to experimental results for the two cases are labeled in the figure. The vertical error bars represent the uncertainty in the pressure reading while the horizontal bars represent the uncertainty in the temperature reading.

As can be seen from Figure 4.3, the inclusion of the volumetric thermal expansion in the model (case 2) results in the reduction of the maximum error (at 175 °F) from 0.88% to 0.54%. This point is used since the experimental uncertainties in previous points overlap with each other. The difference in error between the two cases models is 0.34%, which agrees with the theoretical volumetric thermal expansion of stainless steel at 175 °F (0.31%) estimated from Figure 4.2.

Another experiment was performed but using a lower initial chamber pressure (P_1) of 1,241 psig. The results are shown in the following Figure 4.4. As shown in Figure 4.4, maximum errors

are reduced from 0.53% to 0.21% when including the volumetric thermal expansion effect at (175 °F). The difference in error between the two cases models is 0.32%, which agrees with the theoretical volumetric thermal expansion of stainless steel (0.31%) estimated from Figure 4.2 at the same temperature. The results presented in both Figure 4.3 and Figure 4.4 show that including the volumetric expansion of dome chamber may enhance the accuracy of GLV design set pressure.

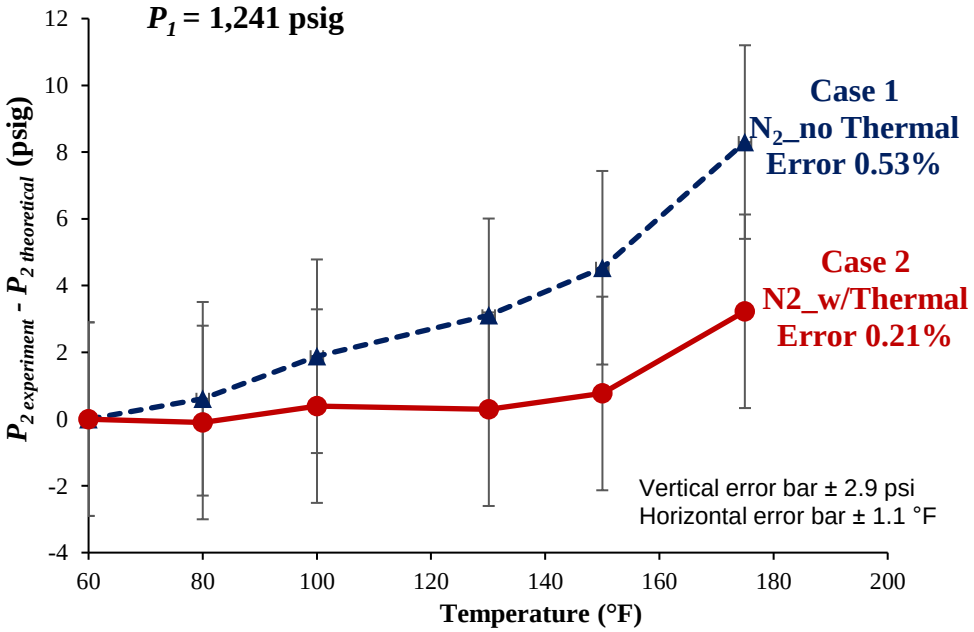

Figure 4.4. Effect of volumetric expansion in reducing the errors at P_1 = 1,241 psig.

It can be seen from Figure 4.3 and Figure 4.4 that as the temperature increases, the effect of thermal expansion in under predicting the final system pressure increases. This effect is expected to further increases after 212 °F, caused by the increase of the volumetric thermal expansion of the stainless steel (Metals, 2001). The maximum excepted pressure reduction due to thermal effects observed in the experiments is 6.7 psig, which occurs at 175 °F and initial chamber pressure (P_1) of 1,495 psig. This is because the higher chamber pressure, the higher the effect of thermal expansion at the same temperature. This effect occurs since initial and final chamber pressures are proportional as per Equation *3.8*. It can be observed that the thermal expansion of the material has more effect at high pressure and temperature applications.

4.1.2. *Effect of Silicone Compressibility*

The silicone fluid used in the experiment is the DC 510 CS 500. Figure 4.5 presents results for silicone compressibility versus pressure using Tichy's method to estimate silicone compressibility for five temperatures. It can be seen from Figure 4.5 that silicone compressibility increases as the pressure and temperature increase. The pressure and temperature range used in this figure cover a wide range of conditions used to set the pressure in a GLV dome (Hernandez, 2016; Winkler et al., 1989). From Figure 4.5, it can be seen that the expected silicone compression under experimental conditions of P=1,981 psig and T=175 °F is 1.42%. These conditions represent the maximum chamber pressure and temperature used in the experiment.

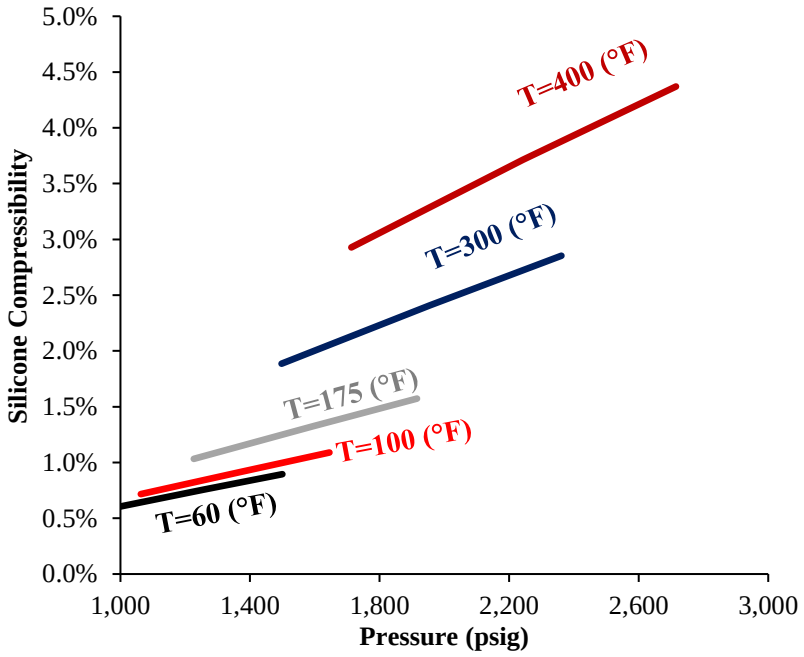

Figure 4.5. Effect of silicone compressibility as a function of pressure and temperature.

The impact of silicone compression will be discussed ignoring all other factors such as silicone thermal expansion and chamber volumetric thermal expansion. When silicone is compressed in

the chamber due to pressure increase (P_2), its final volume is reduced, increasing the chamber volume occupied by the nitrogen (V_2), as shown in Figure 4.6.

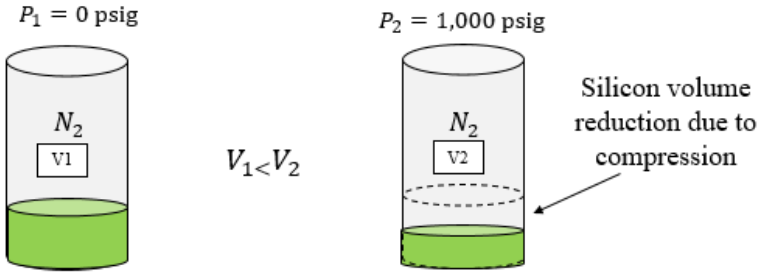

Figure 4.6. Effect of silicone compression on the system final volume (V_2).

If the silicone compressibility is not accounted for the pressure prediction when final volume occupied by nitrogen is increased (V_2), the final chamber pressure (P_2) would be lower than expected.

4.1.3. *Effect of Silicone Volume in the Chamber*

The objective of this analysis is to experimentally evaluate the impact of different silicone volume ratio (silicone volume in the chamber divided by the chamber total volume at standard conditions) in final chamber pressure (P_2) and consequently, GLV dome set pressure. This evaluation helps to understand the importance of having a known volume of silicone in the GLV during its deployment. The experiments evaluate the pressure variation with temperature change in the experimental chamber using different silicone volume ratios of 25, 50 and 75% (silicone fill is shown in Figure 4.7 represented by the green color fill). During the experiments, the temperature is increased in steps from 60 to 175 °F while recording the chamber pressure (P_2). The 25% silicone fill represents a value close to typical silicone fill in a GLV (20%) while 50 and 75% represent possible valve condition after being refurbished.

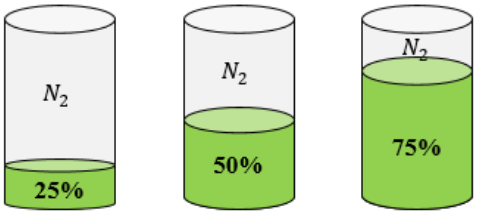

Figure 4.7. (a) Silicone fill 25%, (b) silicone fill 50% and (c) silicone fill 75%.

The typical dome volume for 1 in IPO GLV is 2.7 in^3 and for the 1.5 in IPO GLV it is 5.7 in^3. Because the dome volume of a 1 in valve is 47% lower than for the 1.5 in valve, the same volume of silicone added in the valve dome would result in a much higher silicone volumetric ratio for the 1 in valve. For instance, an addition of 1 in^3 of silicone fluid would increase the silicone fill to 63% for 1 in IPO valve compared to 47% for 1.5 in IPO valve. It can be concluded that adding silicone to a 1 in IPO valve would affect the set pressure more critically than 1.5 in valve.

The theoretical pressure increase due to silicone effect inside the chamber is estimated by calculating the chamber pressure ($P_{2\ theoretical}$) as a function of temperature (T_2) using Equation *3.8* assuming $V_1=V_2$ (which considers nitrogen only and this represents the current recommended practice) and subtracting it from the experimental results ($P_{2\ experiment}$). The experimental results represent the combined effect of silicone presence (mainly expansion), dome thermal expansion and nitrogen. Figure 4.8 shows the experimental pressure increase as a function of silicone fill using initial chamber pressure (P_1) of 1,500 psig. The Y-axis represents the difference in the experimental and theoretical chamber pressure. The X-axis represents the temperature in °F. The vertical error bars represent the uncertainty in the pressure reading while the horizontal bars represent the uncertainty in the temperature reading. The horizontal dashed black line represents the 10 psig error limit that can be tolerated with the GLV design safety factors (API, 1999; Schlumberger, 2000). In addition, Sutton (2014) reported that an error range from 5 to 25 psig

might interfere with normal operations in a well depending upon the application of equipment design.

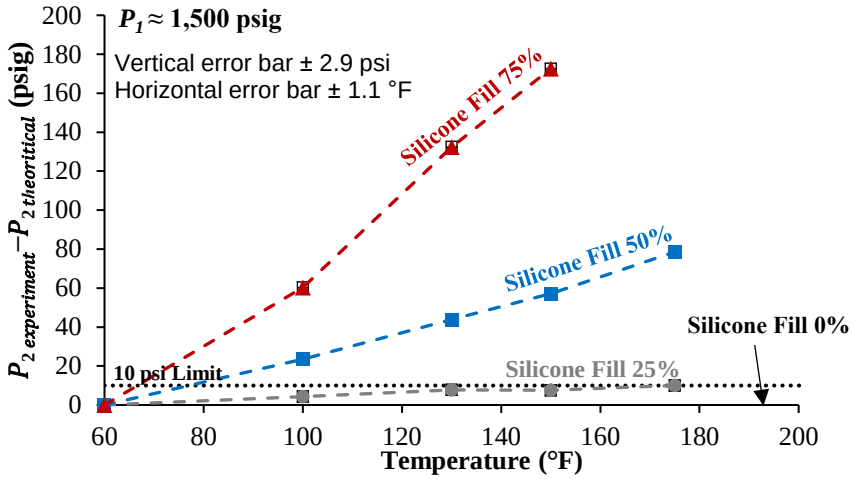

Figure 4.8. Effect of silicone fill in GLV dome pressure at an initial pressure of ≈ 1,500 psig.

Figure 4.8 shows that the presence of silicone in a dome would increase the dome pressure as a function of temperature and silicone fill in all the three silicone volume ratio cases (25, 50 and 75%). It shows that the silicone expansion is the most dominant factor among silicone compression and chamber thermal expansion. Since both silicone compression and chamber volume expansion induce counter effect (increasing of V_2 and thus decreasing P_2) to silicone thermal expansion (decreasing V_2 and thus increasing P_2).

The error effect is lower than 10 psig when the silicone volume ratio is 25%, which is close to the typical silicone volume ratio for new GLV (20%), and it is within the error limits of 10 psig. However, the experiment is limited to a temperature of 175 °F due to equipment limitations. The temperature and pressure in some field applications may reach 350 °F and 3,000 psig respectively (Winkler et al., 1989). This may increase the error more than 10 psig. Expansion factor is typically a linear function of temperature increase. Therefore, at a higher temperature, the expansion of silicone would be higher, occupying a larger amount of the nitrogen volume (reducing V_2) and thus

increase the final chamber pressure (P_2) further, which increases the error due to silicone expansion negligence.

This error is probably would increase further at higher temperature and pressure. Figure 4.9 represents an extrapolation of the experimental results to higher temperatures to investigate potential error at higher temperatures. An extrapolation of the results by linear curve fitting of the experimental results (pressure as Y-axis and temperature and X-axis) with a constant thermal expansion factor for the silicone and chamber. All these factors in addition to silicone compressibility may differ at a higher temperature under real conditions.

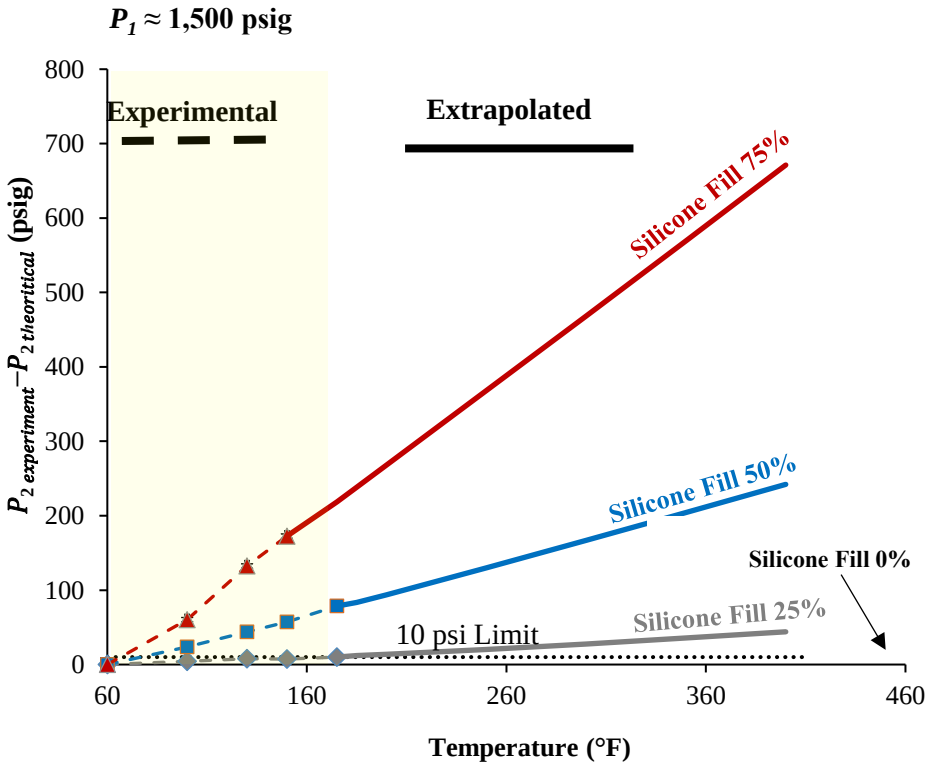

Figure 4.9. Effect of silicone fill in GLV dome pressure at an initial pressure of ≈ 1,500 psig.

Figure 4.9 shows that the pressure error at a temperature of 300 °F and 25% silicone volume ratio is 28 psig and it reaches 44 psig at 400 °F. These errors are significant with respect to the 10 psi safety/design limit. This error increases significantly when using larger silicone fills of 50, and

75% is used since it may reach 167 and 468 psig respectively at a temperature of 300 °F. These error values may lead to serious consequences by failing the unloading operation or lifting at a lower depth.

Figure 4.10 and Figure 4.11 are a repetition of the same experiment but with different initial chamber pressures (P_1) of 1,250 and 975 psig. The effect of the initial chamber pressure (P_1) on the final chamber pressure (P_2) will be discussed on the next section 4.1.4.

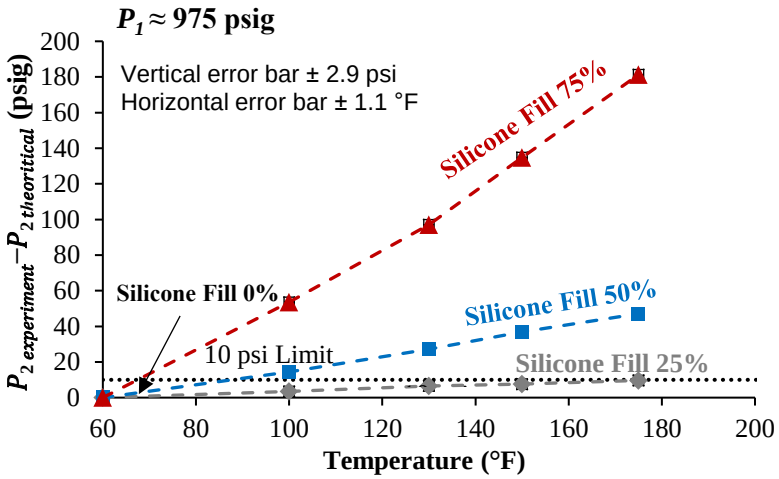

Figure 4.10. Effect of silicone fill in GLV dome pressure at an initial pressure of 975 psig.

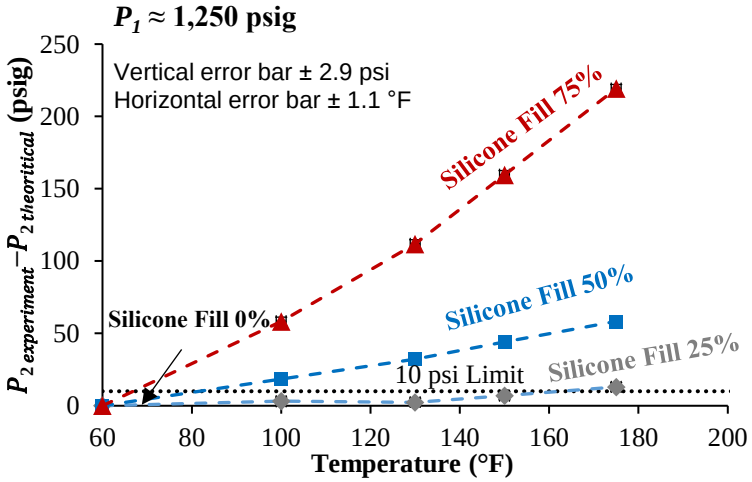

Figure 4.11. Effect of silicone fill in GLV dome pressure at an initial pressure of 1,250 psig.

A similar analysis can be carried in for both Figure 4.10 and Figure 4.11, where it shows that presence of silicone in a chamber would increase the chamber pressure as a function of temperature

and silicone fill in all the three silicone fill cases (25, 50 and 75%). It shows that in all cases, the error limit of 10 psig is reached. Also, it also agrees on the significance of this effect for silicone fills greater than 25%. The initial chamber pressure would affect the pressure increase due to silicone expansion.

The following Figure 4.12 shows experimental results evaluate the pressure variation with temperature change in the experimental chamber using different silicone volume ratios of 7.5, 10, 15 and 25%. The objective of this analysis is to estimate experimentally the threshold silicone ratio at which the silicone effects start to affect the dome pressure (increase) up to 175 °F.

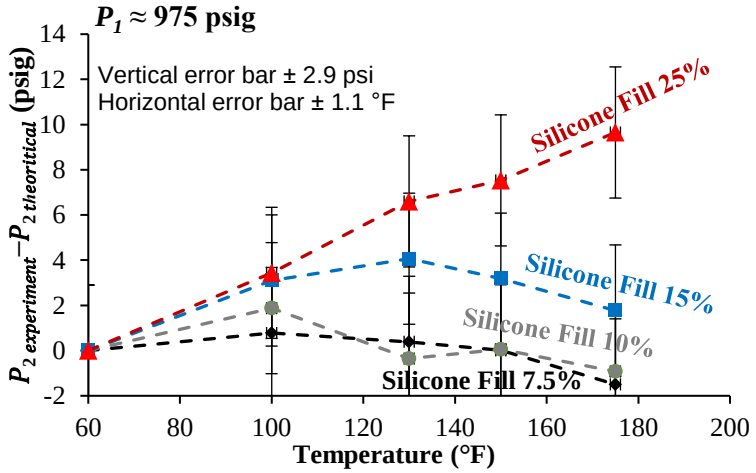

Figure 4.12. Effect of small silicone fill in GLV dome pressure at an initial pressure of ≈ 975 psig.

Figure 4.12 shows that the threshold silicone ratio is not clear for small silicone ratios of 7.5, 10 and 15% since the pressure increase falls within the experimental uncertainty for these cases. However, it can be concluded that all silicone fills (except 25%) start to affect the dome pressure by 4 psig at a temperature of 130 °F and initial pressure of 975 psig. A 4 psi pressure increase falls within the 10 psi safety design margin. Therefore, may not affect the GLV design.

Based on the results presented in this section, it is recommended to measure silicone volume in the GLV dome before the valve deployment in the field. The silicone volume should be

consistent in each valve and included in the design calculations to avoid design failure that may occur especially at high pressure and temperature applications.

The effect of the initial chamber pressure (P_1) increase will be discussed in the next section. Significant errors may occur when using silicone fill of 50% and 75% where the maximum error reached 78 and 218 psig respectively, which vastly exceeds the 10 psig error limit.

4.1.4. *Effect of Initial Dome Pressure*

The objective of this analysis is to experimentally investigate the effect of increasing initial dome/chamber pressure (P_1) on the pressure increase due to silicone presence as a function of temperature (T_2). As mentioned earlier, the current practice utilizes nitrogen correlations or Equation *3.8* to predict the dome pressure as a function of temperature.

Figure 4.13 shows the difference between experimental results ($P_{2\ experiment}$) and the nitrogen correlation results ($P_{2\ theoretical}$) as a function of temperature using three different initial pressures (P_1) of 970; 1,249 and 1,490 psig and a fixed silicone volume ratio of 50%. The maximum typical dome charge is 2,200 psig. However, it may reach 3,000 psig in special applications (Hernandez, 2016; Winkler et al., 1989). The maximum chamber pressure reached in this experiment after heating the chamber is 2,061 psig, which almost covers most of the typical dome charges.

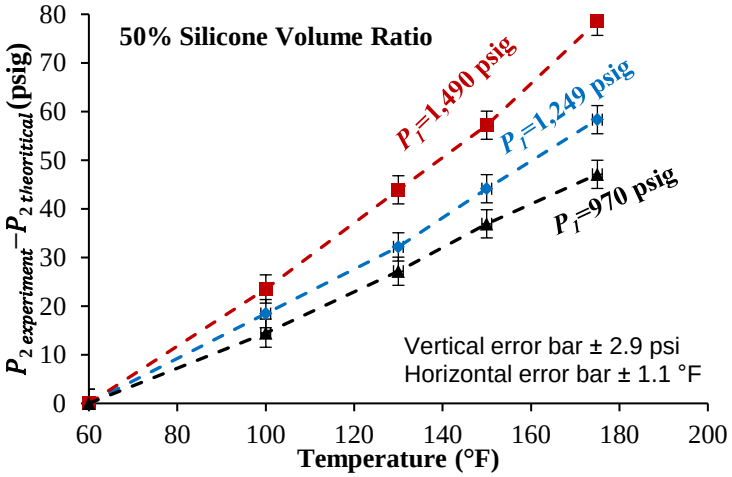

Figure 4.13. Effect of initial dome pressure (P_1) on dome pressure increase due to silicone.

It can be seen from Figure 4.13 that as the initial chamber pressure (P_1) increases, the difference between experimental and theoretical pressures increase due to silicone presence (mainly expansion). The maximum pressure increase occurred at 175°F due to silicone expansion, and it is 79 psig for initial pressure (P_1) of 1,490 psig. At the same temperature of 175°F, silicone effect decreases to 58 psig for the initial pressure (P_1) of 1,249 psig. Finally, the lowest pressure increase due to silicone expansion is 47 psig occurred at the initial pressure (P_1) of 970 psig at the same temperature of 175 °F. This is because the final chamber pressure (P_2) is proportional to the initial chamber pressure (P_1) from Equation *3.8*.

Therefore, the higher the initial chamber pressure (P_1), the higher the deviation from the theoretical chamber set pressure at temperature because of silicone expansion. This highlights the importance of considering the silicone expansion effect at high-pressure applications where the dome pressure exceeds 1,000 psig. The pressure increase due to silicone expansion is significant since most of the pressure increase value is more than 10 psig error/design limit discussed earlier. The effect of the error propagation on GL unloading design will be discussed in section 4.1.6.

The following Figure 4.14 and Figure 4.15 are a replication of the same experiment but using different silicone fill of 75 and 25%. It is shown in Figure 4.14 that as the initial chamber pressure (P_1) increases, the deviation from the expected chamber final pressure (P_2) at temperature increases because of silicone presence (expansion). Comparing the pressure increase due to silicone expansion at 150 °F results in a similar conclusion from the previous Figure 4.13 as follows. The highest pressure difference of 173 psig occurs at the highest initial pressure (P_1) of 1,480 psig. This difference decreased to 160 psig when using moderate initial pressure (P_1) of 1,251 psig. Finally, the lowest pressure difference is 135 psig occurred at the lowest initial pressure of (P_1) 985 psig. The reason of showing this comparison at 150 °F instead of 175 °F is that the

experiment for this case (75% silicone fill and at 175 °F) was not performed due to a limitation in the pressure rating for the chamber.

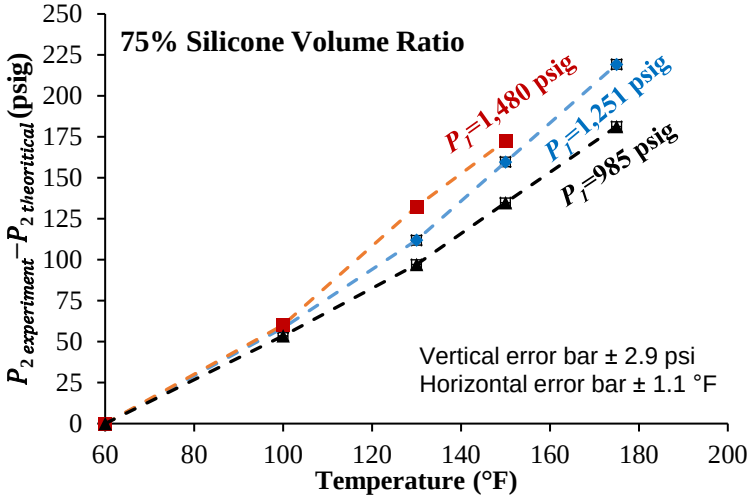

Figure 4.14. Effect of initial chamber pressure (P_I) on dome pressure increase due to silicone effect using 75% silicone fill.

Figure 4.15 does not show clear evidence of chamber pressure effect since the experiment uncertainty for different initial chamber pressure cases (975, 1,256 and 1,500 psig) overlap with the experimental results. This is probably due to a smaller volume of silicone ratio (25%) compared to other cases (50 and 75%). The effect of chamber pressure increase falls within the experimental uncertainty for all the initial pressure cases.

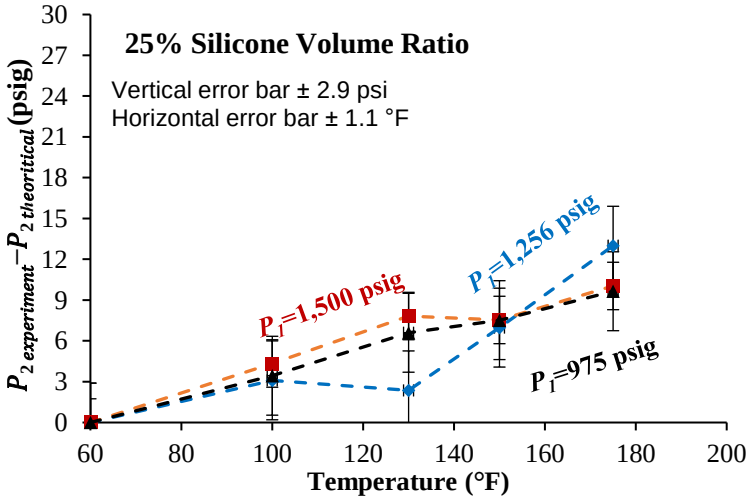

Figure 4.15. Effect of initial chamber pressure (P_I) on chamber pressure increase due to silicone effect using 25% silicone fill.

4.1.5. *Evaluation of the Current Recommended Practice, VPC, and the Model Proposed in this Study*

The objective of this section is to evaluate three different models developed to predict the dome pressure at well conditions compared to experimental results. These models are the current recommended practice nitrogen model (N_2), the VPC model, which is used exclusively in the VPC software, and the author's model. The outcomes of this evaluation would help in determining which model is better predicts the GLV dome pressure, which in turn helps in providing a better GLV design reducing design errors that may fail GLV operations such as unloading.

The current recommended practice utilizes nitrogen correlations to estimate the nitrogen pressure inside the dome as a function of temperature. Several nitrogen correlations are available as discussed in the literature review. Sutton modified DAK correlation (2014) is used in the evaluation and assumed to represent the current recommended practice since it has an accurate estimate compared to other nitrogen correlations and equations. As mentioned earlier, the current recommended practice ignores the effect of silicone presence in the dome (which means ignoring silicone expansion and silicone compression) and thermal dome expansion. In this analysis, the current recommended practice will be referred to as the nitrogen model N_2.

The VPC model utilizes a nitrogen correlation (unknown nitrogen correlation with unknown accuracy since it is not cited in the software manual) and includes the silicone expansion effect. In this evaluation, VPC is assumed to use Sutton modified DAK (2014) equation. The model developed in this study includes in addition to VPC, the silicone compressibility, and dome thermal expansion.

Figure 4.16 shows the experimental pressure difference in the chamber pressure using the N_2 model, the VPC model and the model developed in this study as a function of temperature. In this case, the silicone volume ratio is 25% of the chamber volume, which almost equals the typical

silicone fill in a new GLV (20%). The initial chamber pressure (P_1) is 975 psig at 60 °F (T_1). The vertical error bars represent the uncertainty in the pressure reading while the horizontal bars represent the uncertainty in the temperature reading. The maximum error with respect to experimental results for each model is shown.

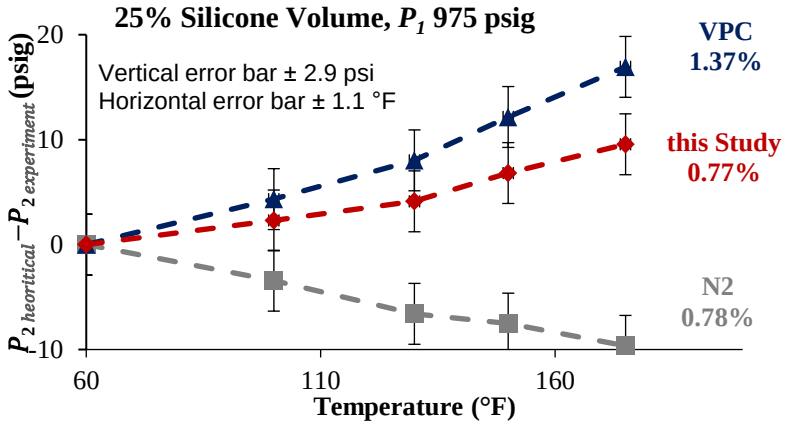

Figure 4.16. Models evaluation using P_1 of 975 psig and silicone fill of 25%.

As can be seen in Figure 4.16, as the temperature increases, the errors coming from silicone presence in the chamber increase since all the models keep diverting apart from the experimental results. The model developed in this study provided a slightly better error percentage compared to N_2 model at a temperature of 175 °F but in the opposite direction. The N_2 underpredicts the experimental results by 0.78% while the model developed in this study overpredicts it by 0.77%. On the other hand, the VPC model provided the highest error among other models by overpredicting the pressure by 1.37%. The N_2 model underpredicts the results probably because it does not include the silicone expansion effect (silicone compressibility and thermal chamber expansion have a lower effect than the silicone expansion as discussed previously). The VPC model overpredicts the pressure more than the model developed in this study probably because it does not include the effect of silicone compressibility and chamber thermal expansion.

It is shown in Figure 4.16 that the effect of silicone expansion is greater than the effect of silicone compression and thermal chamber expansion combined. Since if, the silicone compression and chamber thermal expansion effects are greater than the silicone expansion effect, the experimental results should be equal to or lower than the N_2 model. One possibility of why the model developed in this study overpredicts the experimental results is due to the accuracy of the silicone thermal expansion factor since it is not provided as a afunction of pressure and temperature and assumed constant under any pressure and temperature. In addition, compressibility estimates may involve errors coming from digitizing the data and estimating values using multiple interpolations. Furthermore, nitrogen correlations accuracy and the impurities in the chamber since the chamber is initially contained air at 14.7 psia. Also, the effect of nitrogen solubility may affect this model since this effect is ignored. The experimental uncertainty is large compared to the differences in the Y-axis. Therefore, other cases will be discussed, which have relatively, lower differences between the experimental uncertainty and the models. The same experiment is repeated but with different silicone fill and initial chamber pressure (P_1). In this case, the silicone ratio occupies 50% of the chamber volume, which is considered to represent silicone fill in a refurbished GLV. The initial chamber pressure (P_1) is 1,490 psig at 60 °F (T_1).

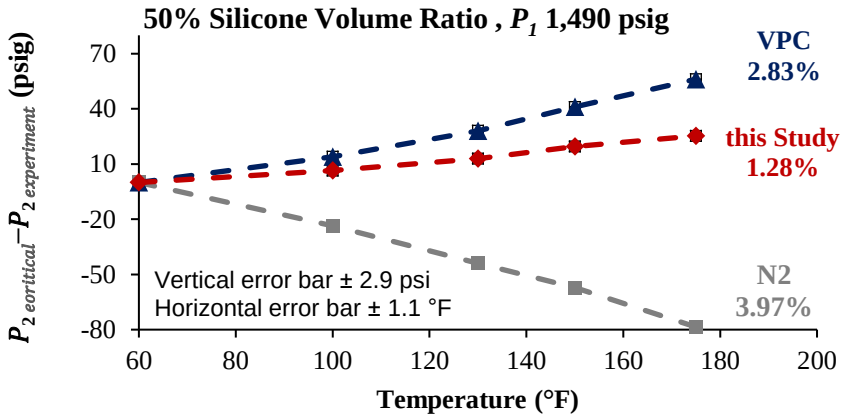

Figure 4.17. The Experimental difference in chamber pressure in three models at P_1 of 1,490 psig and 50% silicone fill.

It can be seen from Figure 4.17 that the best model representing the experiment at a temperature of 175 °F is the model developed in this study where the maximum error is 1.28% (overpredicting), which is significantly better than the N_2 model where the error reached 3.97% (underpredicting) probably because of the following. In this experiment, the silicone fill and initial pressure (P_1) are significantly higher than the previous experiment (P_1= 975 psig compared to 1,490 psig and 25% silicone compared to 50% silicone).

As concluded earlier, the higher the initial chamber pressure (P_1) and the silicone fill percentage, the higher the difference between the N_2 model and experimental results due to silicone effects. The VPC model provided a maximum error of 2.83% (overpredicting) which is higher than the previous experiment where the maximum error was 1.37% (overpredicting). This is probably because of the higher initial chamber pressure (P_1) and silicone fill percentage. The higher the initial pressure (P_1), the higher the silicone compressibility. In addition, the larger the silicone fill, the larger the amount of silicone compressed. Since the VPC does not include the silicone compressibility, it is expected that the VPC error would increase with pressure and silicone fill increase.

The maximum error by the model developed in this study is 25 psig compared to -79 psig by the N_2 and 56 psig by the VPC. This error range exceeds the 10 psig safety/design limit by the industry which necessities the need to increase the safety factors while designing a refurbished GLV or to set a procedure prohibiting/limiting adding silicone during GLV refurbishment since the errors provided may exceed the safety/design limits significantly. As mentioned earlier, many reasons may lead to error increase in the model developed in this study such as the accuracy of silicone compressibility charts, the linear assumption of silicone thermal expansion since the

differences between the experimental results keep increasing with temperature and pressure increase, impurities in the chamber, and accuracy of stainless steel expansion factor.

Figure 4.18 represents an extreme case where the silicone fill is 75%. This case may be rare to reach since it needs adding a significant amount of silicone. However, it may occur if the GLV is refurbished multiple times especially with 1 in IPO valves where the dome volume is small (2.7 in^3). This case shows how significant can the dome set pressure deviate from the expected design set pressure at large silicone fills.

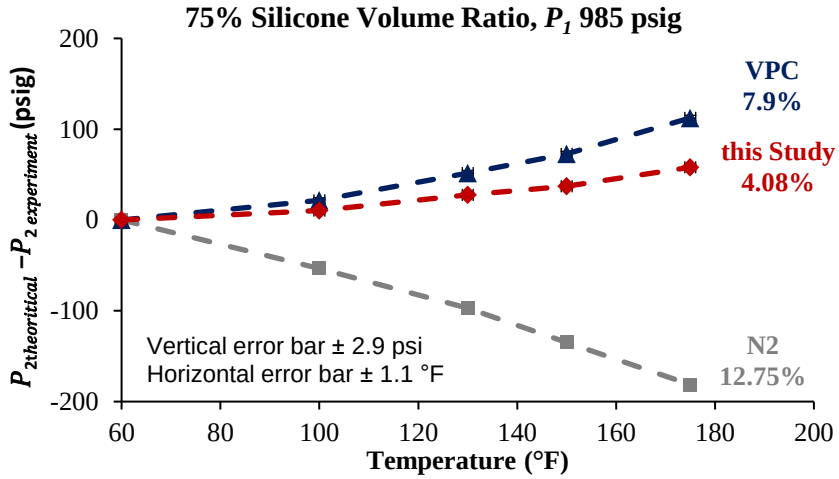

Figure 4.18. The experimental difference in chamber pressure using three models at an initial chamber pressure of 985 psig and 75% silicone fill.

It can be seen from Figure 4.18 that the best model representing the experiment at a temperature of 175 °F is the model developed in this study where the maximum error is 4.08% (overpredicting) followed by the VPC with an error of 7.9% (overpredicting). On the other hand, the worst model representing the experiment is the N_2 model where the error is 12.75% (underpredicting). The probable reason for error increase for the N_2 model is increasing the silicone fill. As mentioned earlier, the higher the silicone fill percentage, the higher the difference between the N_2 model and experimental results due to silicone effects. Larger silicone fills induce larger

changes in the final volume (V_2) as the temperature increases due to expansion and compression, which in turn affect the results significantly.

The VPC model has an error of 7.9% (overprediction) which is higher than the previous experiment where the maximum error was 2.83% (overprediction). This is probably due to silicone fill percentage. The larger the silicone volume ratio, the larger the amount of silicone compressed. Since the VPC does not include the silicone compressibility, it is expected that the VPC error would increase with pressure and silicone fill increase.

The error in the model developed in this study increased from 1.28% (Figure 4.17) to 4.08% (Figure 4.18) probably due to errors in the silicone expansion and compression estimates since it is increased by increasing the silicone amount. Comparing the errors in psig, the model developed in this study error has an error of 58 psig compared to -181 and 112 psig by the N_2 and VPC respectively. These errors are serious and most probably may fail the GLV design since it is larger than the minimum recommended safety factor (10 psig). This experiment confirms the significance of prohibiting adding silicone during the refurbishment processes. Table 4.1 summarizes the maximum error for all the experimental results for nine experiments done using different initial pressures (P_1) and silicone fill. Comparing the model developed in this study, N_2 and VPC models with experimental results, the model developed in this study provided the lowest absolute error in most cases. The average maximum error presented in Table 4.1 for the model developed in this study for all the experiments is 2.21% (overpredicting) followed by the VPC 4.23% (overpredicting) and the N_2 5.22% (underpredicting). In summary, the model developed in this study provided the best results followed by the VPC while the N_2 which represents the current practice provided the least accurate results.

Table 4.1. Summary of all experimental results evaluating three models.

P_1 (*psig*)	Silicone volume fraction (%)	N_2		VPC		This Study	
		$P_{difference}$ (*psig*)	Max. Error (%)	$P_{difference}$ (*psig*)	Max. Error (%)	$P_{difference}$ (*psig*)	Max. Error (%)
≈975	25	-10	-0.78	17	1.37	9.73	0.77
	50	-47	-3.72	36	2.83	20	1.61
	75	-181	-12.75	112	7.90	58	4.08
≈1,250	25	-13	-0.81	22	1.38	12	0.73
	50	-58	-3.55	49	2.95	26	1.55
	75	-219	-12.13	166	9.17	84	4.64
≈1,500	25	-10	-0.52	33	1.72	19	1.01
	50	-79	-3.97	56	2.83	25	1.28
	75	-173	-8.75	156	7.91	85	4.29

4.1.6. *Effect of Error Propagation of the N_2, this study and VPC on GLV Unloading Design*

The objective of this section is to evaluate the impact of utilizing the current practice (N_2) model, the model developed in this study and VPC model on a typical IPO GLV unloading design using various valve silicone fills and safety factors. Also, to suggest improvements on the design practices for IPO valves based on the outcomes from these case studies. The first case (base case) represents unloading design for new valves (25% silicone fill) utilizing the suggested minimum recommended 10 psi decrease in injection pressure between each valve as a safety factor to ensure valve closing for upper valves (API, 1999; Schlumberger, 2000). The second case is a repetition to the first case except that an additional drop in injection pressure (20 psi instead of 10 psi) is used as a safety factor. The third case represents unloading design for refurbished valves with consistent silicone fills (50%) for all the valves utilizing a 20 psi reduction in injection pressure between valves as a safety factor. The fourth case represents unloading design for a well utilizing new unloading valves (25% silicone fill) except the fifth unloading valve, which is a refurbished valve with 50% silicone fill. The following Table 4.2 shows a summary of the cases discussed above.

Table 4.2. Summary of all unloading design cases.

Case #	Silicone Fill	Safety Factor (*psi*)
1	25%	10
2		20
3	50%	20
4	25 and 50%	10

As mentioned in the methodology section 3.1.3, a linear regression is used on the experimental data obtained with silicone fill of 25% (represents new GLVs) and 50% (represents refurbished valves) to predict the real dome pressure at well conditions (P_2) and thus, the expected valve opening pressure (with its associated errors) for each model.

4.1.6.1. *Case 1: Unloading Using New GLVs (25% Silicone Fill) and 10 psi Safety Factor*

Before showing the results of this case, it is important to clarify two important definitions that will be used in analysing the results. These definitions are the valve surface opening pressure under valve uncovering conditions (P_{voU}) and valve flowing conditions (P_{voF}). Valve surface opening pressure under uncovering conditions occurs during unloading when the tubing is filled with kill fluid as shown in Figure 4.19 (a). Therefore, the pressure acting on the valve port (from the tubing side) is because of the kill fluid hydrostatic column. On the other hand, when the well is under flowing conditions, the pressure acting on the valve port (from tubing side) is the flowing tubing pressure (fluid gradient after gas injection) as shown in Figure 4.19 (b). Typically, the hydrostatic column from the kill fluid results in a higher pressure acting on the valve port compared to the pressure resulted from flowing gradient. Which results in a lower valve opening pressure under uncovering condition compared to opening pressure under the flowing condition as per Equation *2.13*. Figure 4.19 shows an example comparing the valve surface opening pressures under uncovering (1,117 psig) and flowing conditions (1,206 psig) for the first valve utilizing well conditions in case # 1. Only one valve is shown in Figure 4.19 for simplicity.

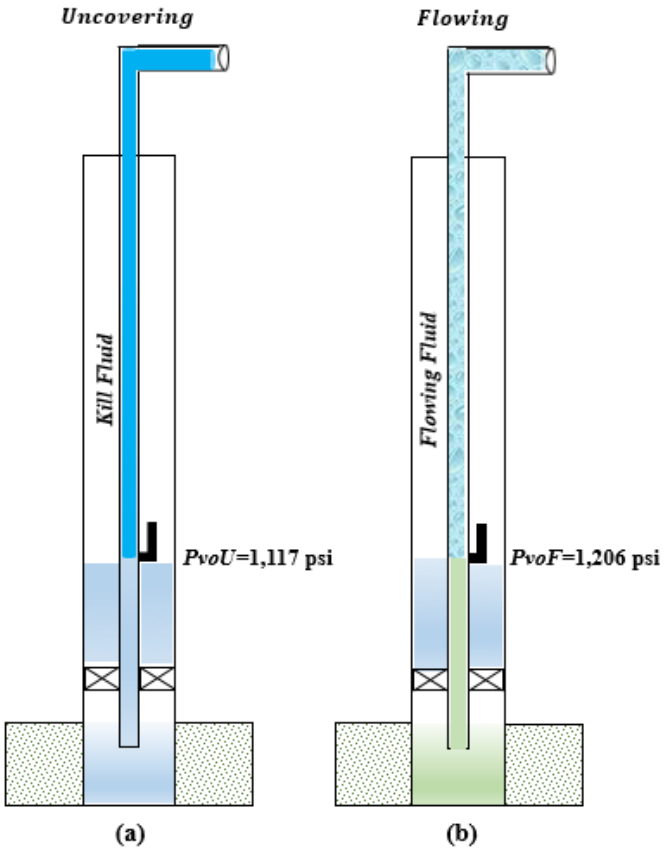

Figure 4.19. Difference between uncovering and flowing conditions.

The following Table 4.3 shows a summary of unloading design results using three different models for the first case (base case).

Table 4.3. Summary of unloading valve design calculations for case # 1 (base case).

Valve #	T_v (°F)	D_v (ft)	P_{inj} (psig)	N_2 Opening (psig)		This study Opening (psig)		VPC Opening (psig)	
				Uncovering	Flowing	Uncovering	Flowing	Uncovering	Flowing
1	130	2,483	1,200	1,117	1,206	1,110	1,200	1,100	1,189
2	147	4,433	1,190	1,131	1,198	1,120	1,188	1,108	1,176
3	159	5,901	1,180	1,141	1,190	1,127	1,177	1,114	1,163
4	169	6,967	1,170	1,146	1,181	1,131	1,165	1,116	1,151
5	175	7,716	1,160	1,148	1,172	1,131	1,155	1,115	1,139

Table 4.3 shows the design surface injection pressure (P_{inj}) for each valve at valve depth (D_v) and temperature (T_v). In addition, it shows the valve surface opening pressure for each model under valve uncovering conditions (P_{voU}) and valve flowing conditions (P_{voF}).

As mentioned in the methodology section 3.1.3, the well data and design procedures follow example # 1 in the API 11V6 recommended practice (1999) with a maximum surface compressor injection pressure of 1,200 psig. When following these procedures, the valve should open at its specified design injection pressure (P_{inj}) under well flowing conditions. However, due to the errors associated with each model (N_2, VPC, and this study), the valve would not open at the exact specified injection pressure.

The valve opening pressure would be either higher or lower than expected opening pressure depending on the model used. For example, the surface opening pressure for the first valve under flowing conditions should equal to the surface injection pressure of 1,200 psig. However, when using the N_2 model for this example, the N_2 model tends to overpredict the opening pressure and therefore, the opening pressure would be 1,206 psig instead of 1,200 psig.

Conversely, when utilizing the VPC model, the model tends to underpredict the valve surface opening pressure and therefore, the opening pressure would be 1,189 psig instead of 1,200 psig. The N_2 model tends to overpredict the opening pressure because it does not include all the physics affecting dome pressure (mainly silicone expansion).

As concluded in section 4.1.3, silicone provides an additional pressure contributing in the chamber as it expands with temperature. During the design stage, the final dome pressure (P_2) at valve temperature is provided to the designer and the initial dome pressure (P_1) in workshop conditions is need to be estimated. Part of the final dome pressure (P_2) is coming from silicone expansion.

When this effect is ignored in the N_2 model, the initial dome pressure (P_1) is overpredicted. When the initial dome pressure (P_1) is overpredicted, the dome is charged with additional amount of gas in the workshop. Thus, the final dome pressure is also overpredicted. An overpredicted

dome pressure (P_2) provides additional closing force to the valve as per Equation 2.13. Therefore, higher than the anticipated valve opening pressure. Conversely, the VPC model tends to underpredict the opening pressure since it does not account for silicone compression and dome thermal expansion, therefore, underpredicting the initial dome pressure (P_1). Which in turn, underpredicts the final dome pressure (P_2) and therefore, provides a lower closing force as per Equation 2.13 which results in a lower valve opening pressure.

The following Figure 4.20 shows a well schematic during unloading operation with the status of each valve during unloading operation for the results presented in Table 4.3 (case 1).

Unloading starts with gas injection in the casing displacing the kill fluid through open valves toward tubing until gas reaches valve # 1. Under this condition, the tubing is filled with kill fluid. Therefore, the valve surface opening pressure under uncovering conditions when utilizing the N_2, VPC and the model developed in this study is 1,117, 1,100 and 1,110 psig respectively, which successfully opens the first valve since the surface injection pressure at this stage is 1,200 psig as shown in Figure 4.20 (a).

Figure 4.20 (a) shows similar successful results would occur for valve # 2 since all the models result in surface valve opening pressure of 1,131, 1,108 and 1,120 psig (under uncovering conditions), which is lower than the current design surface injection pressure of 1,190 psig (the surface injection pressure is decreased from 1,200 psi to 1,190 psi for valve # 2 as a safety factor to ensure upper valve closure since the design opening pressure for the upper valve is 1,200 psig). Therefore, valve # 2 is open and unloading proceeds toward valve # 3.

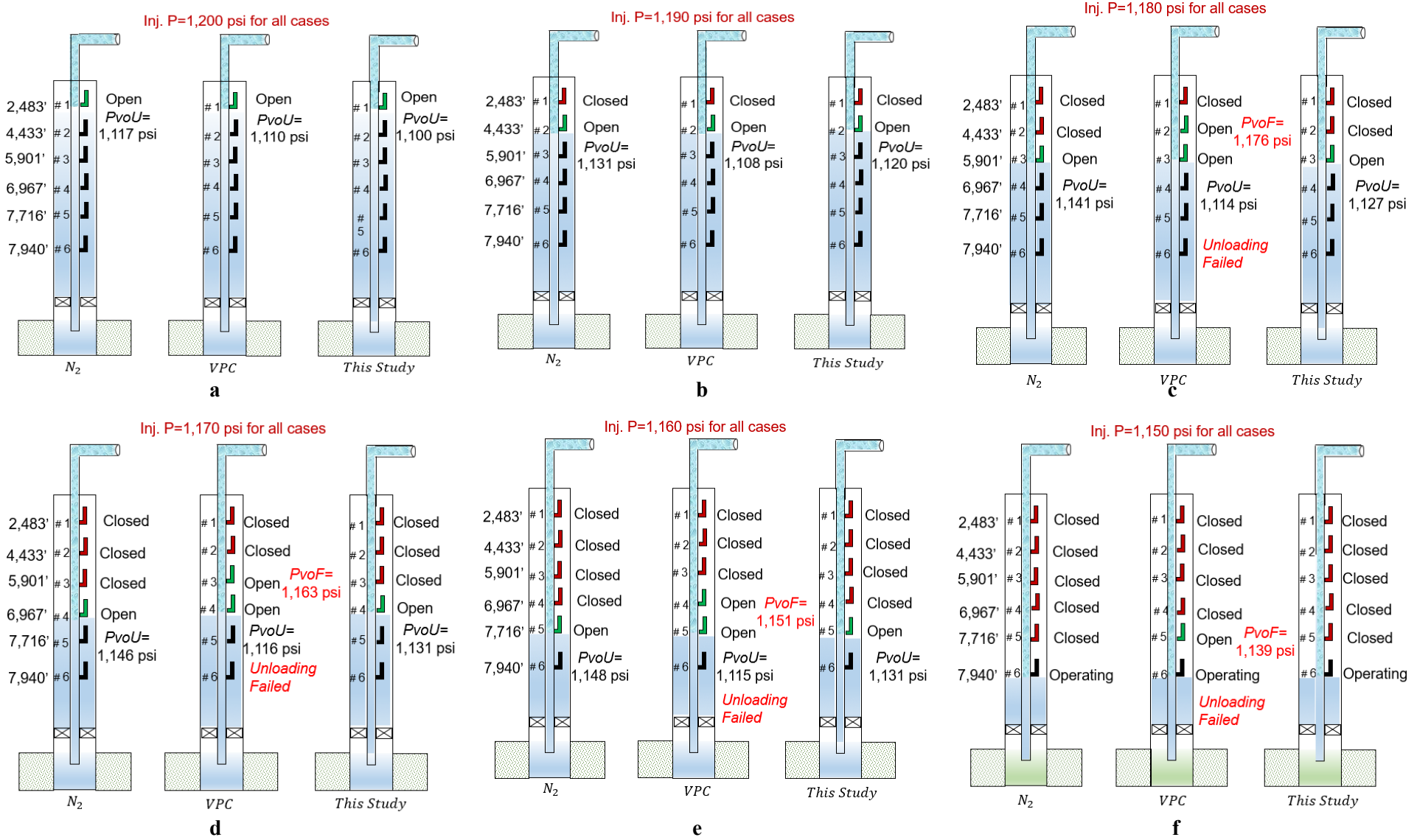

Figure 4.20. Unloading operation for the base case using three different design models.

The analysis for valve # 3 shows that all the models result in a surface valve opening pressure lower than the current surface injection pressure of 1,180 psig at this stage (as mentioned above, the injection pressure for each valve is decreased 10 psi as a safety factor). The N_2, VPC and the model developed in this study results in valve surface opening pressure (under uncovering conditions) of 1,141 and 1,114 and 1,127 psig respectively, which successfully opens the valve, since it is lower than the current surface injection pressure of 1,180 psig. However, when using the VPC model, the surface valve opening pressure at valve # 2 under flowing conditions is 1,176 psig (on this stage, valves # 2 and # 1 are under flowing conditions), which is lower than the current surface injection pressure (1,180 psig) at valve # 3. This results in two valves opening at the same time as shown in Figure 4.20 (c) -VPC model. This problem is defined as a multi-point of injection (API, 1999; Hernandez, 2016; Takacs, 2005) and described in details in section 2.1.3.1. On the other hand, the surface opening pressure for valve # 2 under flowing conditions using the N_2 and the model developed in this study is 1,198 and 1,188 psig respectively, which is higher than the current surface injection pressure (1,180 psig) at valve # 3. Therefore, valve # 2 is kept closed as shown in Figure 4.20 (c) - N_2 and this study models.

Returning to the design example shown in Figure 4.20 (d). During this stage, it is assumed that there is enough amount of gas and pressure in the system to overcome the multi-point of injection problem. Therefore, unloading is assumed to be successful using the VPC model in valve # 3 and gas injection has reached valve # 4. Analyzing valve # 4 with design surface injection pressure of 1,170 psig, all models results in an opening pressure (under uncovering conditions) lower than the current surface injection pressure, which successfully opens the valve # 4. However, the surface valve opening pressure (under flowing conditions) at valve # 3 using the VPC model is 1,163 psig, which is lower than the injection pressure at this stage (1,170 psig) at valve # 4. This

results in multi-point of injection as shown in Figure 4.20 (d) - VPC model. On the contrary, the opening pressures (under flowing conditions) for valve # 3 using model developed in this study and the N_2 model are 1,177 and 1,190 psig respectively, which is higher than the current injection pressure (1,170 psig) at valve # 4. Therefore, valve # 3 is kept closed, and the problem of multi-point of injection does not occur as shown in Figure 4.20 (d) - N_2 and this study models.

When analyzing valve # 5 during this stage, it is assumed again for the VPC model, that the gas injection is successfully reached valve # 5 (although multi-pointing is occurring). Using design surface injection pressure of 1,160 psig, all models result in a surface valve opening pressure (under uncovering conditions) lower than the current surface injection pressure, which successfully opens valve # 5. However, the same problem occurs again when using the VPC model, since the surface opening pressure (under flowing conditions) at valve # 4 is 1,151 psig, which is lower than the current surface injection pressure (1,160 psig) at valve # 5. This again results in multi-point of injection as shown in Figure 4.20 (e) -VPC model. Conversely, this problem does not occur when using the model developed in this study and the N_2 model since the opening pressure for valve # 4 is 1,165 and 1,170 psig respectively, which is higher than the injection pressure (1,160 psig) at valve # 5 as shown in Figure 4.20 (e) - N_2 and this study models.

At the final stage, the injected gas has reached the last valve (operating orifice valve), and the current surface injection pressure is 1,150 psig. As discussed in 1.1.2, orifice valves are always open since there is no closing mechanism for these valves. Therefore, there is no opening pressure for this operating/orifice valve. For this stage, it is assumed for the VPC model that the compressor is capable of delivering the gas to the operating valve (although multi-pointing is occurring). However, the surface opening pressure (under flowing condition) for valve #5 is 1,139 psig, which is lower than the injection pressure at the operating valve (1,150 psig), which results in multi-point

of injection during the production stage. On the other hand, when using the model developed in this study and N_2 model, it results in a surface valve opening pressure (under flowing conditions) of 1,155 and 1,172 psig respectively, which is lower than the surface injection pressure at the operating valve (1,150 psig). Therefore, the upper valve (# 5) is kept closed, and the goal of proper unloading design is achieved by having a single point of injection at the target depth.

In summary, when utilizing the minimum recommended safety factor with new GLVs, the VPC method may results in multi-point of injection during unloading and production stages, which requires larger amount of gas injection and may lead to cease the unloading operation and production losses if an additional amount of gas and pressure are not available. Finally, both the model developed in this study and the N_2 model provided a better design and successfully unloads the well given in the example.

4.1.6.2. *Case 2: Unloading Using New GLVs (25% Silicone Fill) and 20 psi Safety Factor*

The objective of showing this case is to examine the unloading design for three models using new GLVs under additional safety factor (20 psi instead of 10 psi). The following Table 4.4 shows a summary of unloading design results.

Table 4.4. Summary of unloading valve design calculations for case # 2.

Valve #	T_v (°*F*)	D_v (*ft*)	P_{Inj} (psig)	N_2 Opening (psig)		This study Opening (psig)		VPC Opening (psig)	
				Uncovering	Flowing	Uncovering	Flowing	Uncovering	Flowing
1	130	2,483	1,200	1,117	1,206	1,110	1,200	1,100	1,189
2	146	4,410	1,180	1,121	1,188	1,111	1,178	1,099	1,166
3	159	5,838	1,160	1,122	1,170	1,109	1,157	1,095	1,143
4	168	6,852	1,140	1,117	1,151	1,103	1,136	1,088	1,122
5	174	7,541	1,120	1,109	1,131	1,093	1,115	1,078	1,100

Following the same way of analyzing the data in the previous example, the results show that the well would unload successfully using all models. No multi-point of injection occurred for this well using the VPC model with the new safety factor. However, the disadvantage in this design is achieving a lower injection pressure available at the operating valve (1,100 psig compared to 1,150 psig). This is because the decrease in pressure drop between each valve (safety factor) increased from 10 to 20 psig. The reduction in the injection pressure would reduce the injection flow rate and thus, the production rate of the well. Utilizing the minimum safety factor is used in locations where the injection pressure is limited. On the other hand, the new safety factor (20 psi) absorbed the errors coming from the VPC model under the well conditions and unloaded the well successfully.

4.1.6.3. *Case 3: Unloading Using Refurbished GLV (50% Silicone Fill) and 20 psi Safety Factor*

The objective of showing this case is to examine the unloading design for three models using refurbished GLV with consistent silicone fill (50%) for all valves and ample safety factor (20 psi). The following Table 4.5 shows a summary of unloading design.

Table 4.5. Summary of unloading valve design calculations for case # 3.

Valve #	T_v (°*F*)	D_v (*ft*)	P_{Inj} (psig)	N_2 Opening (psig)		This study Opening (psig)		VPC Opening (psig)	
				Uncovering	Flowing	Uncovering	Flowing	Uncovering	Flowing
1	130	2,483	1,200	1,143	1,232	1,117	1,206	1,091	1,180
2	146	4,410	1,180	1,155	1,221	1,116	1,183	1,086	1,153
3	159	5,838	1,160	1,160	1,208	1,112	1,160	1,079	1,127
4	168	6,852	1,140	1,159	1,193	1,104	1,138	1,069	1,102
5	174	7,541	1,120	1,153	1,175	1,093	1,116	1,056	1,078

Analyzing the results in a similar fashion of the base case results in successful unloading operation for the N_2 model and the model developed in this study. The only difference occurs for

the N_2 model in valves # 4 and 5 since it requires to increase the injection pressure up to 1,159 psig instead of designed injection pressure of 1,140 psig. This would operate the system at higher casing pressure than expected. However, it would unload properly through each lower valve since there is available compressor/injection pressure at the surface (1,200 psig).

The VPC model would cause the system to multi-point even with including an additional safety factor of 20 psi. This is because of larger silicone fills added (50%) compared to the base case (25%). As concluded in section 4.1.5, the larger the silicone fill, the larger the amount of silicone compressed. Since the VPC does not include the silicone compressibility and dome thermal expansion, it is expected that the VPC error would increase with silicone fill increase.

In summary, increasing silicone fill affect the VPC model since the problem of multi-pointing occurred even though additional safety factor of 20 psi is included in the design. In addition, silicone fill did not affect the model developed in this study and the N_2 model. Except that for the N_2 model, it required a higher than the designed injection to open the valves # 4 and 5. It can be concluded that adding silicone to the GLV affects the unloading operation more significantly for the VPC model even with an additional safety factor is included. This example considered that all the valves have a consistent amount of silicone fills. However, the amount of silicone added during valve refurbishment is not measured and thus, not consistent with other refurbished valves. The consequence of this practice on the unloading operation is presented in the following example (case 4).

4.1.6.4. *Case 4: Unloading Using New and Refurbished GLV (25 and 50% Silicone Fill)*

The objective of showing this case is to examine the unloading design for three models using new and refurbished GLVs with the minimum recommended safety factor (10 psi). In addition, it

illustrates the importance of measuring silicone amount added to valves during valve refurbishment.

Valve # 5 is a refurbished valve with silicone fill of 50%. All other unloading valves are new valves with 25% silicone fill. The following Table 4.6 shows a summary of unloading design.

Table 4.6. Summary of unloading valve design calculations for case # 4.

Valve #	T_v (°*F*)	D_v (*ft*)	P_{Inj} (psig)	N_2 Opening (psig)		This study Opening (psig)		VPC Opening (psig)	
				Uncovering	Flowing	Uncovering	Flowing	Uncovering	Flowing
1	130	2,483	1,200	1,117	1,206	1,110	1,200	1,100	1,189
2	147	4,433	1,190	1,131	1,198	1,120	1,188	1,108	1,176
3	159	5,901	1,180	1,141	1,190	1,127	1,177	1,114	1,163
4	169	6,967	1,170	1,146	1,181	1,131	1,165	1,116	1,151
5	175	7,716	1,160	1,195	1,219	1,132	1,156	1,103	1,127

Following the same analysis procedures presented in the base case shows that utilizing the N_2 model provides successful unloading until injected gas reaches refurbished valve # 5. At this stage, the surface injection pressure is 1,160 psig. However, the opening pressure (under uncovering conditions) for valve # 5 is 1,195 psig, which is higher than the injection pressure at this stage (1,160 psig). In order to open valve # 5, the surface injection pressure has to increase to 1,195 psig. If the surface injection pressure is increased to 1,195 psig, the upper valves # 4 and 3 will open since the surface opening pressure (under flowing conditions) are 1,181 and 1,190 psig respectively. This would cause multi-point of injection in three valves (# 3, # 4 and # 5), which may lead to cease the unloading operation. Another factor is that the surface opening pressure (under flowing conditions) for valve # 2 is 1,198 psig, which is only 3 psig higher than the opening pressure of valve # 5 (1,195 psig). If the injection pressure accidentally increased 3 psi reaching 1,198 psig, it may cause four valves to multi-point (# 2, # 3, # 4 and # 5). Another factor is the

available surface injection pressure is 1,200 psig, which is very close to the surface opening pressure of valve # 5 (1,995 psig). If in other well/valve conditions (such as larger silicone fill or at higher valve temperature), the available surface injection pressure may not be enough to exceed the opening pressure of that valve, and therefore, it may not be possible to reach the operating valve. Which in turn, may cease the unloading or lead to gas injection at a shallower depth. Injecting at a shallower depth leads to production losses since the bottomhole pressure is increased (API, 1994, 1999; Hernandez, 2016; Takacs, 2005). As mentioned in section 2.1.3.1, if this valve (# 5) is pulled and sent to the workshop for inspection to test its opening pressure, the valve will open at its exact design pressure since the silicone has not expanded significantly at workshop temperature of 60 °F. Therefore, the problem is hard to be diagnosed. On the other hand, the VPC model would cause the system to multi-point in a similar fashion to the base case. Finally, the model developed in this study would successfully unload the well without having the multi-point of injection problem because of its accurate opening pressure predictions.

In summary, silicone amount must be measured if an additional amount of silicone is needed during valve refurbishment. Utilizing un-measured silicone fills would affect the unloading operation significantly when utilizing the N_2 model even with the availability of extra injection pressure at the surface.

4.2. **The Accuracy of the GLV Sizing Equation**

This section is divided into four parts. The first part shows the results related to the use of real gas isentropic exponent (n) on GLV sizing equations for an orifice and an IPO GLV. The second part shows the results of using the velocity of sound to evaluate the accuracy and validity of using the real gas isentropic exponent on GLV sizing equations. The third part discusses the application

of real isentropic exponent on the VPC and API Simplified methods. The fourth part shows the effect of the real gas isentropic exponent (n) on gas-lift operations.

4.2.1. *Ideal Isentropic Exponent (k) versus the Real Exponent (n) Method*

This section discusses the effect of using the real isentropic exponent (n) in the GLV sizing equations, and it presents the comparison to the use of ideal isentropic exponent (k) utilized in current VPC and API Simplified equation. Two GLVs are discussed. The first valve is an orifice valve, which is used as an operating valve as mentioned in the literature. The second valve is an IPO valve, which is utilized as an unloading valve and in some cases as an operating valve.

4.2.1.1. *Orifice GLV*

The valve selected for this analysis is an orifice GLV with 24/64 in orifice size. The valve flow capacity (Cv) is 3.5, and the terminal pressure drop ratio (x_T) for air is 0.54. Valve properties (C_v and x_T) are determined experimentally by a private lab using air. This valve has a large flow capacity when compared to similar GLVs. Large flow capacity valves are typically used in wells with high production rate. Therefore, the consequence of gas flow rate errors as a result of using the ideal isentropic exponent on the production rate may be large. The following analysis is performed using typical natural gas properties. The composition of typical natural gas is listed in Table 4.7 (Lemmon et al., 2007):

Table 4.7. Natural gas composition.

Component	Mass Fraction
Methane	0.888
Nitrogen	0.0014508
Carbon dioxide	0.065432
Ethane	0.032107
Propane	0.0061069
Isobutene	0.0013528
Butane	0.00054114
Isopentane	0.00058776
Pentane	0.00046182

Figure 4.21 is a typical GLV performance curve developed using Equation *2.26*. It shows the gas flow rate in standard conditions with respect to the pressure downstream (P_2) to the GLV (location 4, Figure 2.9). Figure 4.21 presents the results generated using the ideal isentropic exponent (k) of 1.3 for natural gas, and using real isentropic exponent (n) of 1.85. The real isentropic exponent is estimated using FLOWSOLV software at upstream conditions (location 1, Figure 2.9). Upstream conditions for this case is at an injection pressure of 3,000 psig and a temperature of 150 °F.

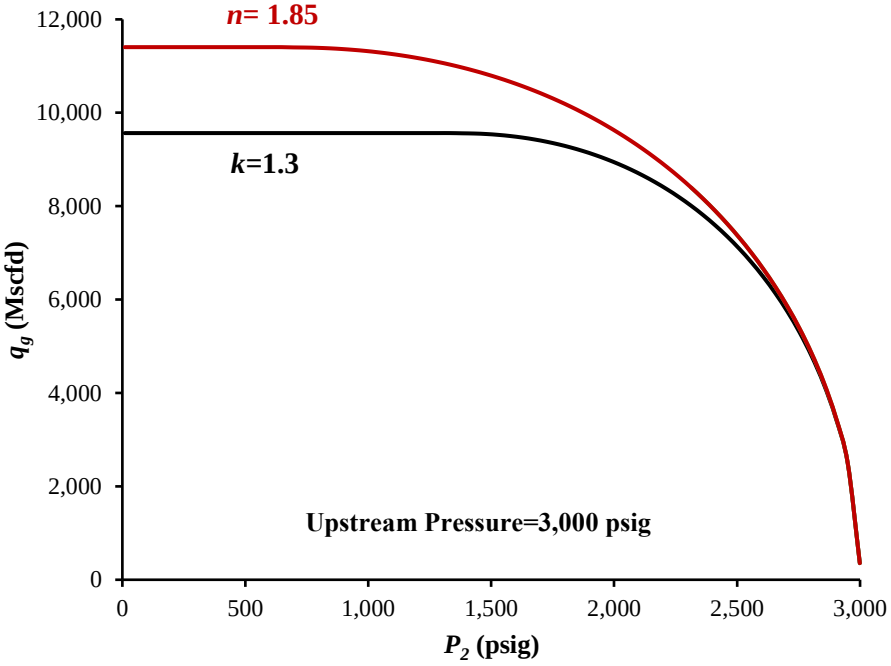

Figure 4.21. Theoretical performance curves for an orifice GLV using ideal exponent (k=1.3) and real exponent (n=1.85) using an upstream pressure of 3,000 psig.

The results presented in Figure 4.21 show that using the ideal isentropic exponent method underestimate the flow for almost the entire performance curve. The maximum flow rate estimate when using the real isentropic exponent (n) is 11,405 Mscfd compared to 9,565 Mscfd by the ideal exponent (k). Using the ideal exponent underestimates the flowrate by 19%, which may result in an oversized GLV.

Two explanations will be discussed. The first explanation is based on thermodynamics. The second explanation is based on mathematical equations derived for sizing the GLVs. Thermodynamically, the expansion processes in valve throat is assumed to be isentropic and governed by Equation *2.23*.

When a larger isentropic exponent is used ($n = 1.85$ compared to $k = 1.3$), it lowers the volume of the gas expanded in the throat (location 3, Figure 2.9) as per Equation *2.23*.

When a lower volume of gas is expanded in the throat, the density of the gas is increased, and thus, the flow is increased. As explained in section 2.2.3, the process of gas expansion adds resistance to the flow. Therefore, the higher the expansion, the lower the flow for the same pressure difference upstream and downstream to the GLV.

Mathematically, the isentropic expansion is used as an *approximate* method to correct for the terminal pressure drop ratio (x_T) for fluids other than air (natural gas in this case) as per Equation *2.24*. The terminal pressure drop ratio (x_T) is used to establish the slope of the expansion factor (Y) with respect to the pressure drop ratio (x) (Equation *2.25*).

A larger value of isentropic exponent results in a larger value of terminal pressure drop (x_T) (in this case, x_T is 0.539 using ideal isentropic exponent, and 0.767 using real isentropic exponent), which in turn, reduces the expansion factor (Y), resulting in a higher flow rate (Equation *2.26*).

Figure 4.22 shows how the expansion factor (Y) varies with pressure downstream the choke for a constant upstream pressure of 3,000 psig as a function of the ideal isentropic exponent (k) of 1.3 and real isentropic exponent (n) of 1.85.

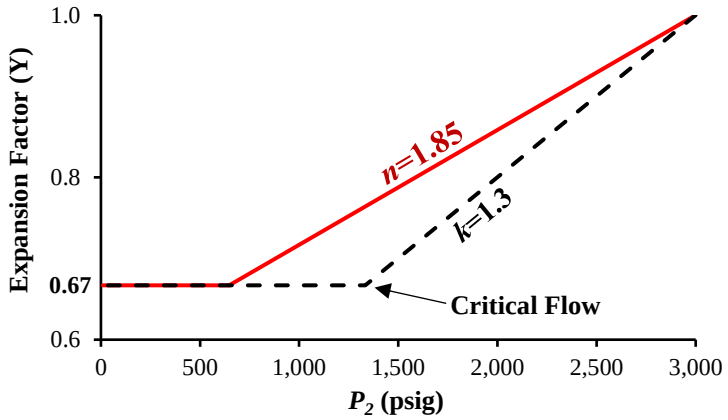

Figure 4.22. Expansion factor (Y) versus downstream pressure for 3,000 psig upstream pressure using ideal (k) and real (n) exponents.

It can be seen from the red-solid line on Figure 4.22 that the use of an ideal exponent of k = 1.3 results in a lower value of expansion factor and the lower the expansion factor, the lower the flow rate. It also shows that the expansion factor reaches the lowest value at Y = 0.67 at a downstream pressure of 1,333 psig, which represents the critical pressure (choked flow). On the other hand, when the real expansion factor is used (n=1.85 at upstream conditions), it would result in a lower slope (higher values of expansion factor). Higher values of expansion factor (Y) mean a lower amount of gas expansion. Therefore, higher gas density in the throat and thus, a higher flow rate as per Equation *2.26*.

One interesting finding is that when using the real isentropic exponent (n) the critical (choked) flow occurs at a significantly lower downstream pressure from the ideal isentropic exponent (k) (647 compared to 1,333 psig). Mathematically, the product of $F_k\ x_T$ (in Equation *2.25*) in the present case (injection pressure of 3,000 psig and temperature of 150° F) would result in a terminal pressure drop ratio (x_T) of 0.767 (using n) compared to 0.539 (using k), which represents a difference of 42%. One other way to prove that the critical flow through valve would occur at larger pressure drop is by using the concept of velocity of sound in the medium. This concept is discussed in 4.2.2.

It is essential to mention that the typical range of application of an orifice GLV used in a well is between 100-250 psig differential (Hernandez, 2016). Therefore, Figure 4.21 is replotted in Figure 4.23 to represent the range of application for an orifice GLV range.

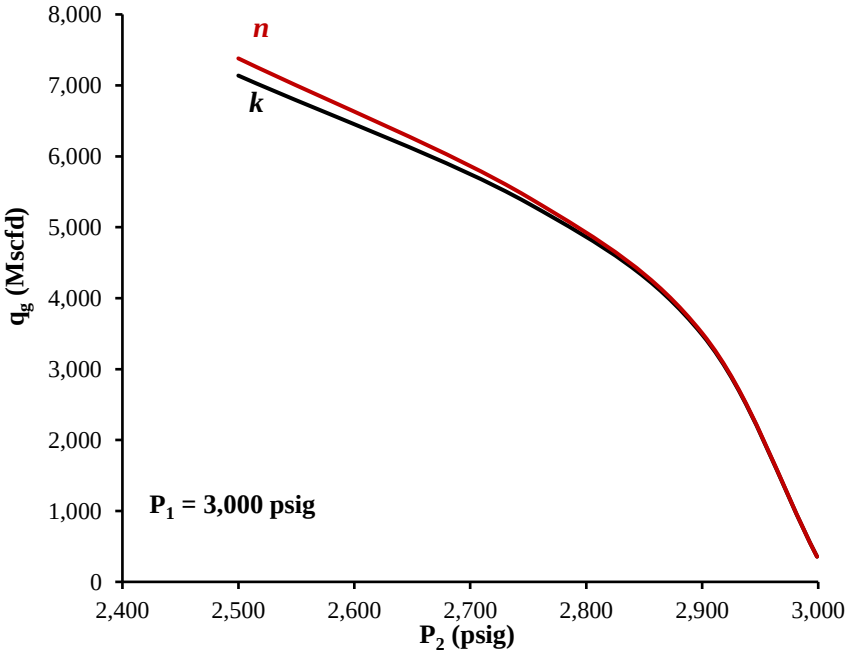

Figure 4.23. Theoretical performance curves for an orifice GLV using ideal (k=1.3) and real exponent (n=1.85) at an upstream pressure of 3,000 psig and differential pressure up to 500 psig.

It can be seen from Figure 4.23 that the difference between the k and n in the flowrate is significantly lower compared to Figure 4.21 since the range of differential pressure is limited to 500 psig. The flowrate difference between the ideal (k) and real (n) isentropic exponents using a typical range of 100 psig is 3,484 Mscfd compared to 3,506 Mscfd respectively. The ideal model slightly underpredicts the flowrate by only 0.62%.

These errors under the typical range application for an orifice GLV are minimal. This effect is probably will be lower when using valves with smaller flow capacities. Therefore, the effect of the real isentropic exponent is probably has a negligible effect on orifice GLV under subcritical conditions.

The reason behind this small difference is due to high expansion factor for low pressure drop ratios.

For low pressure drop, the change in gas density is small and are slightly less than unity. As shown in Figure 4.22, expansion factor in both cases (*n* and *k*) is very similar for low pressure drop ratio.

For example, at a differential pressure of 100 psig, the *n* is 0.986 compared to 0.979 for the *k* case. Since the expansion factors are similar, it means that the flowrates are similar since the expansion factor is the only parameter affecting the flowrate when the isentropic exponent is changed. Therefore, under small pressure drop ratio, the effect of *n* and *k* is minimal.

4.2.1.2. *IPO GLV*

The valve selected for this analysis is an IPO GLV with 3/16 in port size. This valve is chosen for this analysis since it represents a typical IPO valve used for unloading designs (API, 1999). The valve flow capacity (*Cv*) and terminal pressure drop ratio (x_T) as a function of stem travel (d_x) is obtained from API (2001) as follows:

$$C_v = 219.3\, d_x^3 - 149.04\, d_x^2 + 22.58\, d_x \qquad 4.1$$

$$x_T = 734.4\, d_x^3 - 178.3\, d_x^2 + 15.12\, d_x \qquad 4.2$$

The following analysis is performed using natural gas properties at an injection pressure of 3,000 psig and temperature of 150 °F. Figure 4.24 represents a GLV performance curves for an IPO valve developed using Equation *2.26*. It shows the gas flow rate in standard conditions with respect to the pressure downstream (P_2) to the GLV (location 4, Figure 2.9).

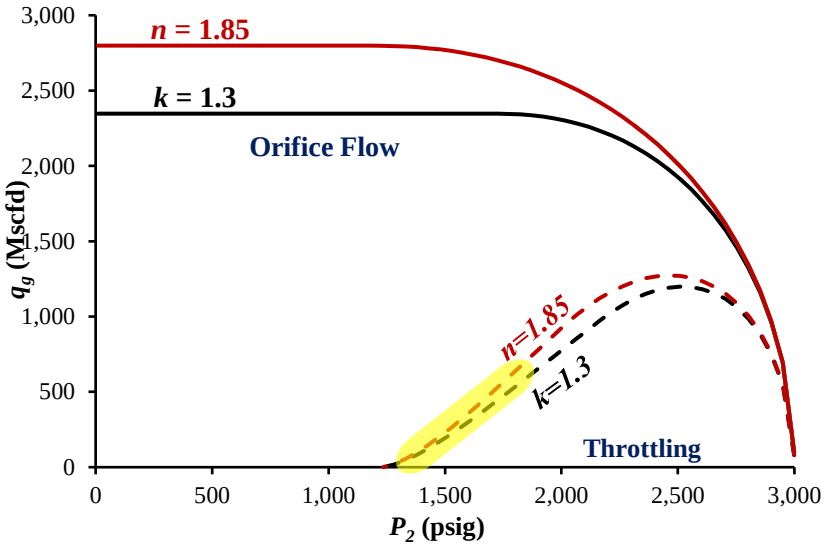

Figure 4.24. Theoretical performance curves result for an IPO GLV using ideal exponent (k=1.3) and real exponent (n=1.85) using an upstream pressure of 3,000 psig.

Two flowing modes are shown in Figure 4.24. The upper two curves represent a comparison between the ideal and real isentropic exponent under orifice flow. Orifice flow in an IPO occurs when the stem of an IPO valve is at its maximum travel, or in other words, fully open (Takacs, 2005). The flow in this IPO valve is similar to the flow for the orifice GLV case presented previously in Figure 4.21. The lower two curves represent a comparison between the ideal and real isentropic exponent under throttling flow. Throttling flow in an IPO occurs when the stem travel is not fully open, and the stem tip interferes with the gas passage through the valve (Takacs, 2005).

Starting with the orifice flow region, the results presented in Figure 4.24 show that using the ideal isentropic exponent method underestimates the flow for almost the entire performance curve. The maximum flow rate estimate (occurring at critical flow) when using the real isentropic exponent (n) is 2,799 Mscfd compared to 2,347 Mscfd by the ideal exponent (k). The ideal exponent model underestimates the flowrate by 19% (maximum difference), which may result in oversized GLV. This difference is similar to the percentage occurred for the orifice GLV analyzed in section 4.2.1.1. This similarity occurred because the real isentropic exponent is the same in both cases, as it is estimated at the same pressure and temperature conditions (P=3,000 psig and T=150

°F). The reasons behind the difference between using *k* and *n* exponent is similar to the reasons discussed in section 4.2.1.1. The only difference is in the flowrate, which is different in this case because the flow capacities for the orifice and IPO valves are different. The consequences of utilizing an oversized GLV on the gas-lift design will be discussed in section 4.2.4.

Moving to the throttling flow region, the results show that using the ideal isentropic exponent method underestimate the flow for almost the entire performance curve. Again, the maximum flow rate difference when using the real isentropic and ideal isentropic exponent is 19% and occurred during the choked flow. The percentage difference in the flowrate remains constant at 19% for the entire range shaded in yellow in Figure 4.24, which represents the critical flow region. The lowest difference occurs at low pressure drop ratios (until downstream pressure ≈ 2,700 psig) due to higher expansion factor as explained earlier in section 4.2.1.1.

It is important to mention that during unloading operation the IPO is expected to reach the critical flow. Therefore, using the ideal exponent may lead to oversized GLV.

4.2.2. *Velocity of Sound (c) Concept to Evaluate the Real Exponent (n) Correction*

Critical (choked) flow occurs when the velocity of a flowing fluid equals the velocity of sound in the medium. Also, the flow rate is a result of the product of velocity and area. As the flowing area is constant, the velocity is directly proportional to the flow rate. Thus, a change in velocity with a certain percentage would induce a change in the flow rate with the same percentage.

The accuracy at which the velocity of sound is estimated is smaller than 0.5%, as shown in Figure 2.10. Due to its high accuracy, the velocity of sound is used as a reference to examine the validity of the correction factor concept outside its experimental limits. As discussed earlier, the correction factor is used outside of its experimental limits (for isentropic exponent $k > 1.65$). This method is not theoretically accurate as originally proposed by (Driskell, 1983).

The velocity of sound (c) at standard condition (14.7 psia and 60 °F) is estimated using FLOWSOLV software (that utilizes the AGA report 10 (2003) method) to be 1,397 ft/s, while at upstream conditions (3,000 psig and 150°F) is 1,708 ft/s. Therefore, the difference in the velocity of sound between standard conditions and upstream conditions is 22% (overprediction with respect to ideal conditions). As mentioned earlier, this 22% difference in velocity represents the same difference in the flow rate. When using the real isentropic method (n) at upstream conditions (3,000 psig and 60 °F) it would result in a 19% difference (overprediction) in critical flow estimates compared to the use of the ideal ratio of specific heats (k) at standard conditions (14.7 psi and 60 °F).

Both methods agreed that the critical flow rate would occur at a higher flow than the ideal estimates. However, the real isentropic method overpredicted the flow by 3% compared to the velocity of sound concept. One of the possible reasons for this difference is that the original development of the ISA (1975) equation is based on experimental work done on nozzles and orifice plates using air and steam with ideal isentropic exponent range between 1.08 and 1.65, assuming ideal gas. Expanding the application of the ISA (1975) method to outside its design limit may lead to this error.

4.2.3. *Application of Real Isentropic Exponent on the VPC and API Simplified Methods*

As mentioned previously, the API recommended practice 19G2 (2010) suggest the use of API Simplified method to predict the flow through GLVs. API Simplified method utilizes Equation *2.26*, which assumes ideal isentropic exponent. When the API Simplified method is used, the injection pressure used to obtain the valve flow capacity and terminal pressure drop is not specified. What is recommended in the API (2010) is to use a minimum injection pressure of 100 psig. The isentropic exponent for air at 100 psig pressure (at 60 °F) is 1.41, which almost equals

the ideal isentropic exponent of 1.4. Therefore, for this case, the effect of the real isentropic exponent on the API Simplified method is similar to the cases presented in Figure 4.21 and Figure 4.23. It can be concluded that, for the case analyzed in this work, the API Simplified method [suggested by the API recommended practice 19G2 (2010)] may lead to oversized unloading GLV. The effect of this real isentropic exponent on the operating (typically orifice) valves is probably negligible since the real isentropic exponent affects more dominantly the critical flow, which is not expected in operating valves.

On the other hand, the VPC method utilizes valve properties obtained experimentally using tests results developed at high injection pressure (with pressures similar to field conditions). Therefore, the ideal exponent of air (k_{air}) is utilized in Equation *2.24* should not be equal to 1.4. This is because the real isentropic exponent for air at these conditions (testing facility with high pressure) is different than the ideal isentropic exponent as dynamic flow tests are performed at high pressures. For example, the isentropic exponent for air at an injection pressure of 3,000 psig and temperature of 60 °F (temperature at test facility) equals to 1.98, not 1.4 as suggested by Equation *2.24*. However, the real isentropic exponent effect is embedded in the resultant valve properties (C_v and x_T) developed at high injection pressure. Detaching the real isentropic exponent effect from these properties is complex and may not be possible. Therefore, effect of this on GLV sizing should be investigated in the future.

Another factor that may influence both VPC and API Simplified is the temperature. Temperature plays a major role in estimating the isentropic exponent (n). Figure 2.11 shows how significant isentropic exponent changes with respect to temperature. For example, the isentropic exponent for natural gas estimated at injection pressure of 3,000 psig and 60 °F (temperature at the testing facility) is 2.5 compared to 1.85 at a temperature of 150 °F (temperature at well).

4.2.4. *Effect of Real Gas Isentropic Exponent on GL Operation*

As explained in section 4.2.1.2, utilizing the ideal isentropic exponent may lead to an oversized GLV. An oversized GLV leads to higher than anticipated gas injection. Higher gas injection may lead to heading (API, 1999). Heading is well flow in unstable conditions, and it occurs due to regular and irregular changes in the flow parameters such as flowrate and pressure (Takacs, 2005). This unstable conditions may lead to sever slugging at the wellhead. As a result of slugging, liquid and gas slugs may overload the surface facilities (API, 1994; Takacs, 2005). Furthermore, in some cases, injected gas may not reach the operating valve (last valve) due to excessive gas injecting through oversized unloading valve above it (Hernandez, 2016). This may lead to production losses or failing the unloading operation.

Conversely, using the non-ideal isentropic exponent leads to proper valve sizing. It is always recommended to use the smallest port size that passes the required gas to unload the well for many reasons (API, 1994, 1999). As explained in section 2.1.2, the production pressure effect factor changes significantly as a function of port size. GLV with smaller port sizes has a smaller production pressure effect factor. Which means that the contribution of the pressure coming from the production/tubing toward the valves' opening pressure is smaller. Therefore, reducing the possibility to cause valves to reopen and cause multi-point of injection, which interferes with the unloading operation especially when higher than anticipated tubing/production pressure occurs. Table 4.8 shows a numerical example of pressure contribution coming from the tubing as a function of port size for a typical 1 in IPO GLV (BK-1) (Takacs, 2005). The tubing/production pressure acting on the valve is assumed to be 1,000 psig. The third column in Table 4.8 is the production pressure effect and results from the multiplication of the tubing/production pressure (1,000 psig) by the production pressure effect factor (column 2).

Table 4.8. Camco BK-1 IPO GLV port sizes with PPEF and PPE.

Port Size (*in*)	PPEF	PPE (*psig*)
1/8	0.073	73
3/16	0.135	135
1/4	0.230	230
5/16	0.456	456
3/8	0.712	712

As can be seen from Table 4.8, the larger the port size, the larger the production pressure effect. This effect increases significantly between ports. For example, the difference between the production pressure effect between 5/16 in and its preceding port size (1/4 in) is 230 psi. This difference represents a 98% increase in the production pressure effect, which in turn increases the possibility of valve reopening significantly if higher than anticipated tubing/production pressure occurred.

Also, the API (1999) recommends using additional safety factors (larger drop in injection pressure to ensure valve closing) for large port valves as shown in Table 4.9. Therefore, oversized GLV used for unloading operation requires larger pressure drop. Larger pressure drop reduces the injection pressure (lift energy) available for the operating valve (last valve). Therefore, reducing the injection flow rate and thus, the production rate of the well.

Table 4.9. Additional safety factor for various IPO valves.

Valve OD *(in)*	Port Size (*in*)	Safety Factor (psi)
5/8	1/8	10
	5/32	15
	3/16	20
1	1/8	5
	3/16	10
	1/4	15
	5/16	20
$1\,1/2$	3/16	5
	1/4	10
	5/16	15
	3/8	20
	7/16	25

5. Conclusions and Future Work

5.1. Conclusions

1. Under the investigated conditions, utilizing the model developed in this study for designing GLV set pressure for unloading operation considering new and refurbished IPO GLVs following the API procedure provided successful unloading operation for all cases compared to other models. This is because the model developed in this study includes silicone compressibility and thermal expansion, which leads to more accurate valve opening pressure, and thus, to proper valve unloading design.
2. Under the investigated conditions, utilizing the VPC model with the minimum recommended safety factor of 10 psi in designing unloading operation for new IPO GLVs following the API procedure may results in multi-point of injection during unloading and production stages due to valve opening pressure underprediction. This is probably because this model ignores silicone compression and thermal expansion. Multi-pointing requires larger amount of gas injection and pressure, and it may lead to cease the unloading operation and production losses if an additional amount of gas and pressure are not available in the system. On the other hand, the model developed in this study and the N_2 model successfully unloads the well for the same base case.
3. Under the investigated conditions, the additional safety factor of 20 psi absorbed the errors coming from the VPC model and unloaded the well successfully (case # 2). However, it reduced the available injection pressure (energy) at the operating valve from 1,150 compared to 1,110 psig, which in turn may reduce the gas injected and, thus the oil production.

4. Under the investigated conditions, utilizing refurbished valves with 50% silicone fill would operate the system at higher than expected casing pressure. However, it would unload properly if there is available compressor/injection at the surface to overcome the increase in valve opening pressure due to N_2 error. The VPC model would cause valves to multi-point even with an additional safety factor of 20 psi since it does not account for silicone compressibility and dome thermal expansion, which leads to further under prediction of valve opening pressure.
5. Utilizing the N_2 model in the unloading design using the API procedure may lead to higher than the anticipated valve opening pressure. This is because this model ignores the silicone thermal expansion effects. During the design stage, the final dome pressure and the temperature is provided to the designer. Part of the final dome pressure (P_2) is coming from silicone expansion. Since this effect is ignored in this model, the initial dome pressure (P_1) is overpredicted. Which in turn leads to overcharged dome pressure (P_1) in the workshop. Thus, the finial dome pressure is also overpredicted. An overpredicted dome pressure (P_2) provides additional closing force to the valve as per Equation 2.13. Therefore, higher than anticipated valve opening pressure.
6. Under the investigated conditions, utilizing the N_2 model in designing IPO valves with different silicone fills may cease the unloading in two ways. Firstly, by not having an adequate amount of injection pressure to overcome increased opening pressure for deeper valves since the valve opening pressure is affected significantly by silicone expansion due to high temperature at depth. Secondly, by multi-pointing (three valves in case # 4) when applying extra injection pressure to open the closed, stuck valve (valve # 5 in the study case), which may lead to cease the unloading operation or lifting

from the shallower depth and thus, production losses.

7. Utilizing un-measured silicone fills in GLV would affect the unloading operation. This effect increases when each valve is filled with a different amount of silicone fluid. Therefore, each valve will have a different amount of expanded silicone and thus, different opening pressure. This problem is not detectable in the workshop since the valves are tested at a temperature of 60 °F. Therefore, the effect of different silicone filling will be undetectable since the silicone has not expanded significantly.
8. Under the investigated experiments, ignoring silicone compression and dome thermal expansion may lead to overpredict the expected dome pressure (P_2) for a GLV. Which in turn affects the opening pressure (underpredicting) for the valve. The range of pressure overprediction for normal silicone fill ratio of 25% and temperature of 175°F is from 7.4 to 13.7 psi followed by 15.5 to 30.8 psi for silicone fill ratio of 50%. The maximum over prediction range difference is from 54.3 to 110 psi at silicone fill ratio of 75%.
9. Under the investigated experiments, utilizing the current recommended practice may lead to underpredict the dome pressure (P_2) for a GLV by 11 psig under normal silicone volume ratio (25%), and temperature of 175 °F up to 219 psig under large silicone volume fills (75%) and temperature of 175 °F due to the negligence of silicone presence and dome thermal expansion. This would results in (overpredicting the valve opening pressure).
10. The higher the pressure, temperature, and silicone fill in a GLV, the higher experimental the dome pressure ($P_{2\ Experiment}$) deviates from the expected dome pressure ($P_{2\ Design}$) if the current recommended practice is utilized.

11. Silicone fill ratios of 7.5, 10 and 15% start to affect the dome pressure (P_2) (increase) by 4 psi at a temperature of 130 °F. However, this effect falls within the safety design margin of 10 psi.
12. Under experimental conditions, utilizing the VPC model in predicting the dome pressure (P_2) may lead to overprediction of the dome pressure (P_2) due to ignorance of silicone compressibility and dome thermal expansion. This would (underpredicts valve opening pressure).
13. Under experimental conditions, the model developed in this study provided the best model, in most cases, in matching the experimental results in predicting the dome pressure (P_2) since it accounts for silicone compression and dome thermal expansion.
14. Using the ideal isentropic exponent k in sizing GLV may lead to underestimating the gas flow rate up to 19%, especially at critical flow estimates.
15. The effect of utilizing the ideal isentropic exponent k instead of real isentropic exponent n in sizing orifice GLV is minimal and may be neglected since the estimated error under typical orifice range is 0.62% (underpredicting). This is because the range of application for orifice valves falls at low-pressure drop ratios. Thus the expansion factor effect is minimal.
16. The effect of utilizing the ideal isentropic exponent k instead of real isentropic exponent n in sizing calibrated (IPO/PPO) GLV may underestimate the gas flow through GLV by 19%, which may lead to oversized GLV. An oversized GLV during the unloading operation may cause heading in the system. In addition, it increases the possibility for the valve to reopen and cause multi-point of injection, which interferes with unloading operation. This is because larger ports have a larger pressure effect

factor. Furthermore, oversized GLV requires additional pressure drop to close it. Additional pressure drop reduces the gas injection pressure available. Therefore, reduce the production rate for the well especially at high rate wells.

17. The effect of utilizing ideal isentropic exponent k instead of real isentropic exponent n in sizing the GLV may affect the API Simplified approach since the valve characteristics (C_v and x_T) may be obtained using low pressure (closer to ideal conditions).
18. The VPC method utilizes high injection pressure (closer to real conditions) in estimating the valve characteristics (C_v and x_T) therefore, utilizing the ideal isentropic exponent k may lead to errors.

5.2. **Novelty and Impact**

According to author's knowledge, the impact of silicone expansion on GLV set pressure was not investigated in the open literature. Furthermore, the enhanced models proposed in this research demonstrated to have an important impact on well unloading and production operations for wells equipped with gas-lift.

5.3. **Future Work**

1. To develop a model that includes the effect of nitrogen solubility in the silicone and how it may affect/enhance the accuracy GLV of the model developed in this study and thus, the GLV design.
2. To test the silicone compressibility experimentally and compare it with the correlations used in this study to evaluate its accuracy. This may enhance the accuracy of the model developed in this study and thus, the GLV design.
3. To test the silicone thermal expansion coefficient experimentally and compare it

with the thermal expansion coefficient provided by the silicone manufacturer to evaluate its accuracy. Similar to the previous suggestion, this may enhance the accuracy of the new model developed in this study and thus, GLV design.

4. Justify the use of silicone in the bellows by implementing the erosion/failure test for the GLV with and without silicone fill inside the valve.
5. Optimize the amount of silicone ratio by experimentally testing the bellow life with the different amount of silicone fills inside the valve.
6. To add the model developed in this study in the VPC software.
7. To evaluate the accuracy of the nitrogen correlation used to predict the dome pressure in the VPC software. This evaluation could be done by using REFPROP software and the methodology presented in Sutton (2014) paper.
8. To evaluate the accuracy of the silicone thermal expansion coefficient provided in the VPC software and to add the option to change it manually.
9. Evaluate the accuracy of Zimmerman nitrogen correlation. This evaluation could be done by using REFPROP software and the methodology presented in Sutton (2014) paper.
10. Study the effect of silicone presence in the valve spread and how it may affect the intermittent GLV operations.
11. Study the effect of silicone presence in changing the bellows load rate and how it may affect the flow rate prediction for the GLV.
12. To study the effect of error propagation coming from formation evaluation techniques on GLV design and unloading operations.

References

AGA. (2003). *Speed of Sound in Natural Gas and Other Related Hydrocarbon Gases*. Retrieved from

AlTarabulsi, K., Coutinho, R., & Waltrich, P. J. (2017). *Effect of Fluid Properties on the Performance of Gas-Lift Valves.* Paper presented at the ASME 2017 36th International Conference on Ocean, Offshore and Arctic Engineering.

ANSI/ISA. (1977). Standard Control Valve Sizing Equations. In *575.01*: ANSI/ISA.

API. (1994). *Gas Lift Book 6 of the Vocational Training Series* (Third ed.): API.

API. (1999). Recommended practice for design of continuous flow gas lift installations using injection pressure operated valves rp 11v6. In. Washington,DC: API.

API. (2010). Flow-control Devices for Side-pocket Mandrels. In *H.11.2 Background and theory of approach* (pp. 74): IHS.

API. (2014). Sizing, Selection, and Installation of Pressure-relieving Devices in Refineries: Part I-Sizing and Selection. In: American Petroleum Institute.

API, R. (2001). 11V2, Recommended Practice for Gas Lift Valve Performance Testing. In: Washington, DC: API.

ASME. (1959). *Fluid Meters: Their Theory and Application*. NY: ASME.

Bagci, S. (2017). *Gas Lift Production Benchmarking Using IPR Risked Inflow Modeling: Case Study*. Paper presented at the SPE Oklahoma City Oil and Gas Symposium.

Beggs, H. (1991). Production optimization using NODAL TM analysis. Oil & Gas Consultants International. *Inc, Tulsa*.

Bertovic, D., Doty, D., Blais, R., & Schmidt, Z. (1997). *Calculating accurate gas-lift flow rate incorporating temperature effects.* Paper presented at the SPE Production Operations Symposium.

BIPM, I., & IEC, O. (1998). Guide to the expression of Uncertainty in Measurement (1995). *Google Scholar*.

Brown, K. E. (1967). *Gas Lift: Theory and Practice. Brown*: Prentice-Hall.

Buresh, J. F., & Schuder, C. B. (1964). Development of a universal gas sizing equation for control valves. *ISA Transactions, 3*(4).

Cook, H. L., & Dotterweich, H. (1946). Report on calibration of positive flow beans manufactured by Thornhill-Craver Company, Inc. *Houston, Texas. Department of Engineer, Texas College of Arts and Industries, Kingsville*.

Corning, D. (1966). *Information About Silicon Fluid Products*. Retrieved from Midland, Michigan:

Corning, D. (2017). Volume Expansion of Fluids. In *Dow Corning*: Dow Corning.

Coutinho, R. (2018). *Experimental and Numerical Investigation of Liquid-Assisted Gas-Lift Unloading.* (Ph.D.), The Louisiana State University (LSU), Baton Rouge.

Cunningham, R. G. (1951). Orifice Meters with Supercritical Compressible Flow. *ASME Trans.*

Decker. (2014). VPC Software Decker Technology, Inc.

Decker, K. (1993). Gas-lift valve performance testing and data correlation. *SPE Production & Facilities, 8*(02), 101-107.

Decker, K., & Sutton, R. P. (2018). *Gas Lift Annulus Pressure.* Paper presented at the SPE Artificial Lift Conference and Exhibition-Americas.

Dranchuk, P., & Abou-Kassem, H. (1975). Calculation of Z factors for natural gases using equations of state. *Journal of Canadian Petroleum Technology, 14*(03).

Driskell, L. R. (1969). New approach to control valve sizing. *Hydrocarbon Processing, 48*(7), 131-&.

Driskell, L. R. (1970). Sizing Valves for Gas Flow. *ISA Transactions, 9*(4), 6.

Driskell, L. R. (1983). *Control valve selection and sizing*: Isa.

Economides, M. J., Hill, A. D., Ehlig-Economides, C., & Zhu, D. (2012). *Petroleum production systems*: Pearson Education.

Fagerlund, A. C. (1988). *A Proposed Method of Control Valve Sizing for Non-Ideal Fluids.* Paper presented at the Proceedings of the 2nd International Conference on Developments in Valves and Actuators for Fluid Control.

Hernandez, A. (2016). *Fundamentals of Gas Lift Engineering*. UK: Gulf Professional Publishing.

Hernandez, A. (2016). *Fundamentals of Gas Lift Engineering: Well Design and Troubleshooting*: Gulf Professional Publishing.

Ho, C. Y., & Taylor, R. E. (1998). *Thermal expansion of solids* (Vol. 4): ASM international.

ISA. (1975). Control Valve Test Procedures. In. NC: ISA.

Jansen, J. D. (2017). *Nodal Analysis of Oil and Gas Production Systems*: Society of Petroleum Engineers.

Johnson, R. C. (1972). Tables of critical-flow functions and thermodynamic properties for methane and computational procedures for both methane and natural gas.

Kirkpatrick, C. (1955). The Power of Gas. *Camco Inc., Houston, Texas*.

Kouremenos, D., & Antonopoulos, K. (1987). Sound velocity and isentropic exponents for gases with different acentric factors by using the Redlich-Kwong-Soave equation of state. *Acta mechanica, 66*(1-4), 177-189.

Kouremenos, D. A. (1986). The normal shock waves of real gases and the generalized isentropic exponents. *Forschung im Ingenieurwesen A, 52*(1), 23-31.

Lemmon, E., Huber, M., & McLinden, M. (2007). REFPROP, NIST Standard Reference Database 23, Version 8.0. *National Institute of Standards and Technology, Gaithersburg, MD*.

Marić, I., Galović, A., & Šmuc, T. (2005). Calculation of natural gas isentropic exponent. *Flow measurement and instrumentation, 16*(1), 13-20.

Metals, H. P. (2001). Technical Data Sheet

Mukherjee, H., & Brill, J. (1999). Multiphase flow in wells. *Monograph from society of petroleum engineers Inc. Richardson, Texas*.

Munson, B. R., Okiishi, T. H., Rothmayer, A. P., & Huebsch, W. W. (2010). *Fundamentals of fluid mechanics*: John Wiley & Sons.

Nasrifar, K., & Bolland, O. (2006). Prediction of thermodynamic properties of natural gas mixtures using 10 equations of state including a new cubic two-constant equation of state. *Journal of Petroleum Science and Engineering*, *51*(3-4), 253-266.

Nederstigt, P. (2017). *Real Gas Thermodynamics and the isentropic behavior of substances*. (Master of Science), Delft University of Technology, Netherlands.

OpenStaxCollege. (2012). Thermal Expansion of Solids and Liquids. *Anatomy and Physiology*.

Rayleigh, J., & Lindsay, R. B. (1945). The Theory of Sound, Two Volumes In One.

Riveland, M. L. (1992). Enhanced valve sizing methods for fluids exhibiting real gas behavior. *ISA SERVICES INC, RESEARCH TRIANGLE PK, NC(USA)*. 111-126.

Riveland, M. L. (2012). The Use of Control Valve Sizing Equations with Simulation Based Process Data. In: ISA automation week.

Rohatgi, A. (2010). Web Plot Digitizer.

Sage, B. H., & Lacey, W. N. (1950). *Thermodynamic properties of the lighter paraffin hydrocarbons and nitrogen: monograph on API Research Project 37*: American Petroleum Institute.

Schlumberger. (2000). Gas Lift Design and Technology. from Schlumberger

Sines, J. (2015). How Do You Use the Expansion Factor to Properly Size Equipment for Compressible Gas Applications?

Smith, J. P., & Clancy, J. (2010). *Understanding AGA Reprot NO. 10, Speed Of Sound in Natural Gas and Other Related Hydrocarbons Gases*. Retrieved from

SOLV. (2017). FLOWSOLVE (Version 5.1). UK: SOLV Company.

Streeter, V. (1969). *Handbook of Fluid Dynamics* (1ST ed.). United States of America: McGraw Hill.

Sutton, R. P. (2014). *Accuracy of Nitrogen Temperature Correction Factors.* Paper presented at the SPE Artificial Lift Conference & Exhibition-North America.

Takacs, G. (2005). *Gas Lift Manual*: PennWell Books.

Tichy, J. A., & Winer, W. O. (1968). A Correlation of Bulk Moduli and PVT Data for Silicone Fluids at Pressures up to 500,000 psig. *ASLE TRANSACTIONS, 11*(4), 338-344.

Waltrich, P. J. (2012). *Onset and subsequent transient phenomena of liquid loading in gas wells: experimental investigation using a large scale flow loop*: Texas A&M University.

Waring, B. (2018). GLtoy (Version Version: 25 March 2018): Burney Waring.

Winkler, H., & Eads, P. (1989). *Algorithm for more accurately predicting nitrogen-charged gas-lift valve operation at high pressures and temperatures.* Paper presented at the SPE Production Operations Symposium.

Winkler, H., & Eads, P. (1993). Applying the Basic Performance Concepts of Single-Element, Unbalanced Gas-Lift Valves for Installation Design. *SPE Production & Facilities, 8*(03), 211-216.

Winkler, H. W., & Smith, S. S. (1962). *Camco Gas lift manual*: Camco.

Wylie, E. B., & Streeter, V. L. (1978). Fluid transients. *New York, McGraw-Hill International Book Co., 1978. 401 p.*

Xu, Z., Richard, B. M., & Kritzler, J. H. (2013). *Smart Gas Lift Valves Enhance Operation Efficiency of Offshore Wells.* Paper presented at the SPE Annual Technical Conference and Exhibition.

Zimmerman, W. G. (1982). *Manual Básico de Gas Lift*. Departamento de Producción, División Occidente. Publicación interna de la compañía, Venezuela.

Vita

Khadhr A KH Altarabulsi, born in Kuwait, worked for the Kuwait Oil Company for more than five years after receiving his bachelor's degree from Kuwait University in 2009. He earned his master's degree in Petroleum Engineering from the same University in 2014. He is planning to work as a faculty member in the Department of Petroleum Engineering at Kuwait University upon his planned Ph.D. graduation in December 2018.